Guo, Du-Jiao (2011) *Microstructure and crystallography of abalone shells.* MSc(R) thesis.

http://theses.gla.ac.uk/2401/

Microstructure and Crystallography of Abalone Shells

Du-Jiao GUO

Thesis submitted for Research Masters Degree

School of Geographical and Earth Sciences, University of Glasgow

October 2010

Abstract

Biominerals are biogenic mineralized products comprising both mineral and organic components. Calcium-bearing minerals comprise about 50% of biominerals with the most common being polymorphs of calcium carbonate, *e.g.* calcite and aragonite.

Abalone (*Haliotis asinina* Linnaeus, 1758; *Haliotis rufescens* Swainson, 1822 and *Haliotis gigantea* Gmelin, 1791) are marine snails, belonging to the Phylum Mollusca, class Gastropoda, family Haliotidae*,* genus *Haliotis.* They can be easily recognized by the row of apertures, which are closed, half-closed and open ones, along the spiral ridges and towards the shell longitudinal growth direction of the dorsal margin.

This study considers the microstructure and crystallography of three species of abalone shells, *Haliotis asinina* from Australia, *Haliotis rufescens* from America and *Haliotis gigantea* from Japan; as well as the aperture infill of *H. asinina*. The microstructure and crystallography are analysed through Scanning Electron Microscopy (SEM) and Electron Backscatter Diffraction (EBSD) respectively.

Abalone shells all have an outer prismatic and an inner nacreous layer. It is confirmed that the shell of *H. asinina* is comprised of aragonite in both prismatic and nacreous layers, with c-axis orientation of crystals throughout the prismatic and nacreous layers of shell. Towards the prismatic-nacreous interface, crystallographic alignment of prismatic layer becomes much more tightly constrained. In nacre, crystallographic continuity persists across several laminae. Along the longitudinal shell growth direction (from posterior part to anterior), there is a trend of gradually thickening tablets towards the shell interior. In addition to this trend from exterior to interior, the tablets formed at the anterior are thicker than those formed earlier at the posterior. It is also confirmed that the nacreous layer in *H. rufescens* and *H. gigantea* is aragonite. The prismatic layer of *H. rufescens* shell is composed of calcite, the c-axis of which is normal to the shell surface. The prismatic layer of *H. gigantea* shell consists of calcite and aragonite, the c-axis of aragonite is normal to the shell surface and that of calcite is parallel to the shell surface. In these three species, there is higher crystallographic constraint in the nacreous layer than in the prisms.

Furthermore, the crystallographic continuity of the nacreous layer persists across as many as 40~50 laminae.

H. asinina is about 800 µm thick, *H. rufescens* is the thinnest at around 600~700 µm and *H. gigantea* shell is the thickest at about 1 mm. Comparing the three species, the prismatic layer to the shell thickness of three species, the calcite prismatic layer (*H. rufescens*) takes up about 50% of the shell thickness compared with aragonite prismatic layer (*H. asinina*) of about 20~30%, and the prismatic layer with calcite and aragonite (*H. gigantea*) is between the two at over 30% of total shell thickness.

Aperture infill of *H. asinina* is also composed of aragonite with both prismatic and nacreous layers. The crystallographic orientation of infill prismatic layer is parallel to the shell surface unlike that of the shell where the crystallographic orientation of the prismatic layer is perpendicular to the shell surface. There is a prism-like layer between aperture infill and the shell. The contact with the shell always occurs within the nacreous shell layer. Aperture infill grows on this prism-like layer and the growth rate of aperture infill is in-keeping with that of the shell growth rate. When individuals reach six months and older, shell growth and aperture infill occur at approximately the same speed.

Table of Contents

List of Figures

List of Tables

Acknowledgements

Declaration

The material presented in this thesis is the result of two and half years independent research carried out at School of Geographical & Earth Sciences, University of Glasgow. The research was supervised by Prof. Maggie Cusack (University of Glasgow) and Dr. Nick Kamenos (University of Glasgow).

This thesis represents my own research and any published or unpublished work by other authors has been given full acknowledgement in the text.

Du-Jiao GUO

January 2011

1 Introduction

1.1 Biminerals

Biomineralisation, the formation of mineralized materials by living organisms is widespread in nature and occurs in all five taxonomic kingdoms (Weiner & Traub, 1984). The biomineral structures perform various functions such as shells providing protection in bivalves, brachiopods, and foraminifera; skeletal support in vertebrates and embryonic chambers in avian eggshells (Cusack & Freer, 2008).

The term "biomineral" refers to biogenic mineralized products comprising both mineral and organic components. Living creatures produce a great variety of minerals, which include bone, teeth, statoliths, otoliths, shells, coccolith scales, eggshells, sponge silica skeletons, algal, radiolarian and diatom silica micro-shells, and a variety of transition metal minerals by diverse organisms (Gilbert *et al*., 2005). Lowenstam (1981) introduced terms to describe two fundamentally different processes of mineral formation, one of which is characterised without organic matrix by bulk extracellular or intracellular mineral formation, exemplified by some bacterial species and algae. The other is an "organic matrix-mediated" mineralization process performed by many animals. In general for animals, a dedicated organ is often defined very early in the embryological development and contains an organic matrix which facilitates and directs the deposition of crystals (Livingston *et al*., 2006). Estimates indicate that there are over 60 different minerals in the biosphere (Lowenstam & Weiner, 1989) and the number of biogenic minerals identified is continuously increasing (Meyers *et al*., 2008). Table 1.1 from Weiner & Addadi (2002) shows the principal biogenic minerals. Calcium-bearing minerals comprise about 50% of biominerals with the most common being polymorphs of calcium carbonate, *e.g.* calcite, aragonite and vaterite (Lowenstam, 1981). Amorphous calcium carbonate (ACC) also occurs as a transient precursor of more stable crystalline aragonite or calcite (Addadi *et al*., 2003).

Inorganic Minerals	**Carbonate**	Calcite	Protodolomite
		Aragonite	Hydrocerrusote
		Vaterite	Amorphous calcium carbonate family
		Monohydrocalcite	
	Phosphate	Francolite	Carbonated apatite (dahllite)
		Whitelockite	Octacalcium phosphate
		Strucvite	Brushite
		Vivianite	Amorphous pyrophosphate
		Amorphous calcium phosphate family	
	Halides	Fluorite	Amorphous fluorite
		Hieratite	Atacamite
	Sulfates	Gypsum	Jarosite
		Celestite	Calcium sulphate hemihydrate
		Barite	Barite
	Silicates	Silica (opal)	
	Oxides and Hydroxides	Magnetite	Amorphous maganese oxide
		Goethite	Amorphous ilmenite
		Lepidocrocite	Todotokite
		Ferrihydrite	Bimessite
		Amorphous iron oxide	
	Sulfides	Pyrite	Galena
		Greigite	Amorphous pyrrhotite
		Hydrotroilite	Mackinawite
		Shalcrite	Wurtzite
Organic Minerals		Whewellite	Uric acid
		Weddelite	Paraffin hydrocarbon
		Wax	Manganese oxalate
		Calcium tartrate	Magnesiumoxalate (glushinskite)
		Calcium malate	Copper oxalate (moolooite)
		Earlandite	Ferric oxalate anhydrous
		Guanine	Sodium urate

Table 1.1 Minerals in biological system

(Data from Weiner and Addadi, 2002)

Scientists have long been fascinated by how organisms form their highly regulated biomineral morphologies in aqueous solutions at ambient conditions. From the materials science perspective, biominerals, as composites of mineral and organic molecules, are compliant and fracture-resistant while inorganic crystals are hard and brittle, and thus there is an ambition to combine the best of these biological properties such as hardness and fracture resistance (toughness) (Currey 1977; Jackson *et al.*, 1988; Schaffer *et al.*, 1997;

Kamat *et al*., 2000; Gao *et al.*, 2003). There are several factors relevant to the properties: structural arrangement, nano-size crystals and chemical composition. Materials scientists have begun to learn how to mimic biosyntheses of new high-performance composite materials that outperform each component taken separately (Heuer *et al*., 1992), such as for nacre (Tang *et al.*, 2003). However, natural biogenic composites produced by living organisms still surpass those of analogous synthetic materials with similar phase compositions in terms of physical and material properties (Rubner, 2003).

1.1.1 Mesocrystals

Biogenetic minerals may be amorphous, paracrystalline, or crystalline (Lowenstam & Margulis, 1980). At a given site, they may occur as a single unit (such as a single crystal), numerous individual units, or aggregates. The latter form structures of varying degrees of complexity (Lowenstam, 1981). In recent years, non-classical crystallization mechanisms such as oriented aggregation have received increasing attention in the scientific literature (Cölfen & Antonietti, 2005; Penn, 2004; Zhang *et al*., 2009; Zeng, 2007). Oriented aggregation involves the self-assembly of primary nanocrystals, crystallographic reorganization and conversion to oriented aggregates, which are new secondary crystals (Penn *et al*., 2004; 1998). These new secondary structures can be composed of a few to hundreds of primary units. Cölfen & Mann (2003) coined the term "mesocrystal" to describe a particle composed of such primary units in crystallographic register.

The formation of a mesocrystal has been suggested as a required intermediate step of oriented aggregation (Schwahn *et al*., 2007) and represents a fundamental step forward in our understanding of the growth mechanism of the oriented aggregation of crystals (Yuwono *et al*., 2010). Figure 1.1 shows a new single crystal formed via mesocrystal intermediates eventually fusing into oriented aggregates with some organic components being included and some excluded.
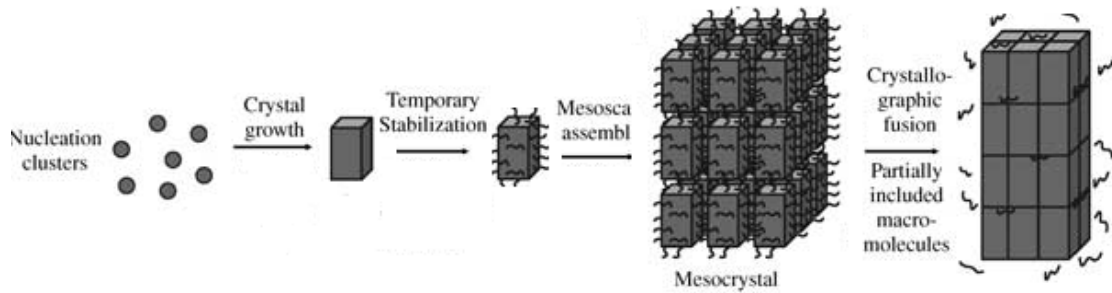
Figure 1.1 Schematics of single crystal formation via mesocrystal intermediate
(From Cölfen & Antonietti, 2005)

Mesocrystals have potentially exciting applications, either in construction materials, as exploited by nature for biominerals or as functional ceramics, *e.g.* with colour or magnetic properties (Cölfen & Antonietti, 2005). However, there is still much to be learned about the forces guiding mesocrystal assembly and the exact mechanisms of formation.

1.2 Mollusca

The invertebrate phylum Mollusca is composed of 110, 000 species in ten classes of eight living classes and two extinct ones (Haszprunar, 2001). The Mollusca is the second largest phylum after the Arthropoda. Some authors combine the Caudofoveata and Solenogasters into one class, the Aplacophora (*Ruppert et al.,* 2004). The class gastropoda accounts for 75.5% classified species of the phylum and are by far the most abundant (Haszprunar, 2001). Figure 1.2 shows the relative abundance of major living classes of the phylum.

Bivalvia (mussels, clams, oysters, scallops, *etc.*)

- **Aplacophora (solenogasters, caudofoveata)**
- **Scaphopoda (tusk shells)**
- **Monoplacophora (trybidia)**
- **Polyplacophora (chitons)**
- **Cephalopoda (squid, octopus, nautilus, cuttlefish)**

Gastropoda (snails, slugs, limpets, nudibranchs)

21.6%

2.9%

75.5%

Figure 1.2 Relative abundance of the major living Classes of the Mollusca in terms of number of species

(Data form Haszprunar, 2001 & Ruppert et al., 2004)

Gastropods are usually characterized by having a single coiled shell. Bivalves possess two valves, joined at one edge by a flexible ligament called the hinge. Cephalopods have one shell, although the shell is internal in squid and cuttlefish. Aplacophorans are worm-like burrowing animals without a shell but with small calcified specules are embedded in the skin. Class Monoplacophora have a single limpet-like shell with a major distinguishing characteristic being that all organ systems occur in multiples. Polyplacophora have eight shells embedded in a broad mantle. Scaphopoda have a singular tubular shell open at both ends. Figure 1.3 presents examples of some classes.

Figure 1.3 Examples of some classes of the Phylum Mollusca

Images from http://en.wikipedia.org/wiki/Mollusca

Allowing for exceptions such as octopus and solenogaster, the generalized gastropod has a single "limpet-like" shell on top, and under shell is a soft body, which consists of three basic parts: a foot, a visceral mass, and a mantle (Ruppert *et al.*, 2004; Figure 1.4). The foot enables locomotion, burrowing and attachment. The visceral mass, located above the foot, contains the digestive system, the heart and other internal organs. The mantle is a layer of tissue that covers the visceral mass and contains glands which secrete a hard shell (Keeton & Gould, 1986).
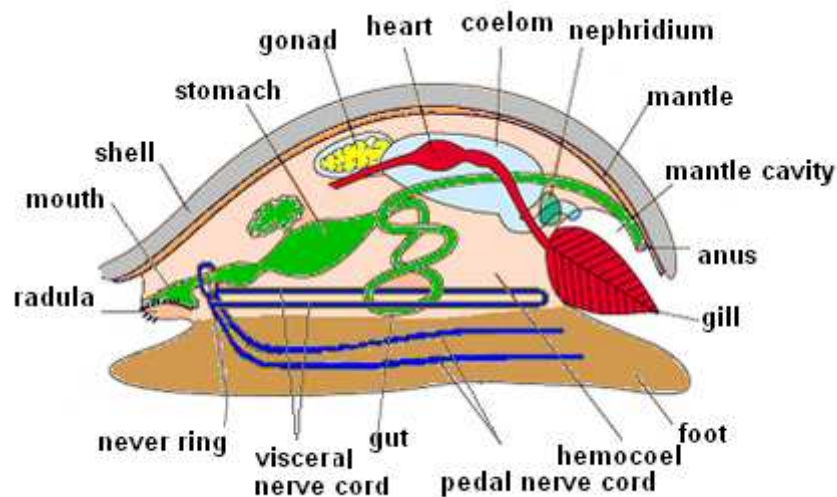
Figure 1.4 Schematic illustration showing the generalized gastropod

(Modified from Ruppert et al., 2004)

Molluscs have more varied forms than any other animal phylum. The majority of species live in the oceans, from the seashores to the abyssal zone, but some form a significant part of the freshwater fauna and the terrestrial ecosystems. The majority of marine molluscs begin their life as ciliated, free-swimming larvae that later metamorphose into adult form. Fresh water and terrestrial snails always develop within the egg and emerge as tiny but fully formed versions of the adult form (Keeton & Gould, 1986).

1.2.1 Abalone

Abalone are marine snails, gastropod molluscs of the family Haliotidae, genus *Haliotis*. Common names for abalone include ear-shells, sea ears, as well as muttonfish or muttonshells in Australia, ormer in Great Britain, *perlemoen* and venus ears in South Africa and *Pāua* in New Zealand (Beesley *et al*., 1998). There are about one hundred species of abalone distributed worldwide, mainly in the South Western Pacific (around Japan and Australia), at the Southern African and the Californian Coast. Abalone are slow-growing single-shelled gastropods which live in rocky and shallow waters near stands of algae, where they can attach firmly on stony ground with their muscular foot. They simply hide in a crevice or under a rock to avoid light and then come out at night, living from

grazing algae (Leighton, 2000). The abalone shell is characterized by having a row of apertures located along the dorsal margin (Figure 1.11, 2.1). The apertures are filled in and new open one form as the animal grows. The open apertures are used for respiration and as outlets for waste products (Geiger & Poppe, 2000).

Abalone are dioecious (separate male and female sexes) and they reproduce by releasing gametes into the water column from April to August, using a process called broadcast fertilization or spawning. The transitions during shell development are presented using *Haliotis asinina* as an example (Figure 1.5). The initial differentiation of biomineralising cells is likely to include a localised thickening of the dorsal ectoderm followed by an invagination of cells to form the shell gland (Kniprath, 1981). Figure 1.5a shows that the shell gland evaginates to form the shell field, which expands through mitotic divisions to direct the precipitation of calcium carbonate via the secretion of organic molecules. In this way the larval shell (protoconch) is formed as shown in Figure 1.5b and 1.5c. The construction of the haliotid protoconch is complete following torsion (Figure 1.5c), and remains developmentally inert until the animal contacts a specific cue that initiates the process of metamorphosis (Jackson *et al*., 2005; Morse *et al*., 1979). The transition from protoconch to teleoconch (juvenile/adult shell) is clearly visible at metamorphosis (Figure 1.5d), and suggests the action of a different biomineralising secretome. The early postlarval shell is more robust and opaque than the larval shell but has no pigmentation. Juvenile *H. asinina* begins to develop a complex colouration in the shell several weeks after metamorphosis (Figure 1.5e, 1.5f). This pattern is gradually lost with growth as the shell becomes thicker and more elongate (Figure 1.5g, 1.5h).
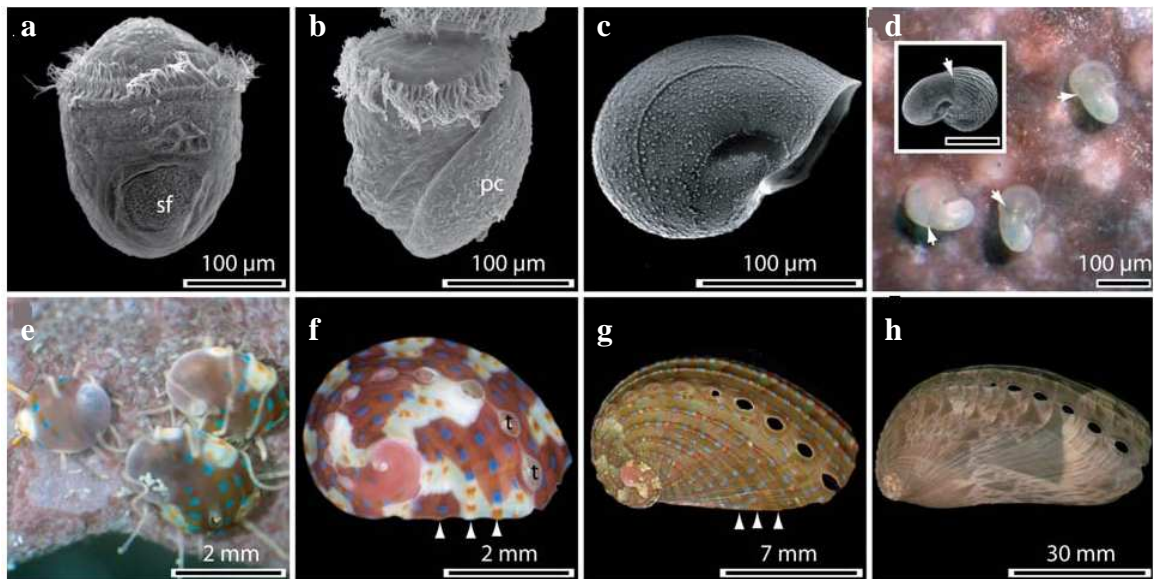
Figure 1.5 Major transitions during shell development of *Haliotis asinina*

a. A newly hatched trochophore larva 9h post fertilization during the initial stages of biomineralisation; the shell field (sf) is evident. b. The calcified protoconch (pc) is present by 11h post fertilization. c. The completed larval shell. d. Newly settled postlarvae on coralline algal surface. An abrupt transition in shell morphology accompanies metamorphosis (white arrows). This initial postlarval shell is unpigmented and displays a rippled texture (inset). e. 1-2 month old juveniles have developed a pigmented shell that is initially a uniform maroon, but soon develops a series of blue and orange dots and cream and maroon fields. f-g. Shell sizes of approximately 1-10mm maintain this complexity in pigmentation with blue and orange dots (arrowheads showing ridges). h. The shell of sexually mature abalone showing a pattern of tan –brown triangles of baring intensity now patterns the shell. (From Jackson et al., 2007)

The studies on abalone growth and longevity reveal a large variation in growth rates and size between species (Day & Fleming, 1992) , which are also influenced by different areas, seasons, and temperatures (Leighton, 2000). Abalone species that occur in temperate regions are bigger than the species found in the tropics (Pollard, 2001). Abalone has several predators including fish, sea birds, otters, crabs and starfish. They are also vulnerable to boring sponges, which erode holes in their shells to open them up to other predators (Leighton, 2000). Their only protection is in their tenacity in clinging to rocks and the protective camouflage of their shell and foot (Leighton, 2000).

1.3 Molluscan Shell

Molluscan shell structures reflect the long evolutionary history of molluscs since the Cambrian (Kobayashi & Samata, 2005). Many marine invertebrate organisms possess annual growth increments in their skeletons, analogous to annual tree rings, which record the marine environment and climatic conditions that the molluscs experience (Rhoads & Lutz, 1980; Clark, 1974). Detailed analysis of element composition of mollusc shells has shown their relationship with environmental parameters (Dodd, 1965; Lorens & Bender, 1980). As a result, the successively deposited shell calcium carbonate layers are potential archives of the varying environmental conditions the mollusc has experienced during its life (*e.g.* Fuge *et al.,* 1993; Stecher *et al.,* 1996; Hart & Blusztajn, 1998).

Mollusc shells (especially in bivalves and gastropods) have also been intensively studied as biomineralisation models for a large variety of microstructures (Carter, 1990; Taylor *et al*., 1969) and their high mechanical performance (Luz & Mano, 2009). The molluscan shell is a composite biomaterial comprising polymorphs of calcium carbonate (95% to 99% per weight) and organic components (1 to 5%) (Marin & Luquet, 2004). The organic matrix is secreted in the extrapallial space by specialized cells of the calcifying mantle and is a complex mixture of proteins, glycoproteins, proteoglycans, polysaccharides, and chitin (Addadi & Weiner, 1992; Lowenstam & Weiner, 1989; Weiner & Addadi, 1997; Weiner & Traub, 1980), which provide a scaffold and control mineral deposition and growth (Weiner & Addadi, 1997). There have also been many advances in our knowledge of the organic components involved in nacre formation (section 1.3.2). In general, molluscs commonly form shells that contain either one or both of the main calcium carbonate polymorphs calcite and aragonite in the prismatic layer; while aragonite comprises the inner nacreous layer. In the bivalve, *Mytilus edulis,* calcite forms the outer prismatic layer and aragonite forms the inner nacreous layer (Lorens & Bender, 1980). Abalone gastropods have an inner nacreous layer while outer prismatic layer is composed of either or both polymorphs. For example, *H. rufescens* contains calcite prisms, *H. glabra* contains aragonite prisms, and *H. tuberculata* has a mixture of these two minerals in the prismatic layer (Mutvei *et al,* 1985; Dauphin *et al.*, 1989).

Recently, biogenic amorphous calcium carbonate (ACC) has been widely discussed and suggested as a transient precursor of more stable crystalline aragonite or calcite (Addadi *et al.*, 2003). ACC is one of six forms of calcium carbonate (Table 1.1) and is the only isotropic form in polarized light. ACC does not diffract X-rays and hence it is described as being amorphous (Lippmann, 1973). As ACC is difficult to detect and especially when it co-exists with one of the crystalline forms of calcium carbonate, it is easy to overlook the presence and so ignore that it may well have a much broader role to play in biology than suspected (Addadi *et al.*, 2003). Raman spectroscopy is a particularly useful method for investigating ACC, because ACC produces a characteristic Raman Spectrum that is quite different from the crystalline $CaCO_3$ phases (Raz, *et al.*, 2000; Weiner *et al.*, 2003; Addadi *et al.*, 2003). With the properties of high solubility and isotropy, ACC can easily be shaped to any morphology prior to crystallization (Greenaway, 1985). The main function of ACC as temporary storage deposit in various vesicles or other tissues has been in this case. Such as Beniashi *et al.* (1997) discovered that ACC is a transient precursor phase prior to the formation of the calcitic spicules of mature sea urchin larvae. Weiss *et al.* (2002) showed a similar function for ACC in the larvae of molluscan bivalves, except in the case it transforms into aragonite. However, little is known about the macromolecules associated with biogenic ACC and whether some proteins are related to the formation and/or stabilization of the ACC components (Addadi *et al.*, 2003). Dey *et al.* (2010) indicate that although the involvement of amorphous phase both *in vivo* and *in vitro* is well established, the mechanism underlying the amorphous to crystalline transformations is still a matter of debate.

1.3.1 Nacre properties

The three main mollusc Classes are Bivalvia, Gastropoda and Cephalopoda, all of which produce nacre. Nacre has highly organized internal structure with optical effects, *e.g.* beautiful lustre (Figure 1.6-a) and mechanical properties. Currey (1977) found that nacre is 3000 times tougher than pure aragonite. Jackson *et al.* (1988, 1990) have shown that nacre is superior to most other artificial composite ceramics in stiffness, strength and toughness. The aragonitic laminar structure consists of polygonal to rounded tablets with fairly uniform thickness arranged in broad, regularly formed parallel sheets (Carter & Clark, 1985). The organic layer plays a role in determining the structure (Addadi & Weiner, 1997;

Walters *et al*., 1997), acting as a powerful toughening component of energy –absorbing filler between the aragonitic layers (Jackson *et al*., 1988; Wang *et al*., 1995). For example, when a crack travels down through and round the layers of crystals, the plates take apart and, in doing so, extend the organic sheets, so that the plates remain connected via the aragonic components and thus cracks are deflected (Jackson *et al*., 1988).

The mechanical properties of nacre have attracted much interest from material scientists, prompting efforts to mimic nacre formation by industrial processes (Addadi *et al*., 2006). Historically, nacre has always been of great interest to the pearl industry (Cuif & Dauphin, 1996). Recently, there is a renewed interest for nacre-related technique application such as the fabrication of bio-inspired super-tough materials and clinical implants. Another fascinating property is that nacre from the bivalve *Pinctada maxima* shows osteogenic activity (Lopez *et al*., 1992; Silve *et al*., 1992). When nacre is implanted in bone, new bone formation occurs without any inflammatory reaction (Atlan *et al*., 1999). It is amazing that such a light and strong material is synthesized at ambient temperature and its formation is still the best-studied example of calcium carbonate biomineralisation.
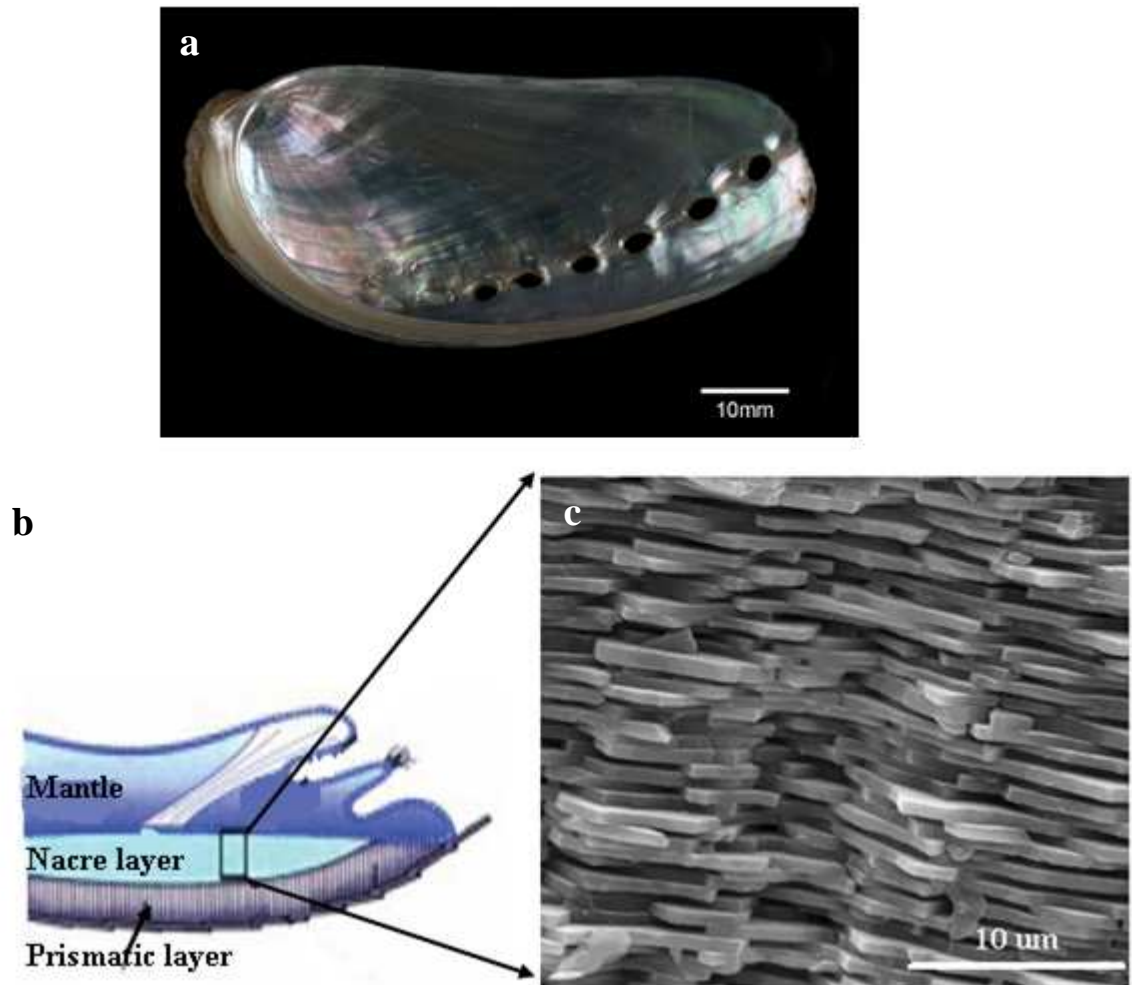
Figure 1.6 The shell of *Haliotis asinina*

a. Shell interior with iridescent nacre layer. The nacreous layer is inside of shell, prismatic layer forms the outer shell. b. Schematic representation of the shell structure and the overlying mantle of the animal. c. Secondary electron image of fracture shell reveals the stacks of nacreous tablets; each layer is about 0.5-1μm thick.

1.3.2 Organic components of nacre

In mollusc shells, mineralisation appears to occur within an organic framework that acts as the template that provides the control of microstructure and crystallography (Bevelander & Nakahara, 1969; Wada, 1972; Schaffer *et al.*, 1997; Nudelman *et al.*, 2006). It is vital to understand the structure of the organic framework and, in particular, its macromolecular layout such as the crystal nucleation. The organic material of the nacreous layer assembled into a 3-dimensional framework has three major components: (1) β-chitin, which is the

main constituent of the inter-lamellar matrix, forms a scaffold where crystals nucleate and grow (Weiner & Traub, 1980); (2) silk-like proteins (Weiner & Traub, 1980; Weiner *et al.*, 1983), present in a hydrated gel-like state, presumably fulfil the task of space-fillers prior to mineral deposition, also providing a hydrophobic micro-environment that contributes to the control of crystal formation (Addadi *et al.*, 2006; Levi-Kalisman *et al.*, 2002); (3) an assembly of acidic glycoproteins (Crenshaw, 1972; Weiner, 1979), some of which specifically nucleate aragonite when absorbed on chitin (Falini *et al.*, 1996; Weiner, 1979). These major components do not function in isolation; *in vitro* experiments have demonstrated that the assembly of all the components is important to induce preferred nucleation of aragonite over calcite (Falini *et al.*, 1996).

Nudelman *et al* (2006) identified four zones of different chemistry on the framework surface of nacre from the cephalopod *Nautilus pompilius* and bivalve *Atrina rigida* (Figure 1.7). There were no holes to facilitate "mineral bridges" observed in the nucleation site regions (including those of Levi-Kalisman *et al.* (2001)). Bezares *et al* (2008) confirm the general findings of Nudelman *et al.* (2006) by working on gastropod *Haliotis rufescens* while observed multiple mineral bridges per tablets for transmission as suggested (*e.g.* by Cartwright & Checa, 2006). Based on direct observation for gastropods, it has been proved that such holes in the matrix exist between mineral layers, and all the crystals in a stack are in fact a single crystals joined by mineral bridges (Schaffer *et al.*, 1997; Song *et al.*, 2002).
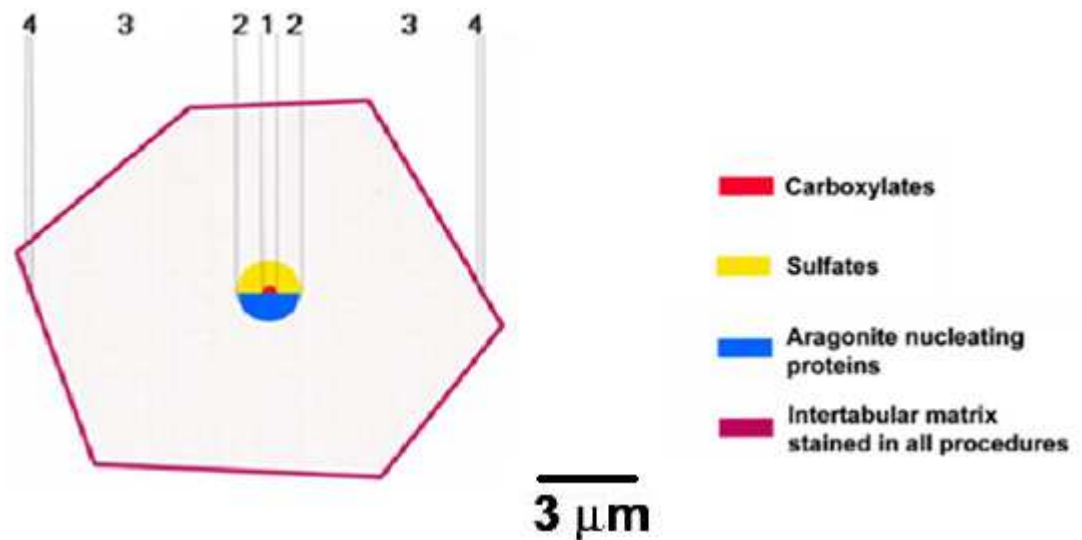
Figure 1.7 Schematic of nacre tablet with zoned distribution of carboxylates, sulphates, and acidic proteins

1. Central zone rich in carboxylates. 2. A zone rich in sulphates (the aragonite-nucleating proteins also map into this region). 3. The region of crystal overgrowth containing either few or no characteristic acidic functional groups. 4. Interface between adjacent crystal tablets, this zone may well contain matrix components that are pushed ahead of the growing crystal and are trapped between adjacent crystals. The elaboration of these zones not only provides insight into the mechanisms of control of the matrix over crystal formation, but can also be sued to assess potential functions of individual matrix components based on their distribution over a crystal imprint (from Nudelman et al., 2006).

1.3.3 Nacre formation, microstructure and crystallography

Nacre forms the inner layer of many mollusc shells and is composed of polygonal aragonitic tablets about 5-15 µm in diameter (Watabe, 1965). These are arranged in continuous parallel lamellae that are typically around 0.5 µm thick (Figure 1.6-c), separated by sheets of interlamellar organic matrices (Gregoire, 1957, 1972; Wada, 1968). Observations of growing nacre shows that each tablet nucleates at a specific location on the matrix surface (Checa & Rodriguez-Navarro, 2005; Crenshaw & Ristedt, 1976; Rousseau *et al*, 2005). The newly formed crystal rapidly grows in a direction perpendicular to the matrix surface and later extended sideways within a-b plane until impinging on one another, no matter whether stacked in columns or layered sheets (Mutvei, 1977). The crystal tablets in bivalve nacre have a staggered "brick wall" like structure. All crystal axes are aligned and b-axis orientation is parallel with the direction of shell growth (Hedegaard & Wenk,

1998; Chateigner *et al*., 2000). In gastropods and to a certain extent in cephalopods (e.g. *Nautilus*), the crystal tablets exhibit a striking columnar appearance and finally coalesce by lateral growth (Figure 1.8; Wise, 1970). Lateral expansion ultimately brings crystals of adjacent stacked into contact, forming the broad mineral laminae which characterize the nacre of all molluscs (Wise, 1970).
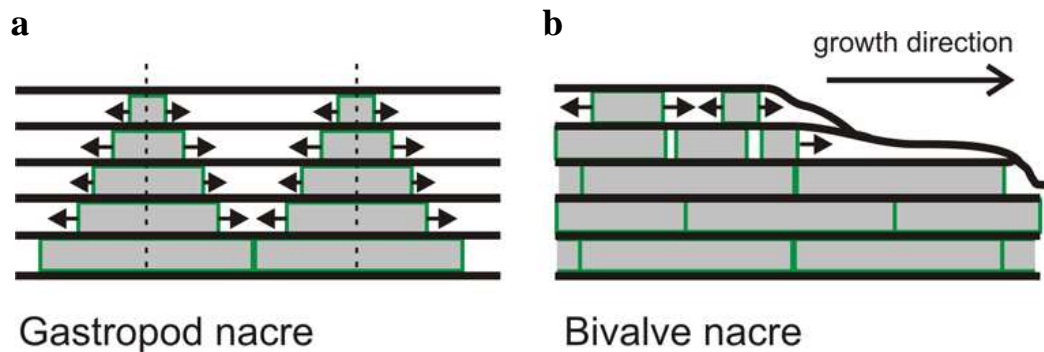
Figure 1.8 Schematic representation of the stacking models of gastropod and bivalve nacre

a. Column nacre stacks in towers, the new tablets formed at the top of the stacks with uniform thickness before the tablets underneath expand laterally to contact neighbours. b. Sheet nacre stacks in "brick wall" pattern, new tablets form at the top surface just when the underneath tablets form flat sheet. Individual tablets (grey) are surrounded by an organic envelope (green) and are laterally separated by organic sheet (black) (Arrow shows the growth direction of the tablets) (from Mann, 2001)

Bivalve nacre is arranged in terraces, the three crystallographic axes of crystals are co-oriented, with the c-axis perpendicular to the nacre surface and the b-axis parallel to the local growth direction of the shell margin (Wise, 1970; Wada, 1972). In gastropod nacre, crystals of the same tower have their crystallographic axes co-oriented, with the c-axis along the stacking axis (Figure 1.9; Mann *et al*., 1994). Crystals in different towers have their c-axis aligned but the a- and b-axes have an azimuthally disorder (Gilbert *et al*., 2008; Metzler *et al.*, 2007). It is interesting to observe that the deposition of organic matrix does not seem to interrupt the epitaxial growth of crystals from one layer to the next; there is always continuity in the preferential orientation of crystals during the shell growth (Checa & Rodriguez-Navarro, 2001). Pores found in organic material are proved as mineral bridges observed by atomic force microscopy (Schaffer *et al*., 1997), transmission electron microscopy (Song & Bai, 2003, Lin *et al*., 2008), and scanning electron microscopy (Lin *et*

al., 2008). Growth through the pores could explain how crystal orientation of the aragonite tablets is maintained between layers. However, the theory is only proposed based on direct observation for gastropods (*e.g.* abalone) not a universal growth mechanism for all mollusc nacre (*e.g.* Nudelman *et al*. 2006 and Levi-Kalisman *et al.* 2001). Recently the possibility of calcium carbonate precursors, such as amorphous calcium carbonate (ACC) formed elsewhere and transported to the sites of tile growth, has been intensively discussed (Nassif *et al*., 2005, Addadi *et al*., 2006; Carwight & Checa, 2006; Bezares *et a*l, 2008). However, it is generally considered that the alignment of the aragonite crystal c-axis is due to microscopic chemical templating by the organic matrix (Mann, 2001; Addadi & Weiner, 1985).
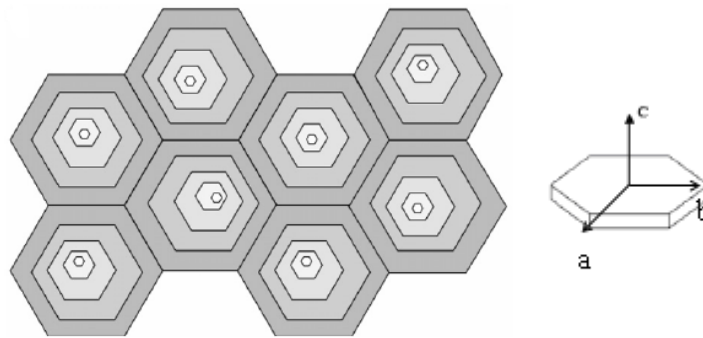
Figure 1.9 Schematic drawing of plan-view of column nacre of abalone

The adjacent column nacre of abalone showing the same c-axis crystallographic orientation, each tile is smaller than the one below it (from Meyers et al., 2008)

Addadi *et al*. (2006) proposed a growth model of nacre formation relying on the organic matrix structure (Figure 1.10). It has been recognized that the microenvironment in which mineralisation occurs is complete and there are still many gaps in our understanding of the steps involved to achieve nacre formation (Addadi *et al*., 2006).
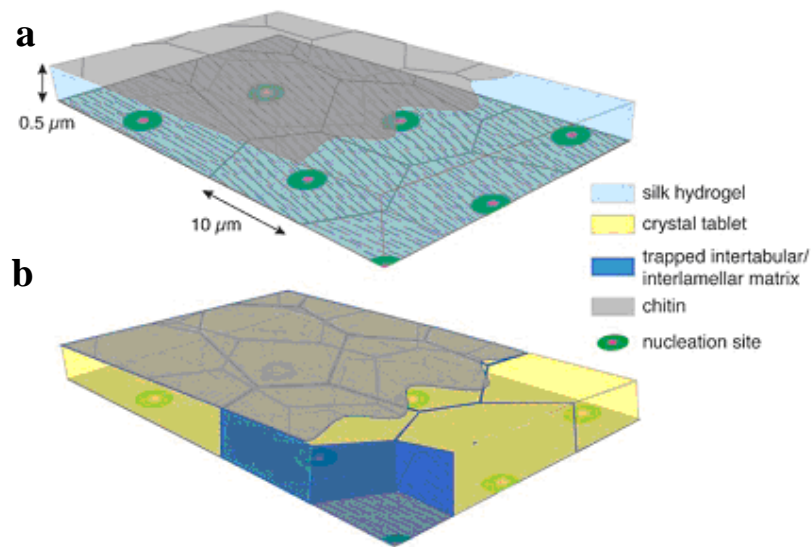
Figure 1.10 Schematic representations of the growth model for nacre formation

a. Before mineralisation. The assembled organic matrix is prior to mineral deposition. The microenvironment is formed by two layers of β-chitin, with a gel comprising silk-like protein filling the space in between. Part of the upper chitin layer (upper right) has been removed to show the silk-like protein gel filling. The gel phase may inhibit crystallization and act as a space filler. The silk gel may already be loaded with colloidal mineral particles. Nucleating proteins are adsorbed on the β-chitin sheet. b. After mineralisation. Nucleation of aragonite (from colloidal particles) is induced on and by the acidic proteins. As the mineral grows, water and silk are displaced. The latter is eventually trapped between adjacent tablets and between the tablet and the chitin layer. Part of the upper chitin layer has been removed together with the underlying interlamellar matrix layer (upper right), to show the mineral tablet surface. A tablet fragment was removed (front corner) to allow visualization of the intertabular and interlamellar matrix (from Addadi et al., 2006).

1.4   Abalone Shell

Abalone can be easily recognized by the flattened shell and the row of apertures along the spiral ridges and towards the shell longitudinal growth direction. Among the apertures there are closed ones, half-closed one and open ones (Fig 1.11). The number of apertures increases during the growth of the shell (Sinclair, 1963; Gerger, 1998a).

Figure 1.11 Abalone shell of *H. asinina* with row of apertures (closed, half-closed and open apertures) along the dorsal margin.

1.4.1 Shell morphology

Species identification is based on numerous characteristics and more than 100 species globally distributed. The terminology mostly used is discussed in the following section and illustrated in Figure 1.12.

The dorsal surface is described in terms of sculptural elements, ordered by their prominence. Ridges are broad and continuous undulations and are divided into spiral and radial ones (Geiger & Poppe, 2000). The shell colouration of most abalone species is extremely variable, which is given in terms of colours and patterns including large uniformly coloured specimens, blotches, patches, spiral bands, tenting and mottling (Geiger & Poppe, 2000). The ventral view shows the inner nacre layer, which has sheen in a similar colour to the pigment colour. The lightness or darkness of the nacre is somewhat species-specific. The muscle scar is found in only a few species (Geiger & Poppe, 2000).

a   b
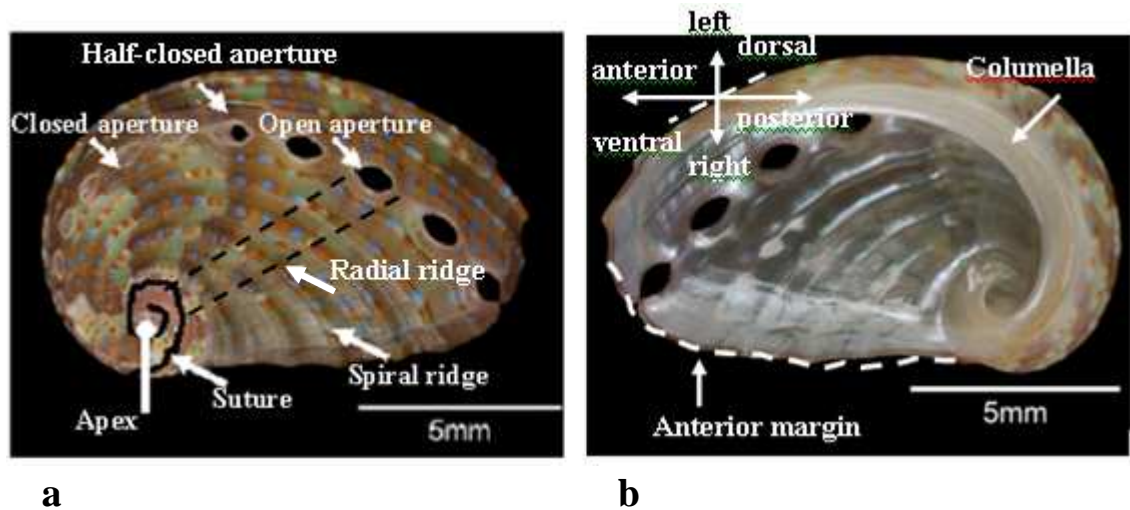
Figure 1.12 Characteristic features of abalone

a. Dorsal view. b. Ventral view with axes of orientation.

1.4.2 Previous work on abalone shells

The abalone shell consists of two main mineral layers underlying the periostracum. The internal layers comprise distinct microstructures (Nakahara *et al.*, 1982; Figure 1.13). There is an inner aragonite nacreous layer, and an outer prismatic layer made of calcite or aragonite or admixture of both (Mutvei *et al*., 1985; Dauphin *et al*., 1989; Dauphin & Denis, 1995). Periostracum refers to the outermost layer of shell and is always ignored in the research work of abalone shell structure.
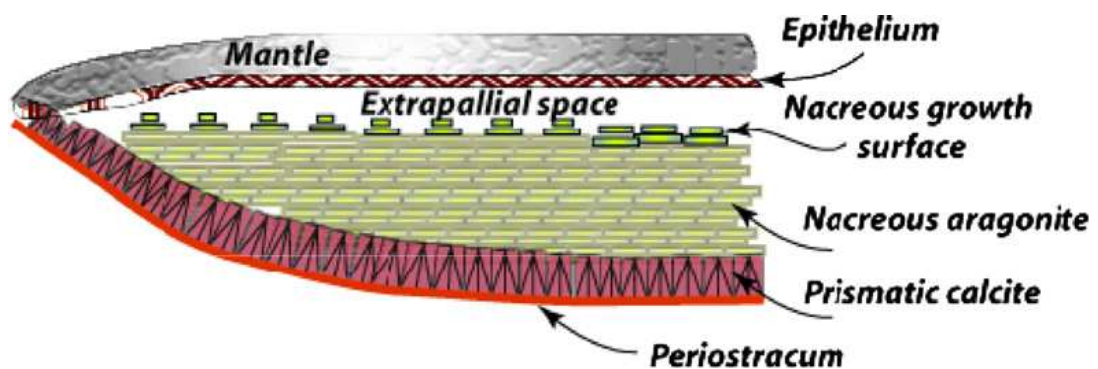
 Figure 1.13 Schematic structure of typical abalone shell

 (From Zaremba et al., 1996)

Abalone nacre is a layered composite biomineral that contains crystalline aragonite tablets confined by organic layers (Gilbert *et al.*, 2008). In red abalone (*H. rufescens*), the organic matrix layers are 30nm thick, and the aragonite tablets are 400-500nm thick and oriented with their [001] crystal axes normal to the layer plane (Metzler *et al.*, 2008; Chateigner *et al.*, 2000; Hedegaard & Wenk, 1998). X-ray diffraction measurements demonstrate that c-axes of different nacre tablets are not all parallel to each other but with misorientation varying ±11˚, and there is no long-range order in a-b orientation (Gilbert *et al.*, 2008; Metzler *et al.*, 2007; Mann, 2001; Levi-Kalisman *et al.*, 2001). Metzler *et al.* (2007) revealed that there are tablets of co-oriented columns varying between 2 and 40 and provided an organic-mediated growth model for abalone nacre formation. The model thought to best resemble bulk columnar nacre has randomly distributed nucleation sites, preformed on organic matrix layers before tablet nucleation and growth. Gilbert *et al.* (2008) identified and clarified another growth model of nacre formation based on oriented tablets growing faster than misoriented ones, that is, the fundamental role played by the mineral phase itself and its gradual ordering, which is not directly controlled biologically or organically. Based on the above work, Coppersmith *et al.* (2009) presents a more detailed dynamic growth model, focusing on how the dynamical development and eventual degree of order depending on model parameters. However, there are still open questions on the incompletely elucidated formation mechanisms.

As a result of the highly ordered hierarchical structure, abalone nacre has remarkable mechanical properties the same as that of other mollusc species (*e.g.* Jackson *et al.*, 1988). Researchers had performed various mechanical tests in abalone shells. *H. rufescens* nacre has an eightfold increase in toughness over wholly inorganic $CaCO_3$ (Sarikaya *et al.*, 1994). Mening *et al.* (2000) and Barthelat *et al.* (2006) found the remarkable strength of abalone nacre when loading is perpendicular rather than parallel to the tiles, which contributes to the high mechanical strength of the whole shell (Chateigner *et al*., 2000). It is also indicated that the organic layer plays a role in the mechanical strength. Meyers *et al* (2008) observed that mineral bridges would result in crack deflection to stop the crack propagating through the composite and therefore the composite is superior to the monolithic material which has no barriers to stop the propagating crack. The result is consistent with the analyses by Gao *et al.*(2003), Ji & Gao (2004), Ji *et al.*(2004). Due to

the unique material properties and hierarchical structure, the formation of abalone shell as a biomineralisation model does inspire materials scientists (Mann, 2001).

1.4.3 Aperture infill

From a biological point of view, the apertures are used for respiration, release gametes, and waste material (Ino, 1952; Tissot, 1992; Voltzow & Collin, 1995). The larval shell has no apertures and the new aperture forms in the anterior (Figure 1.12-b) of the shell as the abalone grows. With the abalone grows, the older apertures are sealed off one by one by aperture infill when they are no longer used (Gerger, 1998a). The growth direction of aperture infill is the same as the longitudinal shell growth direction, from posterior to anterior (Figure 1.12-b). The mechanism of aperture infill is unknown, as well as the ultrastructure, mineralogy and crystallography of the infill material.

1.5 Overall Aims and Objectives

Living systems exert exquisite control on biomineral formation producing functional structures that are light and strong. Much research has focussed on nacre because it has such attractive material properties. Comparison of the dynamic components involved in nacre formation in gastropod and bivalves suggests major differences in nacre formation in these two classes (Checa & Rodriguez-Navarro, 2005; Cartwright & Checa, 2006).

This study aims to characterise the structure and crystallography of gastropod nacre in abalone in order to contribute to this knowledge. Equivalent what could also be carried act on bivalve nacre to determine the extent to which the final product, nacre, is the same in these two molluscan classes despite marked differences in the protein involved in their formation.

The infill of abalone apertures is intriguing from a materials science perspective since the dynamism fills the apertures at a later time and, at the same time, focus new shell at the growth front. The infill is cohesive with the surrounding shell. In this study, the structure and crystallography of the aperture is investigated in order to shed light on this phenomenon.

Scanning electron microscopy (SEM) is used to detail structural information and electron backscatter diffraction (EBSD) used to extract crystallographic data. This thesis builds on previous work done on abalone shells. Here, electron backscatter diffraction (EBSD) is used for the first time to fully characterise the microstructure and crystallography of abalone prisms, nacre and aperture infill. The research focuses primarily on *Haliotis asinina* and also considers *Haliotis rufescens* and *Haliotis gigantea.*

2 Materials and Methods

2.1 Materials

2.1.1 Abalone specimens

In this study, shells of three species of abalone are examined (Figure 2.1). For *Haliotis asinina* (Linnaeus, 1758) shells, the mature and juvenile samples were from Australia (41°-10.5° S, 113°-153.5° E) and provided by Professor Jackson and Professor Degans (University of Queensland). For *Haliotis rufescens* (Swainson, 1822), the only one mature shell was from United States of America (25°-49° N, 125°-73° W) and donated by Professor Taylor and Professor Claverie (University of California). For *Haliotis gigantea* (Gmelin, 1791), the one mature shell was from Japan (31°-46° N, 130°-145.5° E) and kindly provided by Professor Endo (University of Tokyo). Examples of shells of each of these three species are depicted in Figure 2.1. Shells were cleaned using small brushes, transferred to an ultrasonic bath and cleaned using de-ionised water. Clean shells were then air dried and each shell labelled with unique a sample number.

H. asinina

H. rufescens

H. gigantea

Figure 2.1 Abalone shells of three species

Interior and exterior of shells of H. asinina, H. rufescens and H. gigantea. Scale bars= 10, 5 and 5 mm respectively.

Following figure 2.2 reveals the mainly distributions of the three abalone species collected separately, which are all living in the coast of continents.

H. asinina

H. rufescens
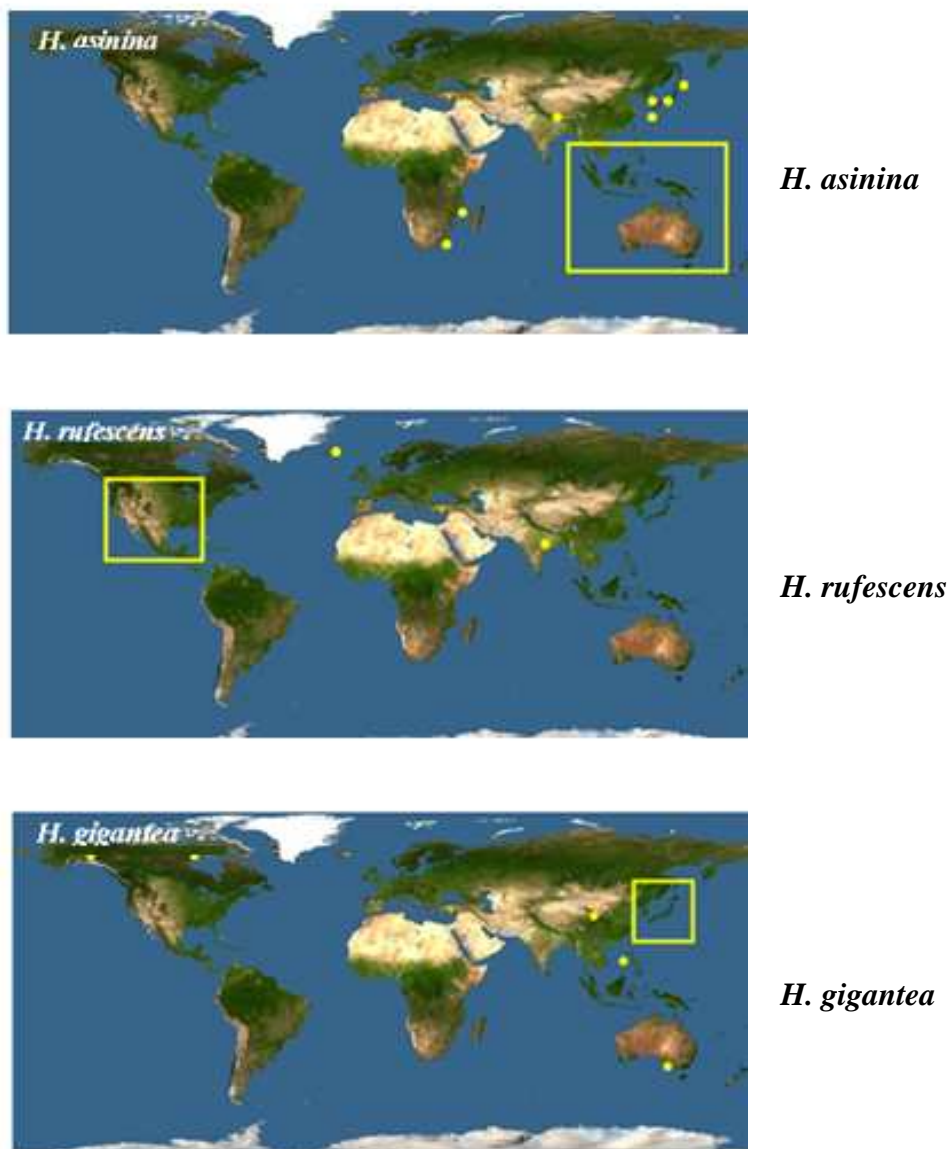
H. gigantea

Figure 2.2 The main distributions (the dots and square) of *H. asinina, H. rufescens* and *H. gigantea*

Data from: *http://www.discoverlife.org*

2.1.2 Chemical information of calcite and aragonite

Calcium carbonate is a chemical compound with the chemical formula $CaCO_3$, which contains mainly two polymorphs calcite and aragonite with different chemical structures. Calcite is the most stable polymorph of calcium carbonate. It is often the primary constituent of the shells of marine organisms, e.g. plankton, the hard parts of red algae, some sponges, branchiopods, most bryozoans, and parts of the shells of some bivalves such as oyster (Harper *et al*., 1997). Aragonite forms naturally in almost all mollusc shells, and as the calcareous endoskeleton of warm- and cold- water corals. In some molluscs, the entire shell is aragonite; in others, aragonite forms only discrete parts of a bimineralic shell (aragonite *plus* calcite) (Runnegar, 1985).

2.2 Methods

2.2.1 Scanning electron microscopy (SEM) imaging

2.2.1.1 Theory of scanning electron microscopy

Scanning electron microscopy (SEM) is one of the most versatile instruments for the examination and analysis of the microstructures of solid specimens. Its main advantages are high resolution and depth of focus, together with ease of instrument operation (Reimer, 1985). It is a type of electron microscope that images the sample surface by scanning it with a high-energy beam of electrons in a raster scan pattern. The electrons interact with the atoms that make up the sample producing signals that contain information about the sample's surface topography, composition and other properties such as electrical conductivity.

The signals result from interactions of the electron beam with atoms at or near the surface of the sample (Figure 2.3). The types of signals produced by an SEM include secondary electrons (SE), back scattered electrons (BSE), characteristic X-rays, and so on. Secondary electrons originate within a few nanometres from the sample surface and they are low energy. Backscattered electrons consist of high-energy electrons originating in the electron beam; that are reflected or back-scattered out of the specimen interaction volume by

interactions with specimen atoms. X-rays are also produced by the interaction of electrons with the sample (Reimer, 1985).
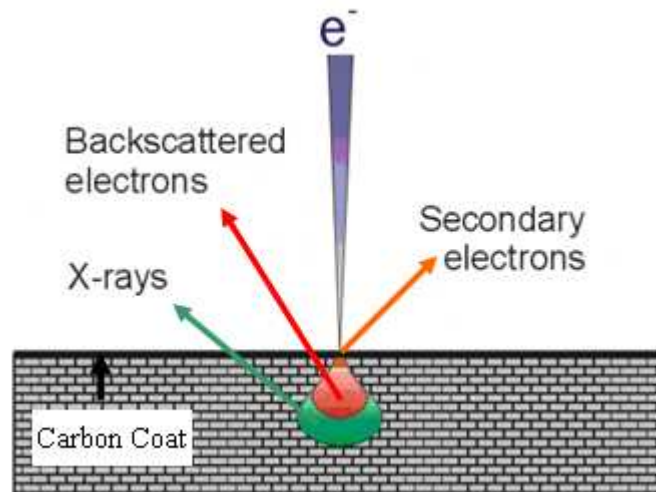
Figure 2.3 Schematic representation of the electron beam interaction with sample and the types of signal generated

(*Refer to Reimer, 1985*)

Secondary electron (SE) imaging. Secondary electrons (SE) are produced when electrons from the primary beam collide with electrons from the specimen and dislodge them. These electrons dislodged from the sample are known as 'secondary' electrons. Due to the low energy of secondary electrons, they originate within a few nanometres from the sample surface (Goldstein *et al*., 1981). Secondary electron imaging is most useful for examining surface structures and offers resolution down to 10nm.

Backscattered electron (BSE) imaging. Backscattered electrons (BSE) consist of high-energy electrons, originating when the electron beam hits the nucleus of the sample and are returned to the detector. Backscatter electrons usually retain about 80% of their original energy. The intensity of backscattered electrons increases with increasing atomic number of the specimen. Therefore, elements of a higher atomic number produce more backscattered electrons and will therefore appear brighter in image than the elements of a

lower atomic number. Thus BSE images can provide information about the distribution of different elements in the sample (Goldstein *et al*., 1981).

Characteristic X-rays are used to identify the composition and measure the abundance of elements in the sample (Goldstein *et al*., 1981).

2.2.1.2 Sample preparation for SEM imaging analysis

SEM samples must be of an appropriate size to fit in the specimen chamber and are generally mounted rigidly on a specimen holder. In order to obtain a good image of most non-conductive specimens in the SEM, the sample must first be covered with a thin coating (few nm) of an electrically-conducting material. The low atomic number coating, such as carbon, maximises signal and improves spatial resolution, especially for backscattered electron imaging (BSE). The high atomic number coating materials, commonly gold, maximises secondary electron yield from within a surface layer of a few nm thick, and suppresses secondary electrons generated at greater depths, producing high topographic contrast and resolution in high-vacuum SEM. Low-vacuum SEM with differential pumping apertures allow samples to be imaged without such coating, and without the loss of natural contrast caused by the coating, but are unable to achieve the resolution attainable by conventional SEM with coated specimens. Secondary electron images were generated from intact and fractured shells including the shell apertures and their infill.

As the backscatter electron (BSE) signal is strongly related to the atomic number, the imaging can provide information on element distribution in samples. BSE imaging also has a high resolution with polished samples and so samples are polished as for electron backscatter diffraction (EBSD) (Section 2.2.2.2).

2.2.1.3 Scanning electron microscopy-conditions for imaging

In a typical SEM, an electron beam, which typically has an energy ranging from a few hundred eV to 40 keV, is focused by one or two condenser lenses to a spot about 0.4 to 5 nm of diameter (Figure 2.4). The beam passed through pairs of scanning coils or pairs of

deflector plates in the electron column, typically in the final lens, which deflect the beam in the x and y axes so that it scan in a raster fashion over a rectangular area of the sample surface.
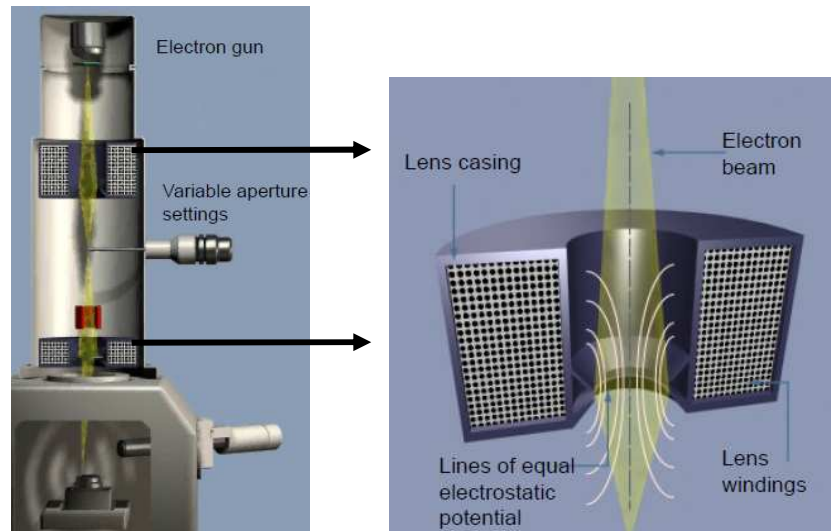
Figure 2.4 Schematic representation of basic probe-forming electron-beam used in the Scanning Electron Microscopy (SEM)

(*From Level 4 class of Focused Beam Techniques, School of Geographical and Earth Sciences, University of Glasgow*)

2.2.2 Crystallographic analyses by Electron Backscatter Diffraction

2.2.2.1 Theory of Electron Backscatter Diffraction

Electron Backscatter Diffraction (EBSD) is a significant tool in the field of materials science (Wright & Adams, 1991, 1992; Adams *et al*., 1993; Wright *et al*., 1994; Schwartz *et al*., 2000). EBSD analysis is conducted in a scanning electron microscope (SEM) under vacuum with a specialized camera integrated with a phosphor screen detector (Figure 2.5a). When an electron beam interacts with a crystalline material under low angle incidence, the electrons are diffracted by the material before backscattering. These diffracted electrons interact with the phosphor screen to produce distinct bands, termed 'Kikuchi bands'

(Figure 2.5b) that form a pattern unique to that crystal lattice in a particular orientation. When the electron beam is scanned across the surface to produce point-to-point data, the patterns of each point are collected to construct maps of orientation (Figure 2.5c), and phase for a selected surface area (Schwarzer, 1997a, 1997b).
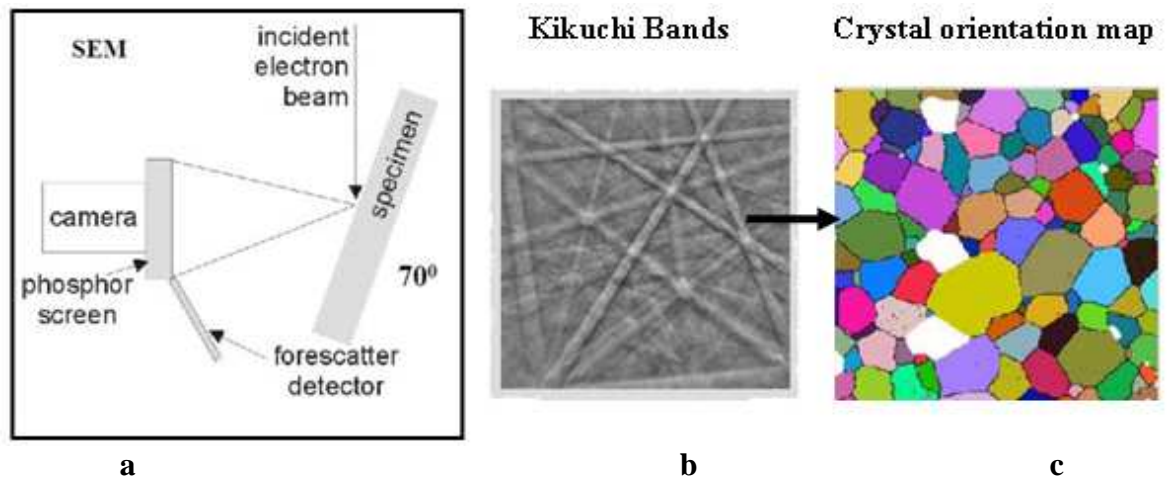
Figure 2.5 Main features of Electron Backscatter Diffraction (EBSD) analysis

a. A polished and coated sample is tilted to 70°toward the phosphor screen and a focused electron is directed at the sample surface. b. The backscatter electrons diffracted by the material interact with the phosphor screen to produce 'Kikuchi bands'. c. These Kikuchi bands are used to determine crystallographic phase and produce crystal orientation map. (From Orientation Imaging Microscopy User's Manual (Mahway, 2005))

2.2.2.2 Electron Backscatter Diffraction sample preparation

Sample preparation is crucial for electron backscatter diffraction (EBSD) analysis, especially for biogenic carbonates. Before grinding and polishing procedures, the influence of the choice of resin and the thickness of the carbon coating is also very important (Pérez-Huerta & Cusack, 2009).

Samples were cut and embedded in resin (EpoxiCure epoxy resin/hardener with a mix weight ratio of 5:1). Because diffracted electrons escape from within only a few tens of nanometres of the specimen surface, specimen preparation for EBSD is critical to achieve good results. If material near the surface is deformed, or has any surface contaminant,

oxide or reaction product layers present, then EBSD pattern formation may be suppressed. Epoxy resin types generally have the best characteristics with respect to hardness and shrinkage (*Oxford Instruments, http://www.oxford-instruments.com/Pages /home.aspx*).

After 20hs, the resin blocks are polished through a series of grinding and polishing steps prior to analysis (Cusack *et al*., 2008b). Initially, samples are ground using frit papers: P180/220 (82/68µm; 3 min), P320 (46µm; 3 min), P800/1000 (21/18µm; 3 min), P1200 (15µm; 3 min), P2500 (8µm; 3 min), and P4000 (<5 µm; 5 min). The polishing stages are performed with alpha aluminium oxide at 1µm and 0.3µm with final 5 min treatment of 0.06µm colloidal silica on a short nap disc. The colloidal silica stage is essential for EBSD analysis to remove any residual damage surface layers with local stress and deformity produced by the harder compound grinding and polishing (Prior *et al*., 1999; Nowell *et al*., 2005). Finally, samples are cleaned in an ultrasonic bath and dried at room temperature.

Carbon coating is applied to reduce the sample surface charging during EBSD analysis. The coating thickness is critical with the requirements, for sufficiently thin to enable the diffracted beam to be backscattered while must be sufficiently thick to dissipate charge (Prior *et al*., 1999). The thickness of carbon coating was controlled using a Precision Etching-Coating System (Model 682) by Gatan Inc. Two ion guns sputter an ultrathin layer of amorphous carbon on the sample, and an electronic monitor measures the precise thickness of the even carbon layer. Carbon coating provided further reduction of excess surface charging. A sufficiently thin coat is required to enable the diffracted beam to be backscattered while the carbon coat must be sufficiently thick to dissipate charge (Prior *et al*., 1999). Pérez-Huerta & Cusack (2009) have demonstrated that a uniform layer of 2.5nm thickness of carbon gives optimal results and that the intensity of diffraction begins to decrease with more than 5nm in carbon thickness.

Carbonate materials are insulators and surface charging of specimens during EBSD analysis can result in weaker Kikuchi pattern quality. Silver paint is applied to the edges of the sample and used as a strong adhesive between the sample block and the aluminium stub providing a conduit for charge dissipation during EBSD analysis (*Oxford Instruments, http://www.oxford-instruments.com/Pages /home.aspx*).

2.2.2.3 Electron Backscatter Diffraction analysis conditions

EBSD analyses were carried out in the School of Geographical & Earth Sciences at Glasgow University. Using a FEI Quanta 200F field-emission scanning electron microscope (SEM) in high (5.5×10^{-6} Torr) and low (5.2×10^{-1} Torr) chamber pressure vacuum modes with an aperture and spot size of 4. Finally data were analyzed using Orientation Imaging Microscopy (OIM) 5.2 software from EDAX-TSL Company.

The angle of tilt is important for EBSD analysis. Nowell & Wright (2005) demonstrated the variation on Kikuchi pattern intensity at varying angles of tilt with a 70° angle producing optimal pattern intensity. The distance of the sample to the electron gun, the working distance (WD), is another important factor in EBSD analysis. The optimum range is for pattern collection being established between 6-12mm. The beam aperture is set with spot size 4 and an accelerating voltage of 20kV. This yields a sufficiently strong beam but with surface charge effects minimized resulting in optimal Kikuchi patterns. The Kikuchi patterns are indexed using the OIM Data Collection database, which contains structure files of calcite and aragonite.

The phosphor screen camera control settings are set to collect the clearest Kikuchi patterns that could be quickly indexed, therefore producing a sufficient frame rate for quicker scans to be performed within reasonable time frames to generate sufficient detail, avoiding beam damage to sample and excessive SEM time. Scan rates are dependent on frame rate and step size, both of which are dependent on magnification of the scanning area. At lower magnifications, larger step sizes are employed to cover the areas. Smaller step sizes are used to produce high resolution maps at higher magnifications. This underlines the importance of choosing appropriate step sizes during EBSD mapping, which depend on the materials investigated (Wu & Jensen, 2008).

2.2.2.4 Electron Backscatter Diffraction data processing

EBSD data and maps are interpreted and presented by way of diffraction intensity, pole figures (PF) and crystallographic orientation maps.

Crystal orientation of the crystal lattice is displayed with respect to the sample reference frame. Crystallographic orientation map and pole figure plots (Figure 2.6) are all presented with reference to three orthogonal reference directions: normal direction (ND, normal to the sample surface), reference direction (RD, parallel to the direction of sample tilt) and transverse direction (TD, running horizontally across the sample surface) (Figure 2.7). All the pole figures in this thesis are relative to the reference direction (RD).
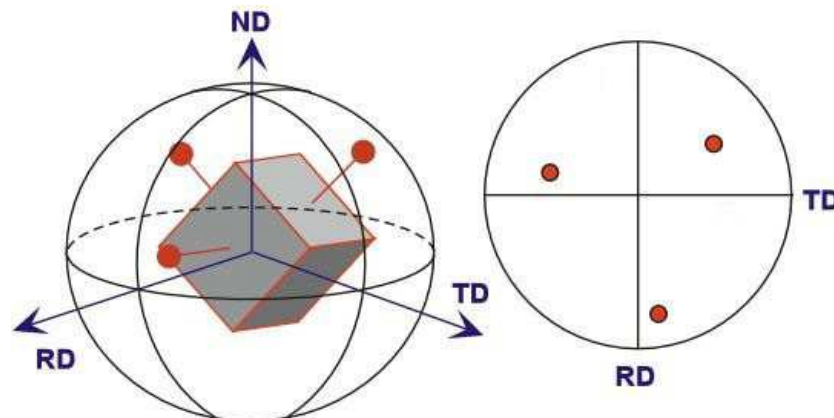
Figure 2.6 Principle of pole figures in crystallography

The three symmetrically equivalent planes of a cubic crystal in 3D space each produces a perpendicular pole to the crystallographic plane which plot as a single point on a hemispheric projection (left). These are viewed as a 2-D stereographic projection (right). (From Orientation Imaging Microscopy User's Manual (Mahway, 2005))
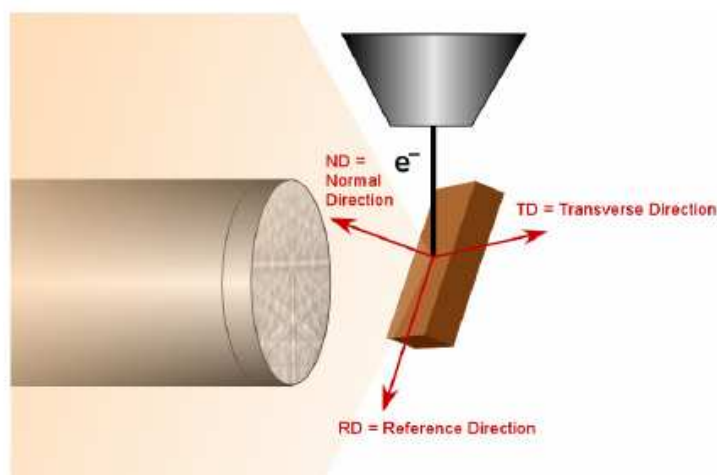
Figure 2.7 Schematic representations of three orthogonal reference directions, normal direction (ND), reference direction (RD) and transverse direction (TD)

(From Schwartz et al., 2000)

Crystal orientation map is produced using the same reference frame with the crystallographic orientation reported here. Using this frame of reference, crystal faces parallel to the field of view (poles normal to field of view) will be coloured according to the crystal colour key (Figure 2.8).
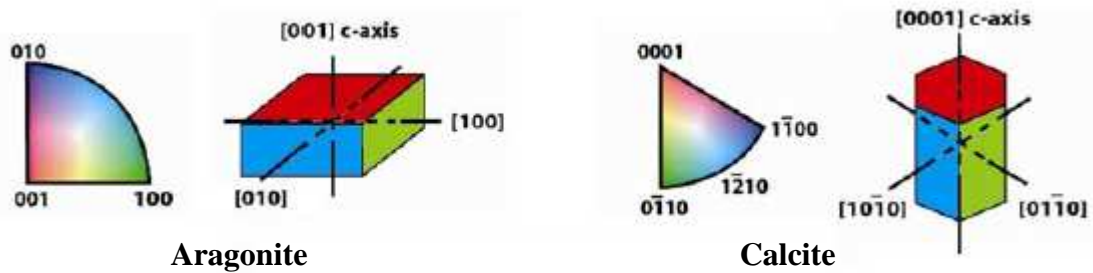
Aragonite   **Calcite**

Figure 2.8 Colour keys of aragonite and calcite with reference to the normal direction (c-axis)

The respective wire frames show a simplified view of the individual crystal faces of the unit cells and how they are coloured in a crystal orientation map. ND[001], RD[100] and TD[010] for aragonite; ND [0001] for calcite. (From Schwartz et al., 2000)

2.2.3 EBSD data analysis

EBSD data were interpreted and maps produced through Orientation Imaging Microscopy (OIM) Analysis 5.2 software. OIM maps were subject to two clean-up algorithm procedures to ensure reliable data was displayed (Mathway, 2005). EBSD data processing includes screening of the confidence index (CI) of each. By imposing a CI value (*e.g.* CI>0.1), the user can efficiently filter points with bad quality patterns or uncertain indexing. The intensity of the diffraction pattern indicates the quality of diffraction such that bright areas indicate good diffractions. Factors affecting the quality of an EBSD pattern in localized areas can be crystal inhomogeneity, presence of organic material, and crystal edges (Dalbeck, 2008).

For the cleanup, Grain Dilation was applied with a Grain Tolerance Angle of 5˚ (the default), minimum grain size of 5 and making sure the Single Iteration box is checked on. The Grain Dilation cleanup method essentially grows grains one point at a time around the

perimeter. The dilation process can continue to iterate until each point in the scan is associated with an OIM grain. One different cleanup method of Grain Certification Identity (CI) Standardization was applied with a Grain Tolerance Angle of 5°and minimum grain size of 2, with grains of CI≥0.1 displayed in the result OIM map. This removed unreliable data from the final data set and points with unreliable confidence index were also removed (*OIM Analysis Tutorial*, *http://www.edax.com*).

2.2.4 Sample preparation

The shells' microstructure and crystallographic orientation of three species are investigated in Chapter 3 and 5, as well as the aperture infill of *H. asinina* shell in Chapter 4. Microstructure is determined using scanning electron microscopy (SEM) and polymorph distribution and crystallographic orientation are identified using electron backscatter diffraction (EBSD) analysis. For SEM imaging, fractured samples are gold coated with 7.5nm thickness. For EBSD analysis, samples are polished firstly and carbon coated with 2.5 nm thickness.

3 Structure and Crystallography of *Haliotis asinina*

3.1 Introduction

3.1.1 Specific research questions

This chapter uses scanning electron microscopy (SEM) and electron backscatter diffraction （EBSD）to address the following questions.

- What are the characteristic morphological features of the external and interior surface of the shell?

- Are the nacreous tablets of uniform thickness throughout the shell?

- What is the mineralogy and crystallographic orientation of the prismatic and nacreous layer?

3.1.2 Biological information

Haliotis asinina (Linnaeus, 1758) is common in the Pacific islands, southern Japan and northern Australia (Poutiers, 1998; Figure 2.2). They live from the lowest intertidal to 8 m depth, on the edge of reefs, in reef flats and in the vicinity of living corals (*Acropora spp.*) and algae (Geiger, 2000). *H. asinina* species are most active at night, but activity is also linked to low tide and they prefer peaceful environment (Geiger & Poppe, 2000; McNamara & Johnson, 1995). Species mature at 30-35 mm shell length (Capinpin *et al.*, 1998) and grow to marketable size of 55-60 mm within one year, surpassing the growth rates of other tropical and sub-tropical abalones (McNamara & Johnson, 1995).

H. asinina has a pelagobenthic life cycle that includes a minimal period of three to four days in the plankton (Jackson *et al.*, 2002; 2005). The first biomineralisation events occur shortly after hatching, with the fabrication of the larval shell (protoconch) over about a 10h

period (Figure 1.5b). These structures allow the veliger larva to completely retract into a protective environment and rapidly fall out of the water column. The next phase of biomineralisation does not commence until the competent veliger larva contacts an environmental cue that induces metamorphosis (Jackson *et al*., 2002). Postlarval shell (teleoconch) is laid down rapidly following metamorphosis with marked variation between individuals in the rate of its production. While the initial teleoconch is not pigmented (Figure 1.5d), it is textured and opaque such that post larval shell is easily discerned from the larval shell (Figure 1.5d *inset*). Subsequently, the teleoconch rapidly develops a uniform maroon colouration similar to the crustose coralline algae that the larva settled upon (Figure 1.5e).

H. asinina is medium to large, growing up to 117mm (Hutsell *et al*., 1997). The shell is lightweight, elongated along the axis of growth, arched and convex, in clear resemblance to the ear of a donkey (Geiger & Poppe, 2000). Apertures are medium size, somewhat oblong, hardly elevated and usually 4-7 open (Geiger & Poppe, 2000). As the abalone grows, a new aperture forms in the dorsal margin of the shell, while the older open aperture will be filled in gradually when no longer used. Juvenile (<35mm) shells always show the spiral cords with rows of dots in combination of white, red and blue (Geiger & Poppe, 2000; arrows in Figure 3.1a). With further growth, the ridge-valley structures fade and give rise to a smooth adult shell structure, with irregular brown-green triangles on a light brown background (Geiger & Poppe, 2000; Figure 3.1b). Ontogenetic changes of pigmentation and structure in *H. asinina* shell match changes in the habitats occupied during development (Jackson *et al,* 2007). The interior surface of the shell is strongly iridescent, with shades of pink and green (Geiger & Poppe, 2000; Figure 3.1).
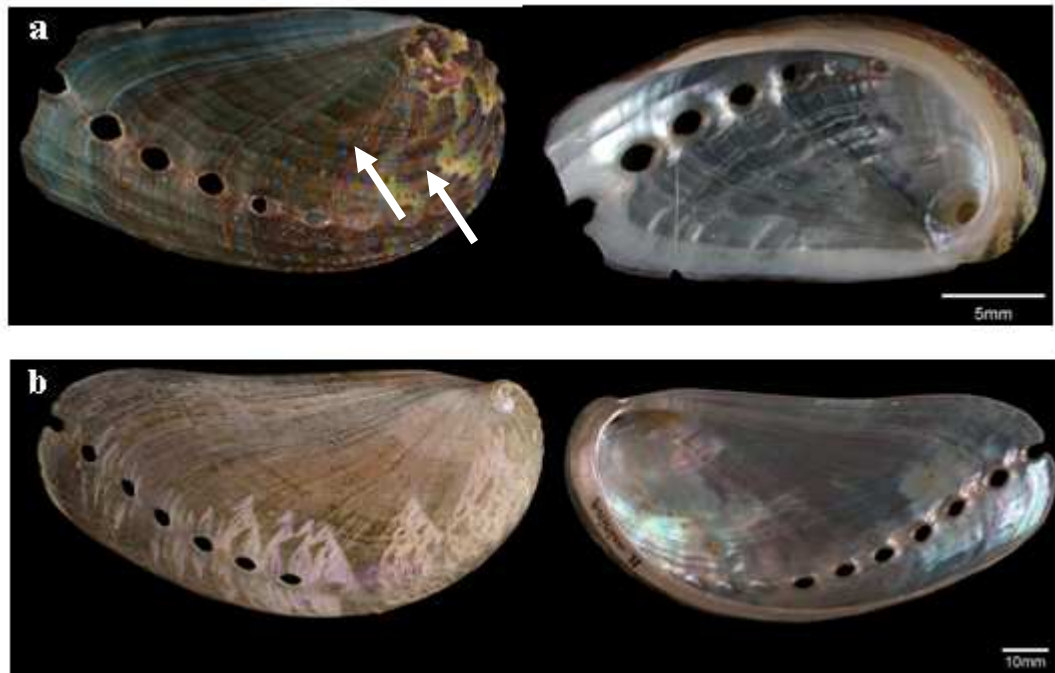
Figure 3.1 Exterior and interior of *H. asinina* shells

a. Juvenile shell (arrows show the spiral cords). b. Mature shell. Scale bars are 5mm and 10mm respectively

3.2 Results

3.2.1 Microstructure of juvenile shell

3.2.1.1 External shell

Using scanning electron microscopy (SEM) to observe the exterior surface of the juvenile shell, it reveals pronounced series of spiral ridges and a row of apertures (Figure 3.2a). The radial lines are smooth and thin, perpendicular the spiral ridges (Figure 3.2b). The most elevated region of the shell (umbo) shows characteristic morphology of zig-zag spiral lines with not uniform distances between them (Figure 3.2c); and the lines gradually grow flat (Figure 3.2d). But have not being able to look at external surface of other species, such as *H. rufescens* and *H. gigantea*.
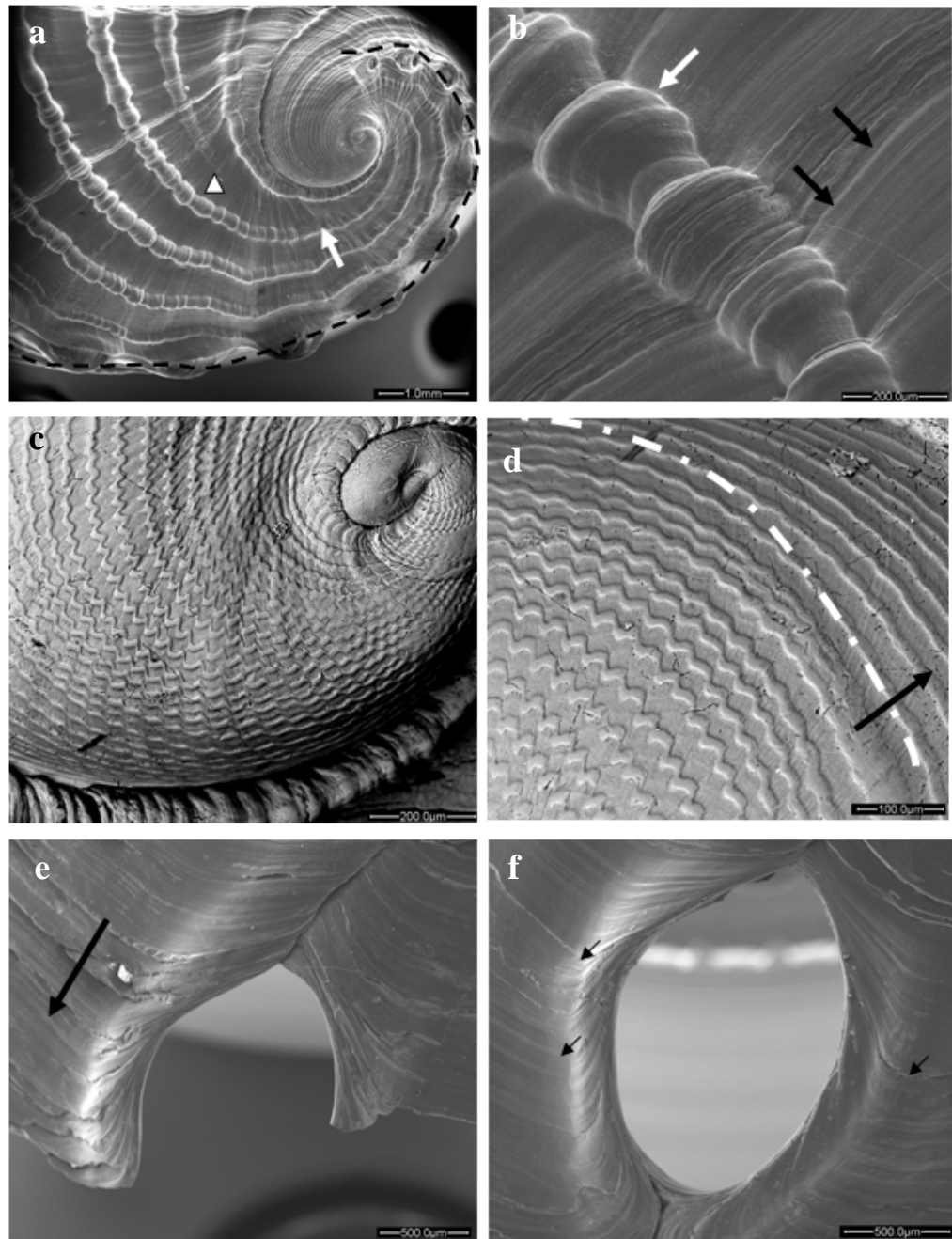
Figure 3.2   Secondary electron images of external juvenile *H. asinina* shell

a. Plan-view of shell surface showing pronounced series of spiral ridges (arrow) and a row of apertures (dashed line). Some new spiral ridges present with the shell growth (arrowhead). b. Radial lines (black arrows) are crossed with the spiral ridge (white arrow). c. The ornament at the umbo comprising zig-zag spiral lines with not uniform distance between them. d. Interface (dashed line) between zig-zag spiral lines and flatter spiral lines in umbo area of shell (arrow shows the growth direction). e. New aperture forming at growing edge. Arrow indicates growth direction. f. Open aperture with the radial lines (arrows) of shell on either side of aperture. Scale bars for a-f=1mm, 200, 200, 100, 500, 500 μm respectively.

New aperture is formed along the longitudinal shell growth direction (Figure 3.2e). The formed aperture is like a gap with the radial lines of shell on either side of it (Figure 3.2f). The open apertures are gradually filled in one by one along the longitudinal shell growth direction from the posterior to the anterior of the shell (Figure 1.12b).

The infill has the same growth direction as the shell (Figure 3.3a). The aperture infill grows, showing the morphology of circular growth lines, from start (Figure 3.3b, c) to the end (Figure 3.3d). The growth lines of the aperture infill are not contiguous with the shell radial lines (Figure 3.3c). Figure 3.3e shows the detailed crystal morphology of aperture infill and Figure 3.3f shows the final of infill being composed of small granular crystals.
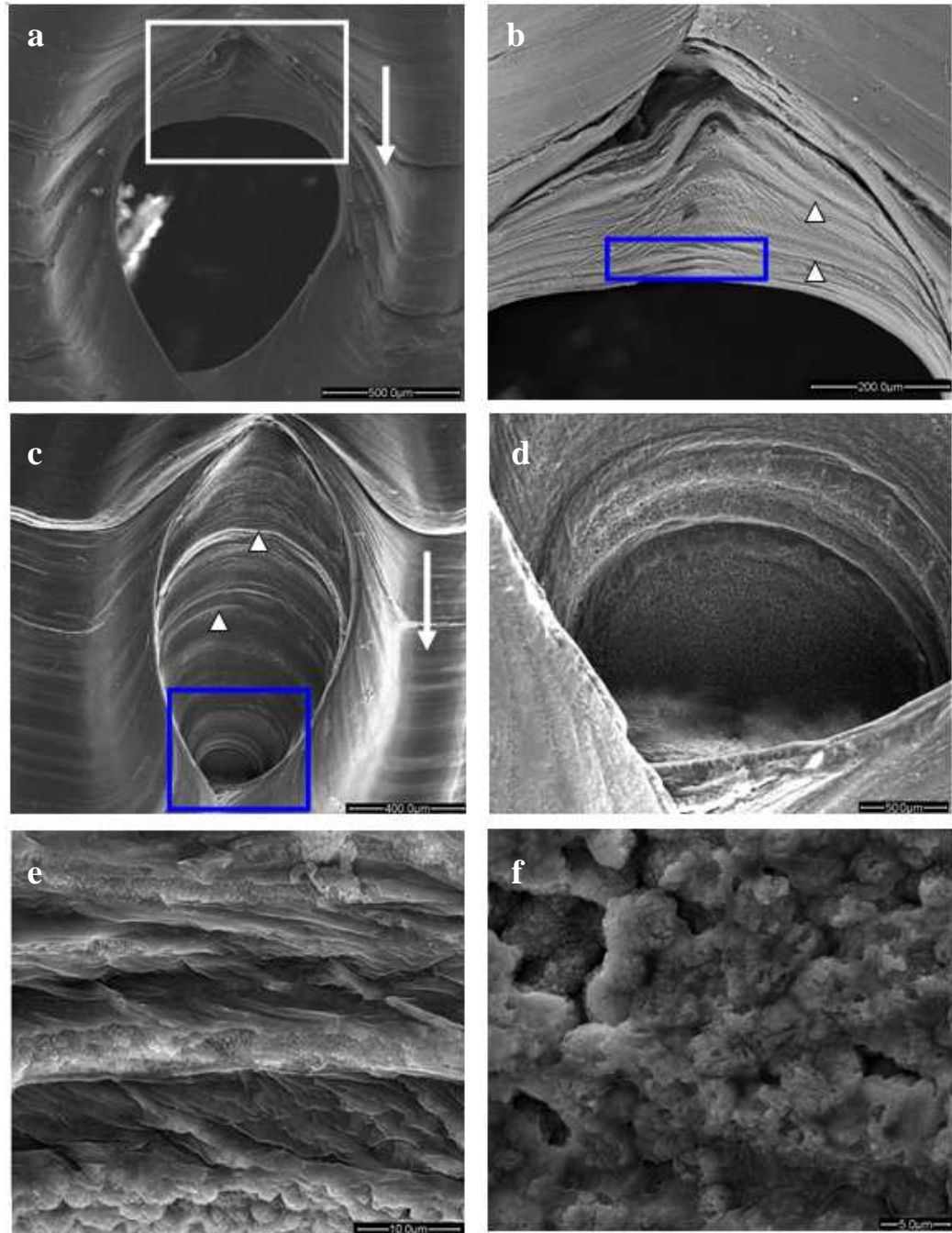
Figure 3.3 Secondary electron images of aperture infill of juvenile *H. asinina* shell

a. Half-closed aperture (arrow shows the growth direction of infill and shell). b. Higher magnification image of boxed area in (a) showing growth lines in circular arc form (arrowheads). c. One closed aperture showing growth lines (arrow heads). d. Higher magnification image of boxed area in (c) showing the end part of aperture infill. e. Higher magnification image of boxed area in (b) showing the crystal morphology of growth lines. f. Higher magnification image of final part of aperture infill (d) showing the crystal morphology. Scale bars for a-f=500, 200, 400, 50, 10, 5 μm respectively.

Details of aperture infill will dealt with in Chapter 4.

3.2.1.2 Nacre surface of the shell

Scanning electron microscopy was used to observe the anterior area of interior surface (Figure 3.4).
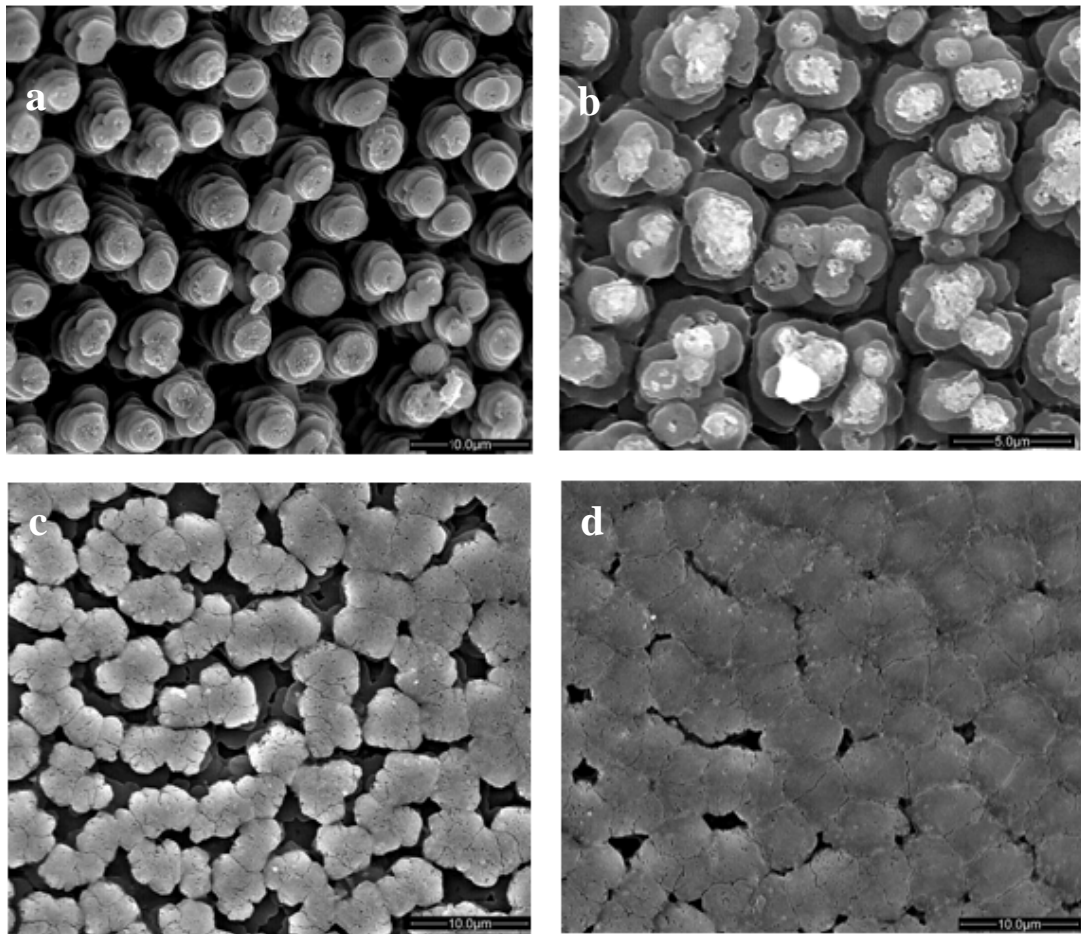
Figure 3.4 Secondary electron images show the major transitions of nacre growth of *H. asinina*

a. The aragonite tablets in a "stack of coins" arrangement perpendicular to the shell surface. b. Tablets start to grow laterally and because coherent with neighbours while new crystals nucleate on top of the tablets. c. Organic material grows to cover the top tablets' surface. d. Mature nacre with polygonal tablets in contact with neighbours. Scale bars for a-d=10, 5, 10, 10 μm respectively.

Nucleation sites have been described in nacre (Nakahara *et al*, 1982; 1991). Nucleation sites in *H. asinina* are indicated by black arrows in Figure 3.5a. The interface surrounding each tablet is indicated by white arrows in Figure 3.5a. There are nanoscale asperities found on the surface of stacked nacre tablets (Figure 3.5b). Asperities were first found on aragonite platelet surface by Wang *et al*. (2001). Lin *et al*. (2008) used transmission electron microscopy (TEM) to demonstrate that the asperities are remnants of mineral bridges. Between the tablet there is organic 'glue' (Lin & Meyers, 2009), which is evident in Figure 3.5b.
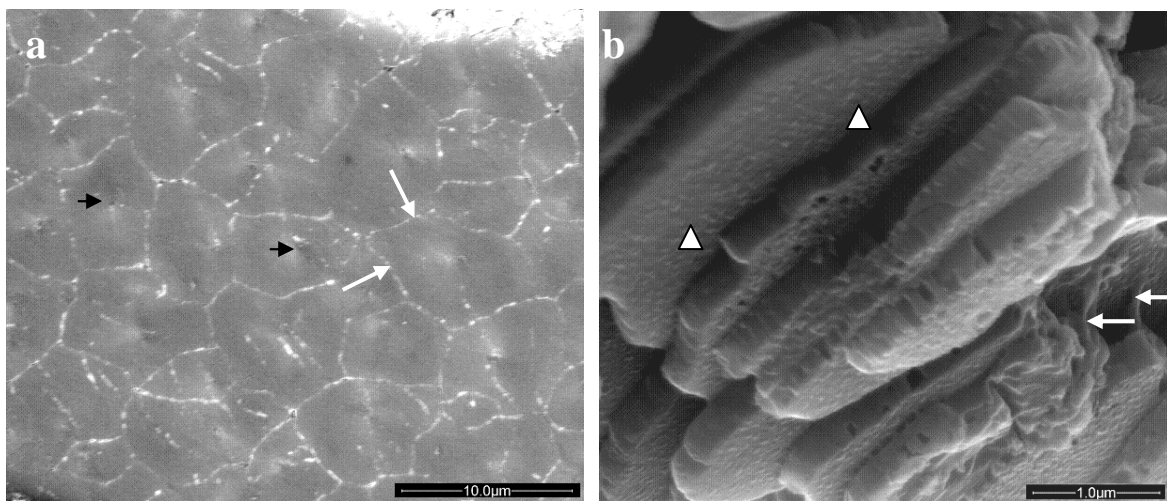
Figure 3.5 Secondary electron images of nacre layer of *H. asinina* shell

a. Plan-view of nacreous layer with nucleation sites (black arrows) on each tablet which is surrounded by intra-crystalline matrix (light white lines indicated by white arrows). b. Cross-section view of stacked tablets with nanoscale asperities (arrowheads) on the surfaces and tablets are adhesive by 'glue' organic (arrows). Scale bars for a-b=10, 1 µm respectively.

From cross-section view of the shell anterior edge, the different crystal morphology of the aragonite of the prismatic layer (Figure 3.6a) and nacreous layer (Figure 3.6b) is evident.
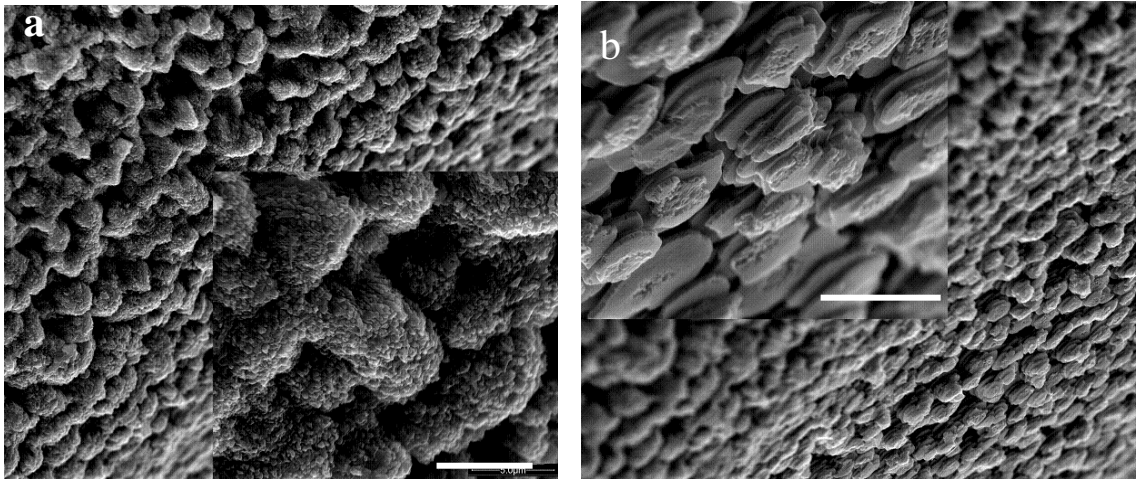
Figure 3.6 Secondary electron images of crystal morphology in prismatic layer and nacreous layers of *H. asinina* shell

a. Prismatic layer image with an inset of magnified crystal morphology. b. Nacreous layer image with an inset of magnified crystal morphology. (5 µm scale bar in insets)

3.2.2 Microstructure of mature shell

3.2.2.1 Morphology of prismatic layer and nacreous layers

SEM imaging of the fractured sample from the mature *H. asinina* shell clearly reveals the different morphology of the prismatic and nacreous layers (Figure 3.7). In the prismatic layer, prisms are smaller torwards the shell exterior (Figure 3.7b). In the nacreous layer, tablets are stacked in columns (Figure 3.7a). The surfaces of tablets are not smooth presenting nanoscale asperities (Figure 3.7c)
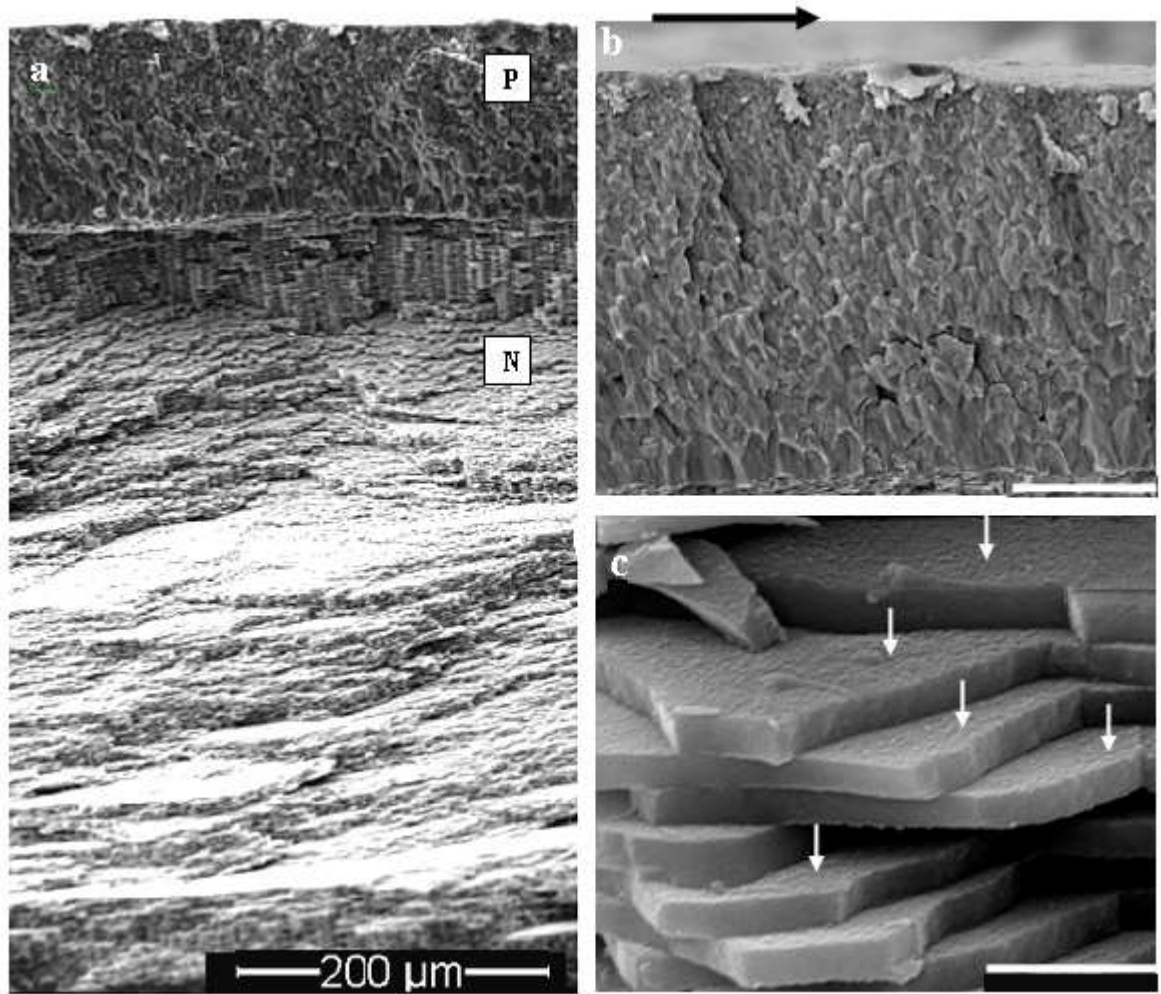
Figure 3.7 Secondary electron images of fractured *H. asinina* shell

a. Different crystal morphology of prismatic and nacreous layers. b. Prismatic layer with arrow indicating the longitudinal shell growth direction. c. Nacreous layer of stacked tablets being not smooth surfaces with nanoscale asperities (arrows). Scale bars for a-c= 200, 50, 2 µm respectively.

3.2.2.2 Thickness of nacre tablets

Nacreous tablet of abalone are described of about 0.5 µm thick (Nakahara *et al*., 1982, *H. rufescens*). The uniformity of nacreous tablet thickness was investigated in three polished samples from mature *H. asinina* shell from posterior to anterior (Figure 3.8a). Each sample is chosen from three areas in nacreous layer: outer (near the prismatic layer), mid and inner

(near the interior surface of shell) (Figure 3.8b). The thickness of 30~40 continuous tablets was measured in each area.
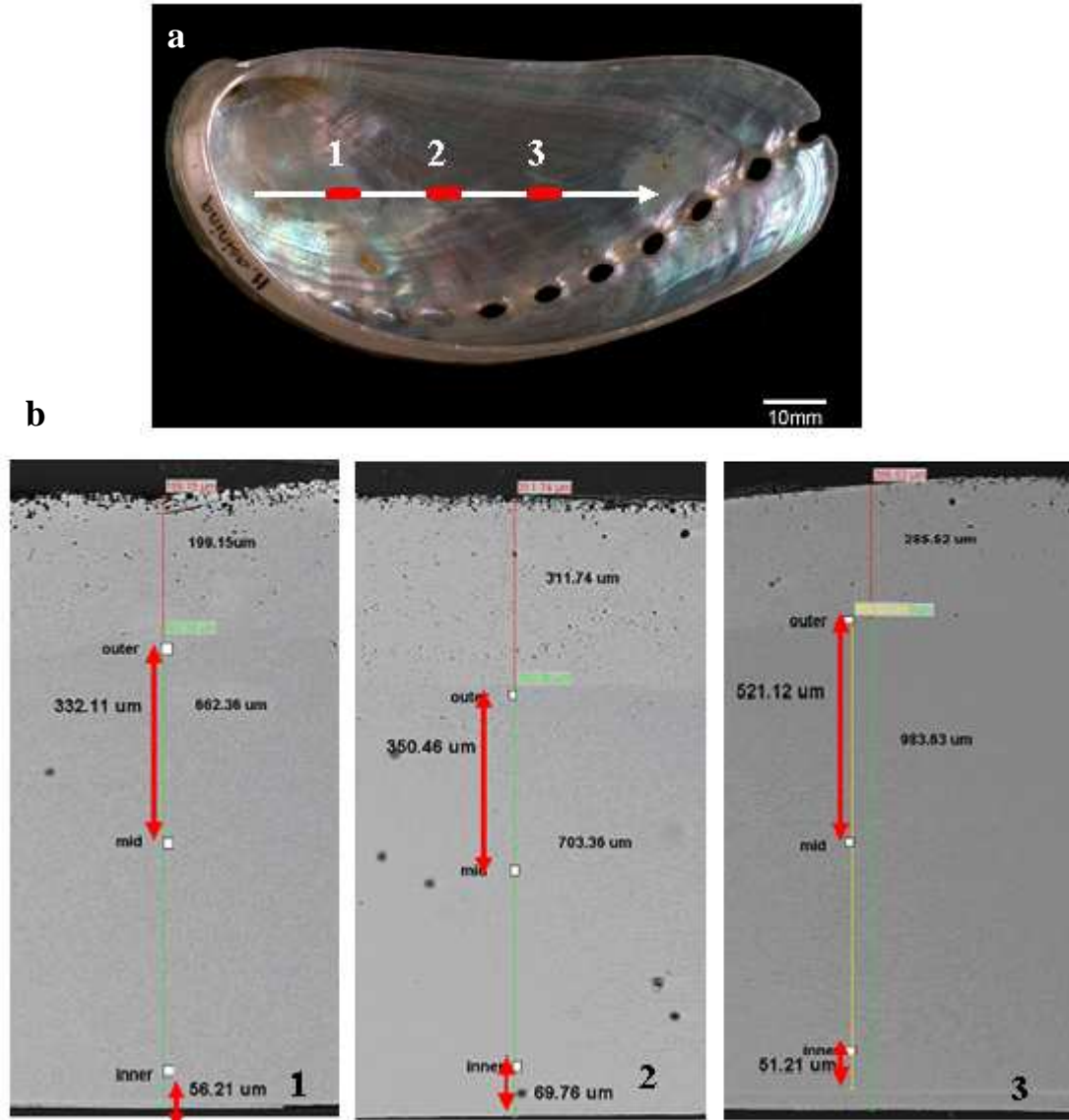
Figure 3.8 Three polished samples of *H. asinina* shell for measuring tablets thickness

a. Three samples were obtained from the longitudinal shell growth direction (from posterior to anterior, arrow). b. Detailed information of chosen areas from three polished samples separately, white squares showing the chosen areas at outer, mid and inner regions.

The tablets in the outer part (near the prismatic layer) are thinner than mid and inner regions (Figure 3.9).
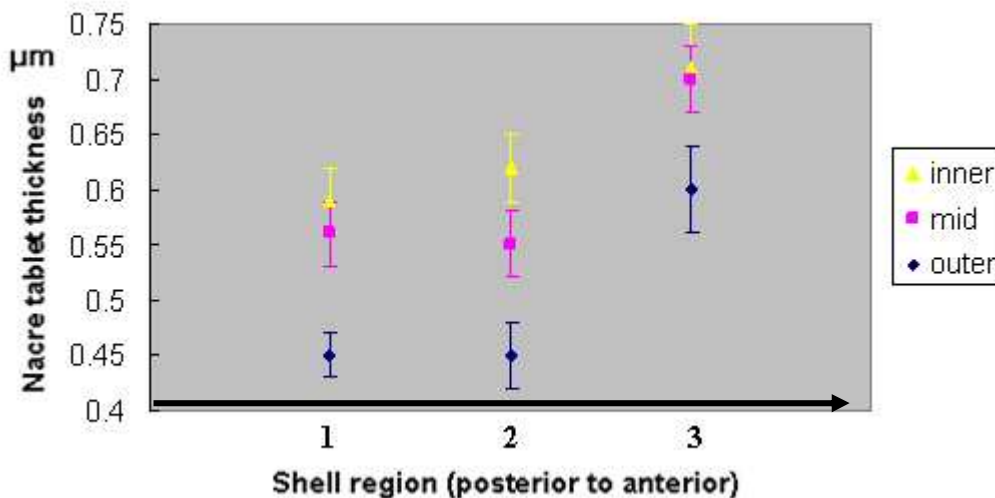
Figure 3.9 Average thickness of nacre tablets throughout *H. asinina* shell

Mean (and standard deviation) of tablet thickness in region 1, 2 and 3 of the outer, mid and inner regions. For each mean value, 30-40 tablets were measured. Along the longitudinal shell growth direction (from posterior part to anterior), there is the same trend of gradually thickening tablets forwards the shell interior. In addition to this trend from exterior to interior, the tablets formed the anterior are thicker than those formed earlier at the posterior (Figure 3.9). Thinnest tablets (450nm) occur at the anterior posterior while thickness tablets (700 nm) occur at the innermost anterior.

3.2.3 Crystallographic of mature shell

3.2.3.1 Shell phase

Electron backscatter diffraction (EBSD) indicates that both prismatic and nacreous layers of *H. asinina* shell are composed of the same polymorph of calcium carbonate, aragonite (Figure 3.10).
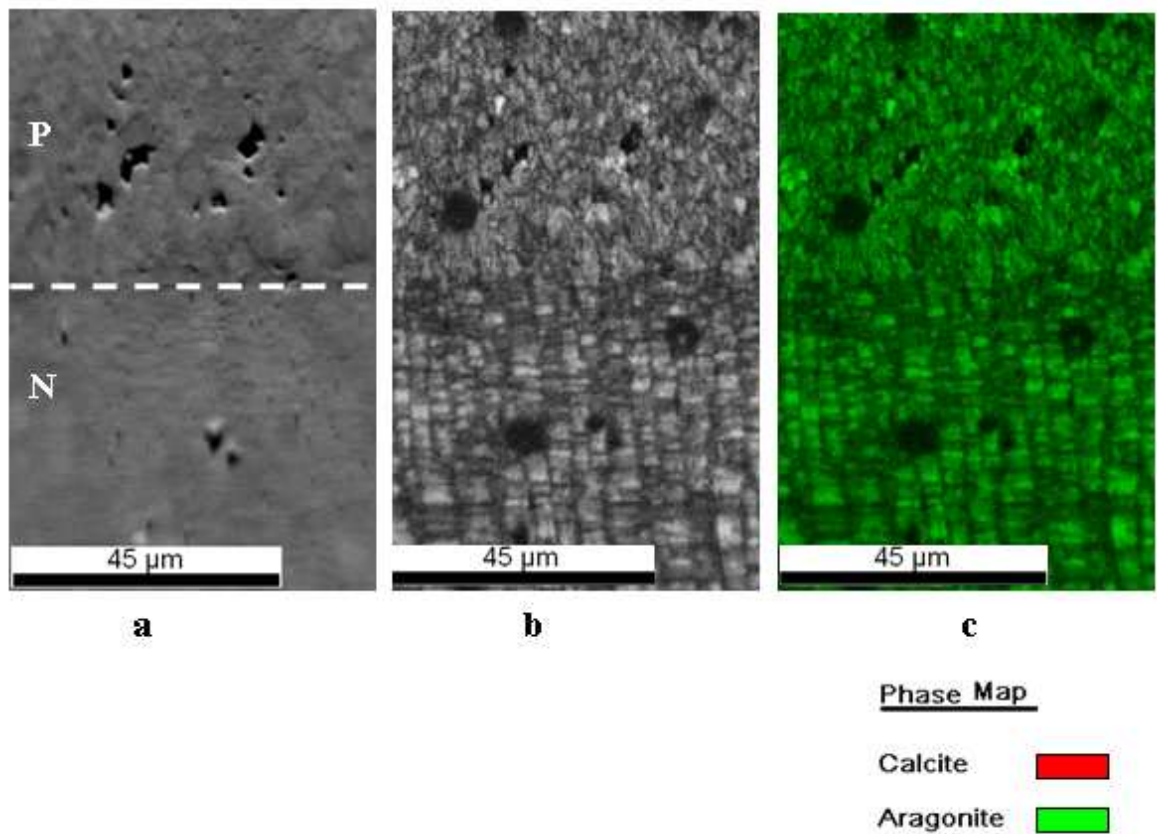
Figure 3.10 Interface between prismatic and nacreous layers in *H. asinina* shell.

a. Secondary electron image of polished interface between prismatic (P) and nacreous (N) layers. b. EBSD diffraction map of (a). c. EBSD phase map with calcite in red (none seen) and aragonite in green.

3.2.3.2 Shell crystal orientation

EBSD was used to investigate the crystallography of *H. asinina* shell. Data are presented in the form of pole figures (Figure 3.11c). Throughout the shell, c-axis tends to be perpendicular to the shell exterior. In the initial part of the prismatic layer, the crystallographic orientation is more poorly concentrated by the loose cluster in the pole figure (Figure 3.11c). Towards the prismatic-nacreous interface, crystallographic alignment becomes much more tightly constrained. The c-axis is well constrained throughout the nacreous layer (Figure 3.11c). In the crystal orientation maps, the nacre layer is composed of columns which show crystallographic continuity across laminae and the number of

tablets with the same crystallographic orientation in co-oriented columns varies between 2 and up to 50 (Figure 3.11c).

a

b

c

Aragonite
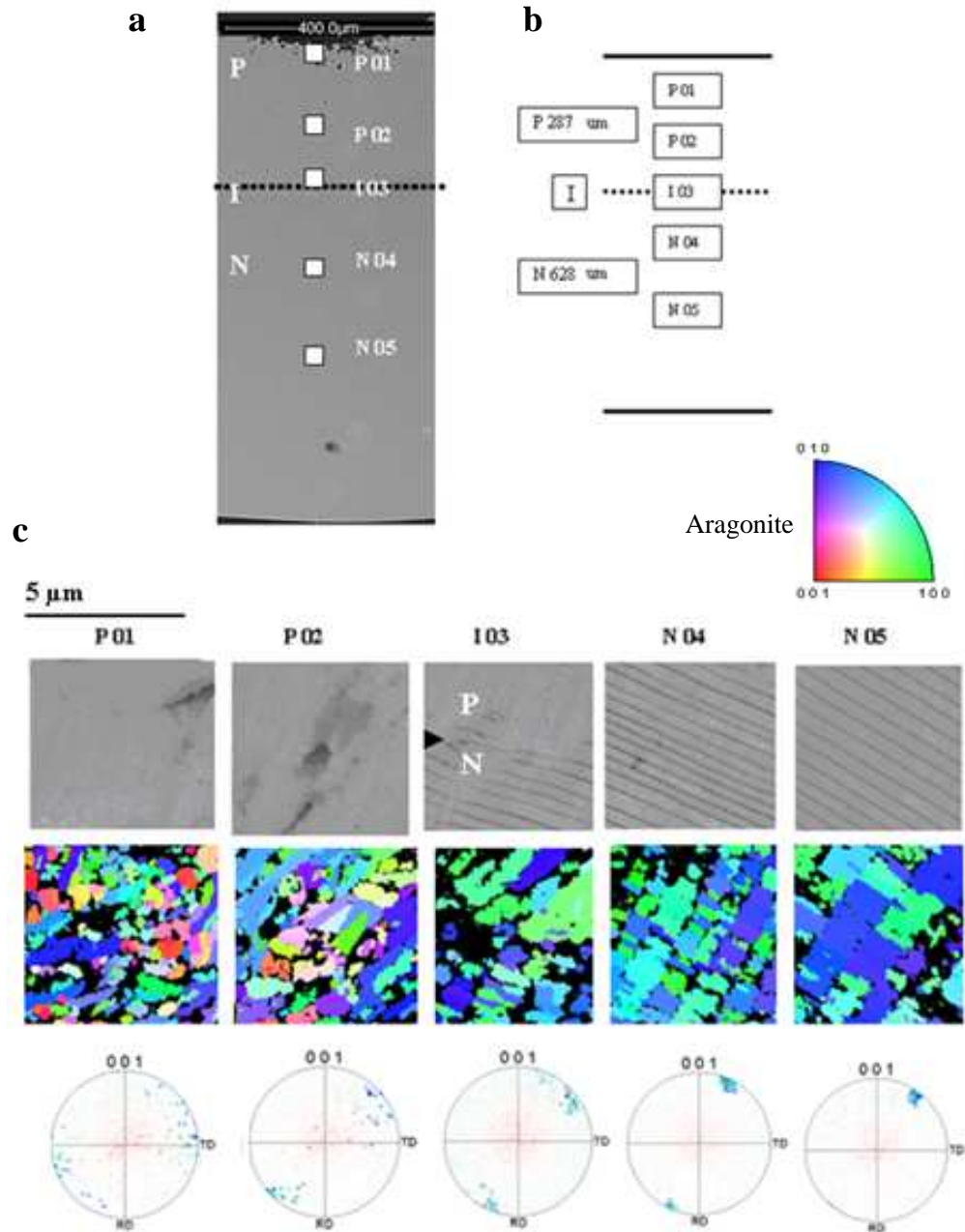
Figure 3.11 Crystallographic orientation of cross-section sample of *H. asinina* shell

a. Secondary electron image of polished section of prismatic (P) and nacreous (N) layers with P=prism, N=nacre and I=interface. b. Schematic illustration of (a) with five areas analysed. c. Secondary electron images of the five areas according to (b), and including corresponding crystal orientation map and pole figures according to aragonite crystal colour key.

3.3 Discussion

Scanning electron microscopy inquiring of the exterior of the shell of *H. asinina* reveals characteristic features (Figure 3.2). In *H. asinina* shell, the spiral and radial lines are clear (Figure 3.2b). The spiral lines are more raised and thicker compared to the radial ones. The radial pattern at the umbo area shows two different morphologies of zig-zig spiral lines and flatter spiral lines (Figure 3.2d), which are not reported before and may be unique to *H. asinina* shell. However, to know more on abalone protoconch, investigations including other abalone species are required.

The interior of growth nacre exhibits the "Christmas-tree-like" like growth fields of each tile being smaller than the one below it (Figure 3.4b; Simkiss & Wilbur, 1989; Fritz *et al*., 1994; Belcher, 1996), which is associated with tiled aragonite growth (Shen *et al*., 1997; Zaremba *et al*., 1996; Fritz *et al*., 1994; Fritz & Morse, 1998).

One theory of heteroepitaxial nucleation, termination of crystal growth by heteroepitaxial capping followed by heteroepitaxial nucleation of the next crystal layer (Schaffer *et al*., 1997), suggests that the organic layers covering each tile layer and each tablet nucleates at a specific location on the matrix surface (Checa & Rodriguez-Navarro, 2005; Crenshaw & Ristedt, 1976; Rousseau *et al*, 2005). Specifically, the ring shaped nucleation sites observed by Nudelman *et al*. (2006) would simply have pores at their centre through which the underlying crystal grows (Addadi & Weiner, 1997). The nucleation sites on each aragonite tablet are observed here in nacre in *H. asinina* (Figure 3.5a). The deposition of organic matrix does not seem to interrupt the epitaxial growth of crystals from one layer to the next, indicating continuity in the preferential orientation of crystals (Figure 3.11c; Checa & Rodriguez-Navarro, 2001). It is suggested that aragonite growth continues through pores in the organic membrane, which support the theory of "mineral bridges" (Nakahara *et al*., 1982; Schaffer *et al*., 1997). Atomic force microscopy (Schaffer *et al*, 1997), transmission electron microscopy (Schaffer *et al*, 1997; Song & Bai, 2003), and scanning electron microscopy (Lin *et al*., 2007) have also been used to observe the existence of mineral bridges in abalone nacre. In the microstructure of *H. asinina* nacre, the nanoscale asperities are easily observed on the aragonite platelet surface (Figure 3.5b, 3.7c); which are remnants of mineral bridges (Lin *et al*., 2008) and may explain how

crystal orientation of the aragonite tablets is maintained between layers. On the other hand, it was suggested by Evans *et al.* (2001) and Wang *et al.* (2001) that the rough nature of tile surface's asperities leads to inter-tile friction. They hypothesize that friction is the principal source of shear resistance between tiles.

Recently, the possibility of calcium carbonate precursors has been intensively discussed, with the suggestion that amorphous calcium carbonate (ACC) may be formed and transported to the sites of tile growth where the crystal orientation is determined by a separate templating mechanism (Nassif *et al.*, 2005, Addadi *et al.*, 2006; Cartwright & Checa, 2006; Bezares *et a*l, 2008). There is no direct evidence of the presence of ACC in the nacreous or prismatic layers (Archan *et al.*, 2009). However larval mollusc shells were shown to from an ACC precursor (Weiss *et al.*, 2002).

Nacre tablets are described as 0.4~1.2μm thickness by Nakahara *et al.* (1991). While nacre tablets of abalone are usually described as 0.4~ 0.5 µm thickness, such as *H. rufescens* (Nakahara, 1982; Mayer, 2005; Lin & Meyers, 2005; Gilbert *et al.*, 2008) and *H. laevigata* (Chateigner *et al.*, 2009). These studies do not provide any information on the spatial distribution of tablets of different thickness. Here, in *H. asinina*, there is a pattern of more recently formed tablets being thicker and the tablet thickness increasing gradually between 0.45~0.70 µm from exterior to shell interior (Figure 3.9). It is proposed that the growth rate of nacre approximately 0.5μm per day (Lin *et al.*, 2008). Whether the different thicknesses of nacre tablets in *H. asinina* reflect environmental factors or the ageing of the organism affecting shell growth needs more investigation.

In *H. asinina*, the prismatic layer comprises about one third of the shell thickness (Figure 3.8c) with abrupt transition to the nacreous layer (Figure 3.7a). The prismatic layer in *H. asinina* is composed of aragonite as described by EBSD analysis (Figure 3.10c), conforming the reports by Mutvei *et al.* (1985) and Dauphin *et al.* (1989) using EDS analysis. In Chapter 5, more detailed information of the prismatic layer of *H. asinina*, *H. rufescens* and *H. gigantea* as described by EBSD analysis are presented.

The c-axis of crystal orientation is perpendicular to the shell exterior in both prismatic and nacreous layers (Metzler *et al.*, 2008; Chateignera *et al.*, 2000; Hedegaard & Wenk, 1998).

Crystallographic orientation is more highly ordered in the nacreous layer than in the prismatic layer (Figure 3.11c). It is also revealed that the number of co-oriented columnar tablets varies between 2 and 50 (Figure 3.11c), comparing with *H. rufescens* of 2 and 40 varying co-oriented tablets (Metzler *et al*., 2007). Unfortunately, these data have no spatial context and whether this represents for the whole shell requires further investigation.

4 Aperture Infill of *Haliotis asinina*

4.1 Introduction

4.1.1 Specific research questions

In this chapter, following questions on aperture infill are addressed.

- What is the growth rate of aperture infill, changeable or stable with the shell growth?

- What is the crystallographic orientation and mineralogy of aperture infill?

- How is the aperture infill cohesive with the shell and what is the relationship of shell and infill in terms of crystallographic orientation?

4.1.2 Biology information of abalone

Abalone can be easily recognized by one row of apertures along the spiral ridge of the shell. Some apertures are closed, those at the anterior are open and sometimes one is half-closed between them. The open apertures are used for respiration, release of gametes and waste (Ino, 1952; Tissot, 1992; Voltzow & Collin, 1995). As the abalone grows, new apertures form at the anterior margin of the shell and the older apertures at the posterior are filled in (Figure 4.1).
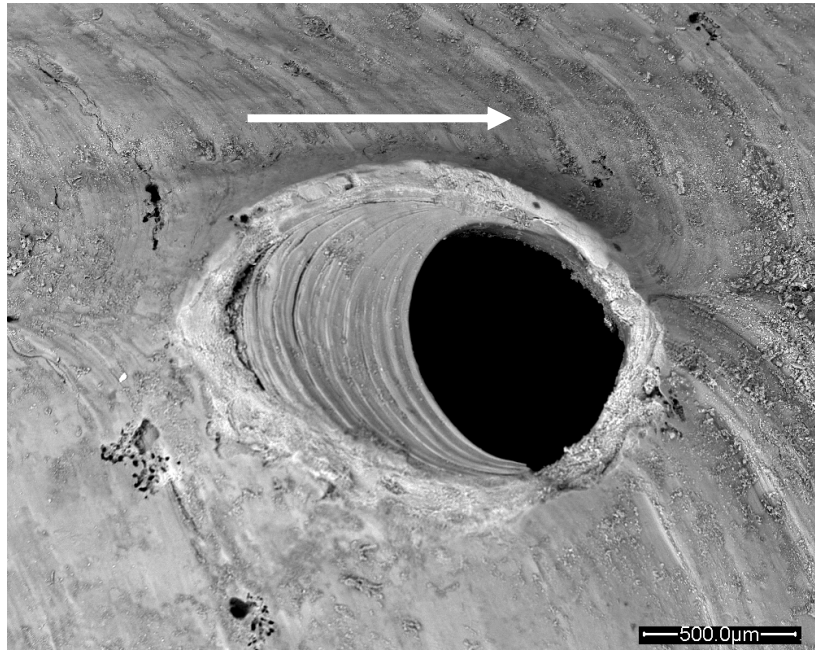
Figure 4.1 Half-filled aperture of *H. asinina*

Secondary electron image of one half closed aperture showing the elevated encircle and aperture infill with shell growth direction (arrow)

From the secondary electron image of Figure 4.1, the growth direction of aperture infill coincides with the longitudinal shell growth direction.

4.2 Results

4.2.1 Growth rate of aperture infill

McNamara & Johnson (1995) did researches on 451 mature shells and 68 juvenile shells (2-36mm) to estimate that *H. asinina* grows to 35 mm shell length in 6 months, to 55-60 mm in one year, and to approximately 70-75mm in three years. By measuring the shell length of an ontogenetic series of *H. asinina* shells, according to the *H. asinina* shell growth rate equation (McNamara & Johnson, 1995), the age of each one can be calculated. The equation is as follows,

$$y =4.27*L \wedge (2.03)*e \wedge (-u)$$

y is the shell growth rate (mm/year), L is the shell length (mm), u= 0.27* L^ (0.88) (2.5mm <L< 98.5mm)

Subsequently, by comparing with the number of apertures (closed, half-closed and open) in nearby shells of known age, the time period required to fill in one aperture can be estimated (Figure 4.2).
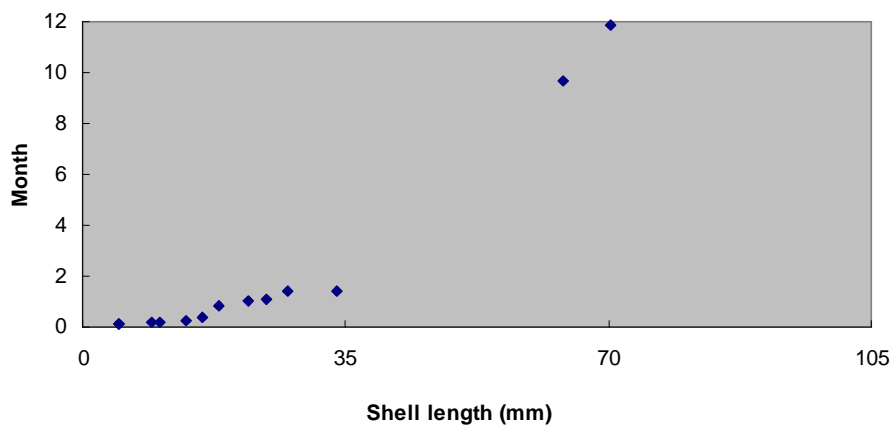
Figure 4.2 Time period of completely filling in one aperture of *H. asinina*

The length of most recently formed aperture infill was compared with that of the nearby ontogenetic shell and then divides the age gap of the two comparing shells; in order to determine the growth rate of aperture infill based on the shell length (Figure 4.3). In young *H. asinina* (<6 month) the shell growth is about 60% faster than that of the aperture infill; while in individuals older than 6 months, shell growth and aperture infill occur at nearly the same speed (Figure 4.3).
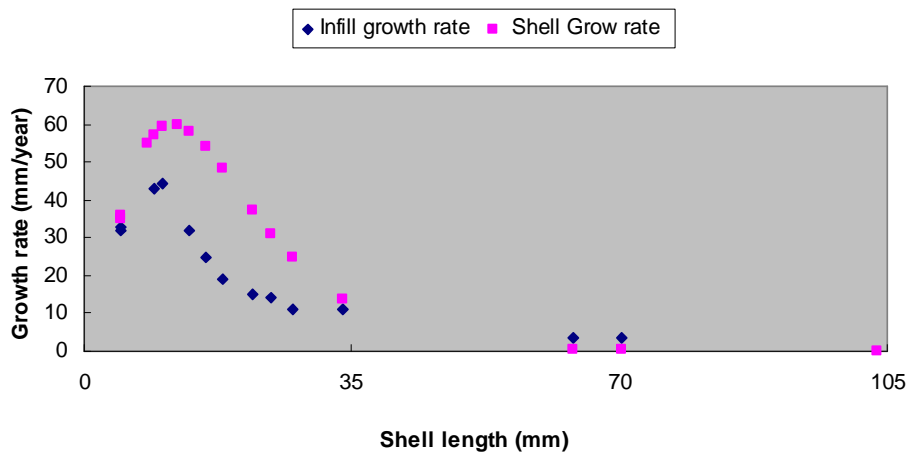
Figure 4.3 Growth rates of aperture infill and shell of *H. asinina*

4.2.2 *Composition and ultrastructure*

The aperture infill, like the shell, consists of outer prismatic and inner nacreous layers (Figure 4.4).
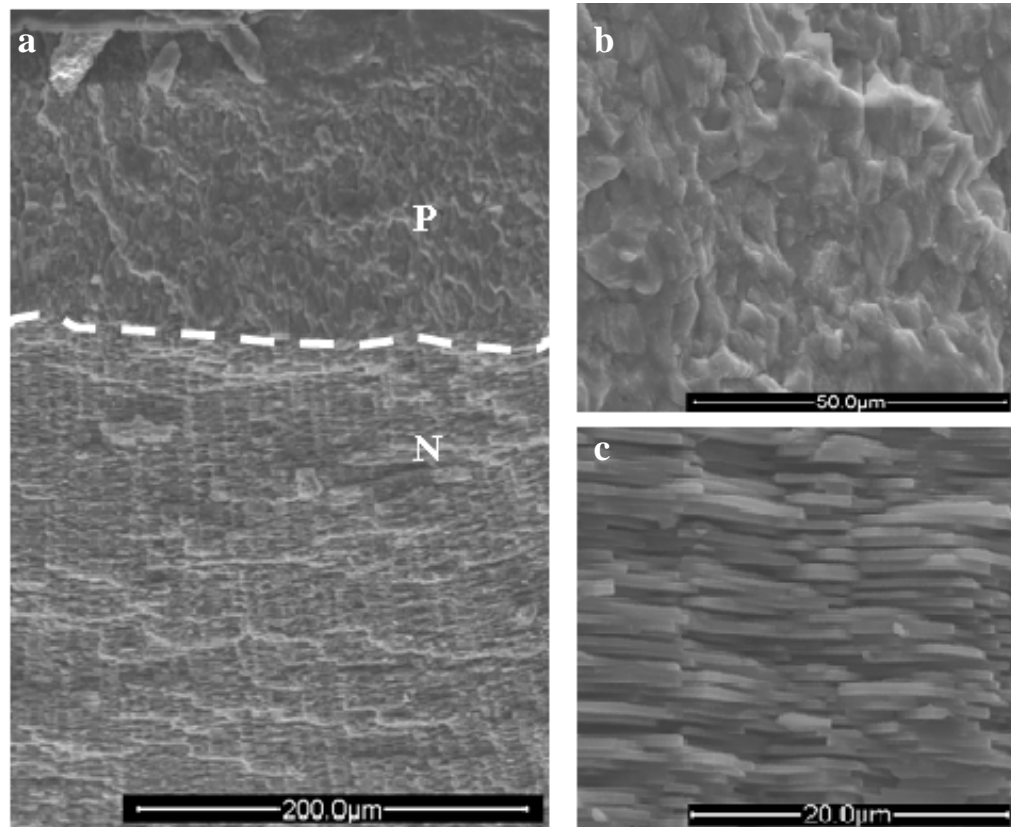
Figure 4.4 Secondary electron images of fractured aperture infill of *H. asinina* shell

a. Different crystal morphology of prismatic (P) and nacreous (N) layers (dash line shows the interface). b. Magnified image of prismatic layer. c. Magnified image of nacreous layer.

Scanning electron microscopy has been used to provide detailed microstructure information of aperture infill of *H. asinina* from transverse sections (Figure 4.5a) and longitudinal sections (Figure 4.5b) separately.
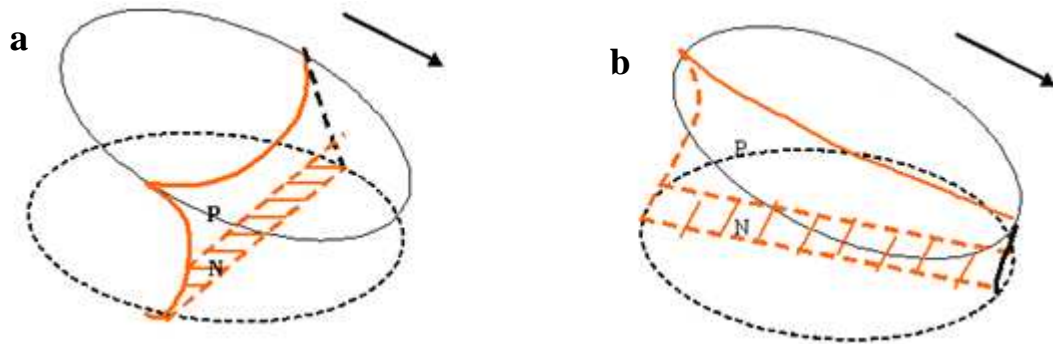
Figure 4.5   Graphical representations of aperture infill sample of plane section of aperture infill in *H. asinina*

a. Transverse section with prismatic (P) and nacreous (N) layers. b. Longitudinal section sample with prismatic layer (P) and nacreous layer (N). (Arrow shows the growth direction of infill and the shell).

4.2.2.1 Transverse sections

In transverse section, the prismatic and nacreous layers are evidently distinct (Figure 4.6). In prismatic layer, the organic material shows morphology of parallel layers and uniform space between them (Figure 4.6d). In the initial nacreous layer, large amounts of organic material are observed (Figure 4.6e). In mature nacreous, the aragonite tablets are stacked in the form of columns (Figure 4.6f) and a new structural layer of aragonite about 20μm thick is in the innermost region (Figure 4.6g).
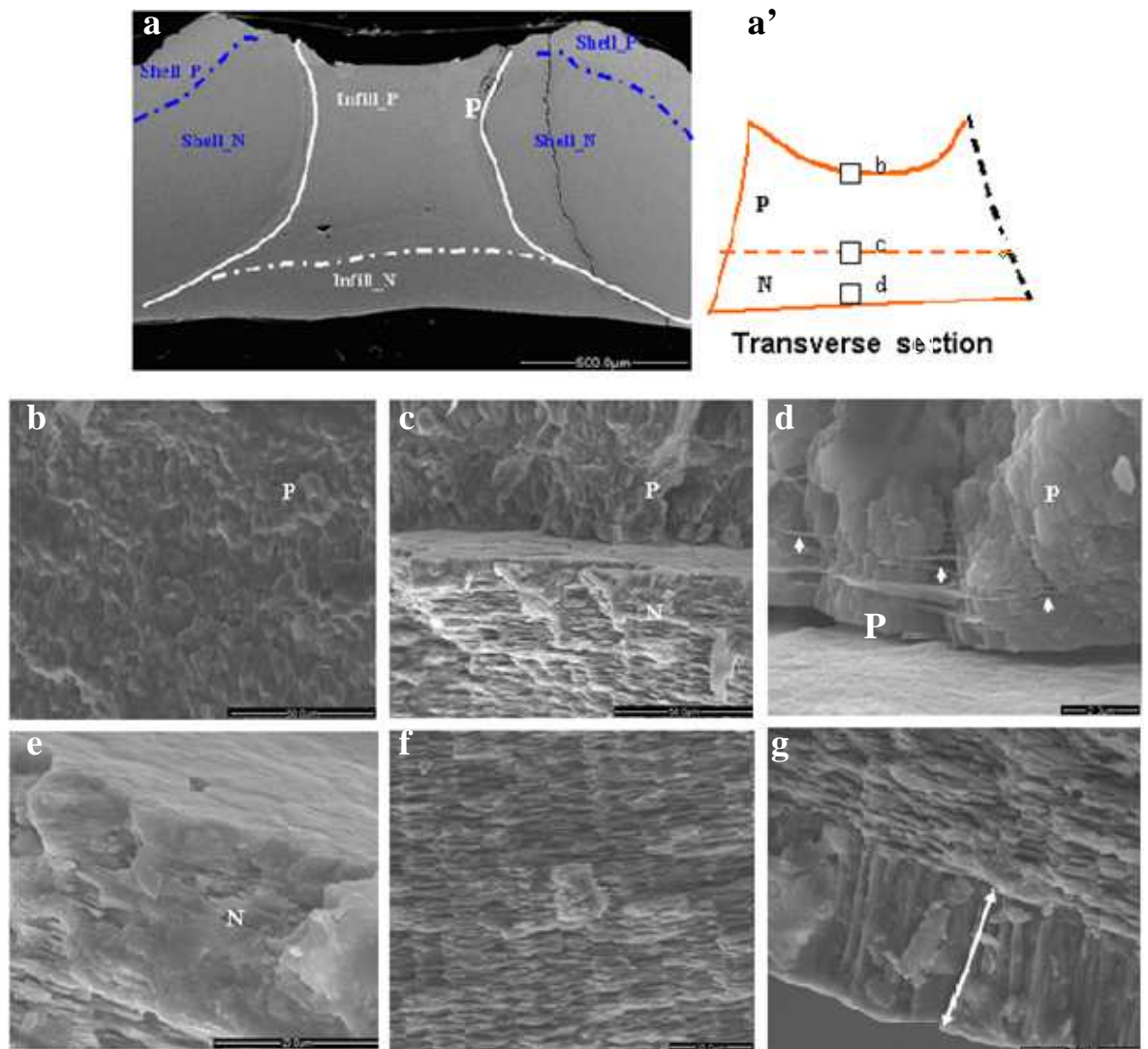
Figure 4.6 Secondary electron images of aperture infill of *H. asinina* shell in transverse section

a. Aperture infill is cohesive with the shell, and both infill and shell including prismatic and nacreous layers. a'. A sketch representation of (a) with 'b' (in prismatic layer), 'c' (in interface area) and 'd' (in nacreous layer) three magnified areas. b. Prismatic layer (P) of area 'b' in (a'). c. Interface of prismatic (P) and nacreous (N) layers of area 'c' in (a'). d. Magnified image of prismatic layer with organic material in the form of parallel layers (arrowheads). e. Magnified image of initiate nacreous layer with organic material filling in their space. f. Mature nacreous layer of area 'd' in (a') is composed of stacked tablets in column form. g. A new structural layer is about 20µm thickness in the innermost region of nacre. Scale bars for a-g=500, 50, 50, 2, 20, 20, 20 µm respectively.

4.2.2.2 Longitudinal section

In longitudinal section, the morphology of prismatic and nacreous layers of infill is presented with the aperture rim evident and the growth direction indicated (Figure 4.7a). In the infill prismatic layer, prisms firstly grow against the shell nacreous layer perpendicularly (Figure 4.7b), and from small crystals develop to long cylinder shape (Figure 4.7b, c). Near the infill prism-nacre interface, the prisms become a little disordered (Figure 4.7d) and nacreous layer starts to grow on the prisms (Figure 4.7e). The mature nacreous layer of the infill has columnar morphology (Figure 4.7f) and a new structural layer about 20µm thickness is in the innermost part (Figure 4.7g).
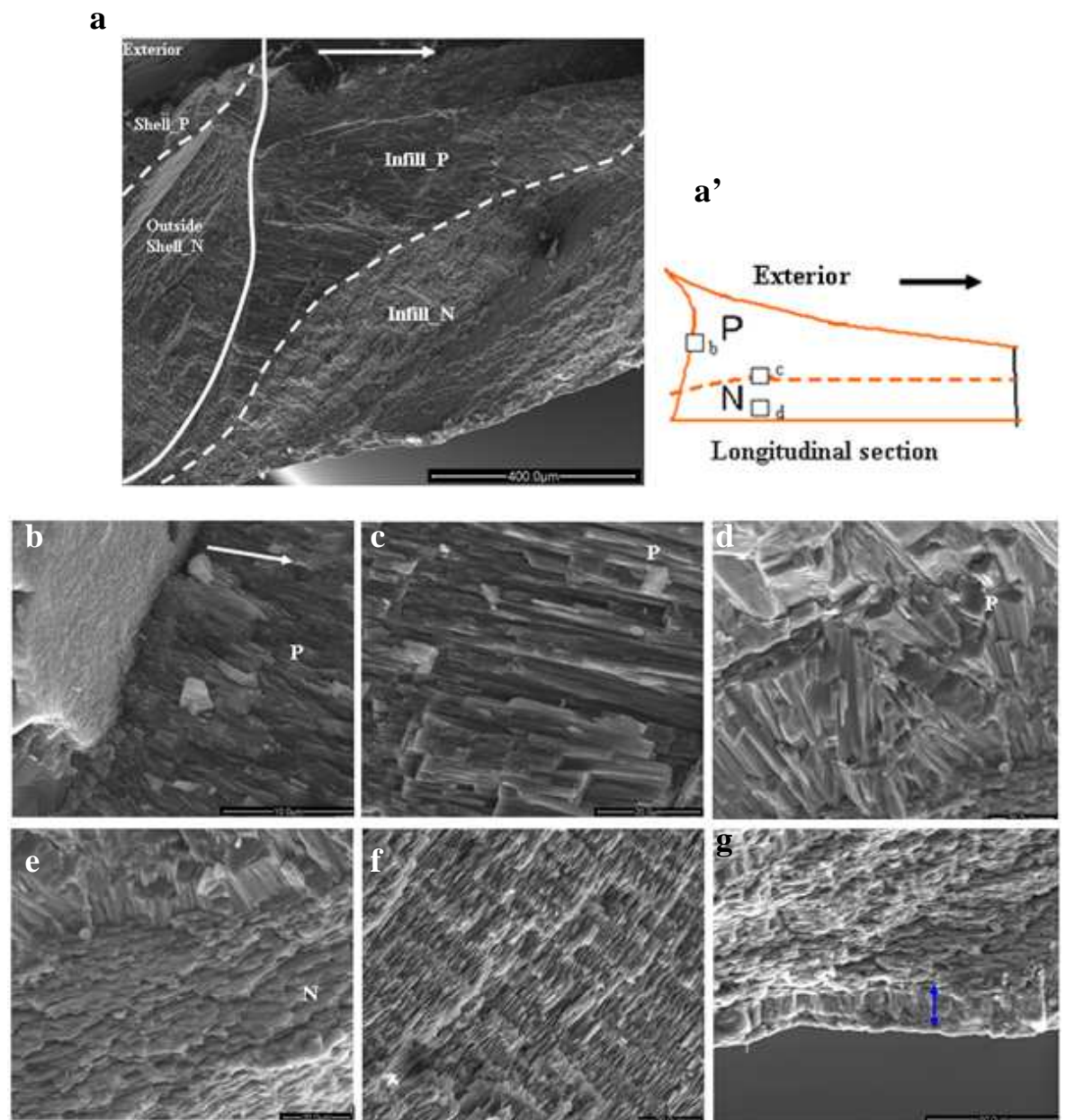
Figure 4.7   Secondary electron images of fractured aperture infill of *H. asinina* in longitudinal section

a. Aperture infill is cohesive with the shell nacreous layer including prismatic and nacreous layers. a'. A sketch representation of (a) with 'b' (in prismatic layer), 'c' (in interface area) and 'd' (in nacreous layer) three magnified areas. (Arrow shows the growth direction of infill and shell). b. Prisms grow on the shell nacreous layer perpendicularly. c. Prisms grow to be cylinder shape toward the growth direction. d. Slightly disordered prisms near the interface of 'c' area in (a'). e. Initiate nacreous layer grows on the prisms perpendicularly. f. Mature nacreous layer with column morphology. g. New structural layer is of about 20 µm thickness in the innermost region. Scale bars for a-h= 400, 10, 20, 20, 20, 20, 50 µm respectively.

4.2.3 Crystallographic orientation

4.2.3.1 Prismatic layer of aperture infill

In transverse section of aperture infill in *H. asinina* (Figure 4.8a), electron backscatter diffraction is used to identify the polymorph of calcium carbonate and crystallographic orientation. The prismatic layer is composed of aragonite. The initial anterior most prisms are small granules and gradually develop to polygonal shape (Figure 4.8b). Although diffraction is poor, it is evident that the c-axis becomes preferentially oriented, parallel to the shell surface and along the growth direction of infill and shell (Figure 4.8c, d).
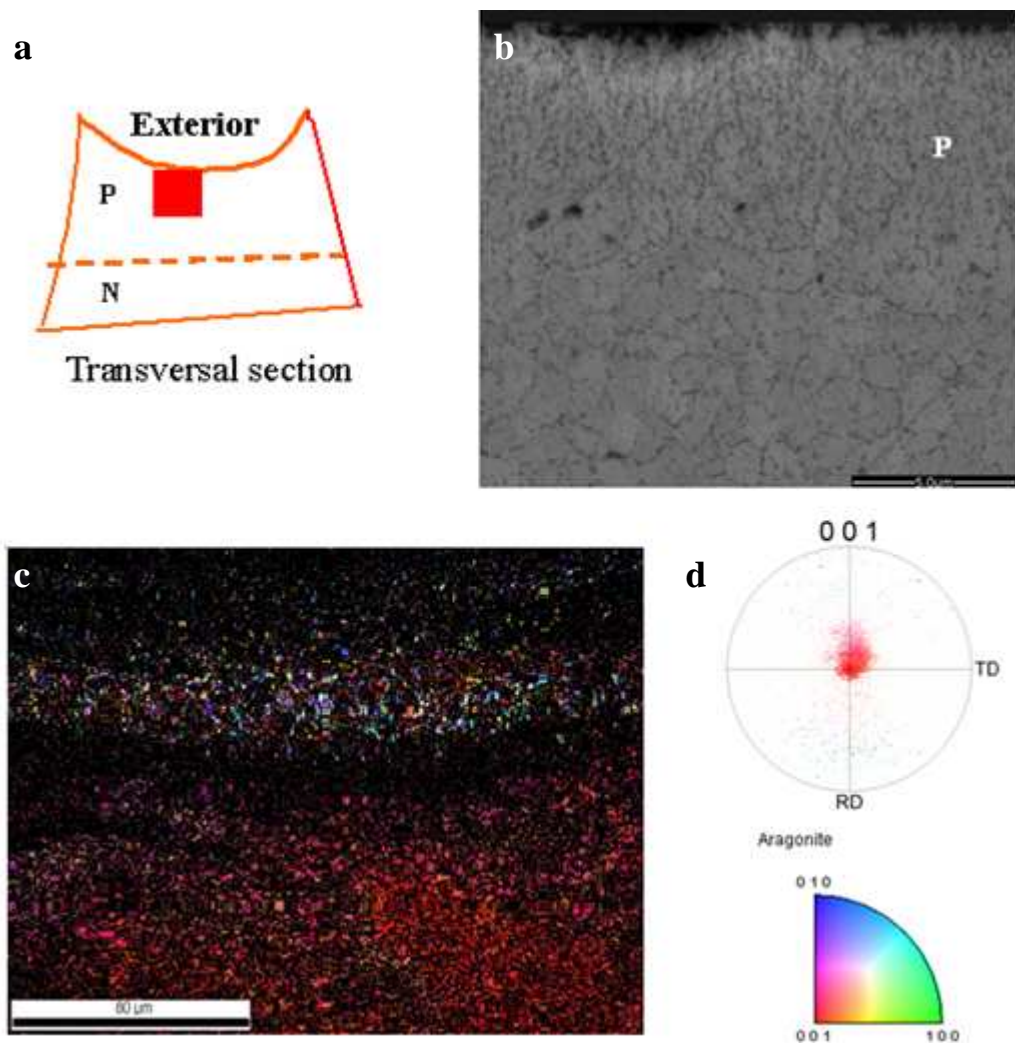
Figure 4.8   Crystallography of prismatic layer of aperture infill of *H. asinina* in transverse section

a. A sketch representation of transverse section sample with an analysed area in the prismatic layer (P). b. Backscatter electron image of the area in (a) shows that the initial prisms are granules and develop to polygonal shape. c. Crystal orientation map of area in (a) according to the aragonite colour key. d. Pole figure of the same area in (a) according to the crystal orientation map (c). Scale bars for b-c=5, 80 µm respectively.

In longitudinal section of aperture infill in *H. asinina* (Figure 4.9a), the prisms firstly grow small crystals perpendicular to the aperture wall, and develop to long polygons with larger diameter (Figure 4.9b). By using electron backscatter diffraction it is confirmed that the infill prismatic layer is aragonite and the c-axis of crystal orientation is parallel to the growth direction of infill and shell (Figure 4.9c, d).
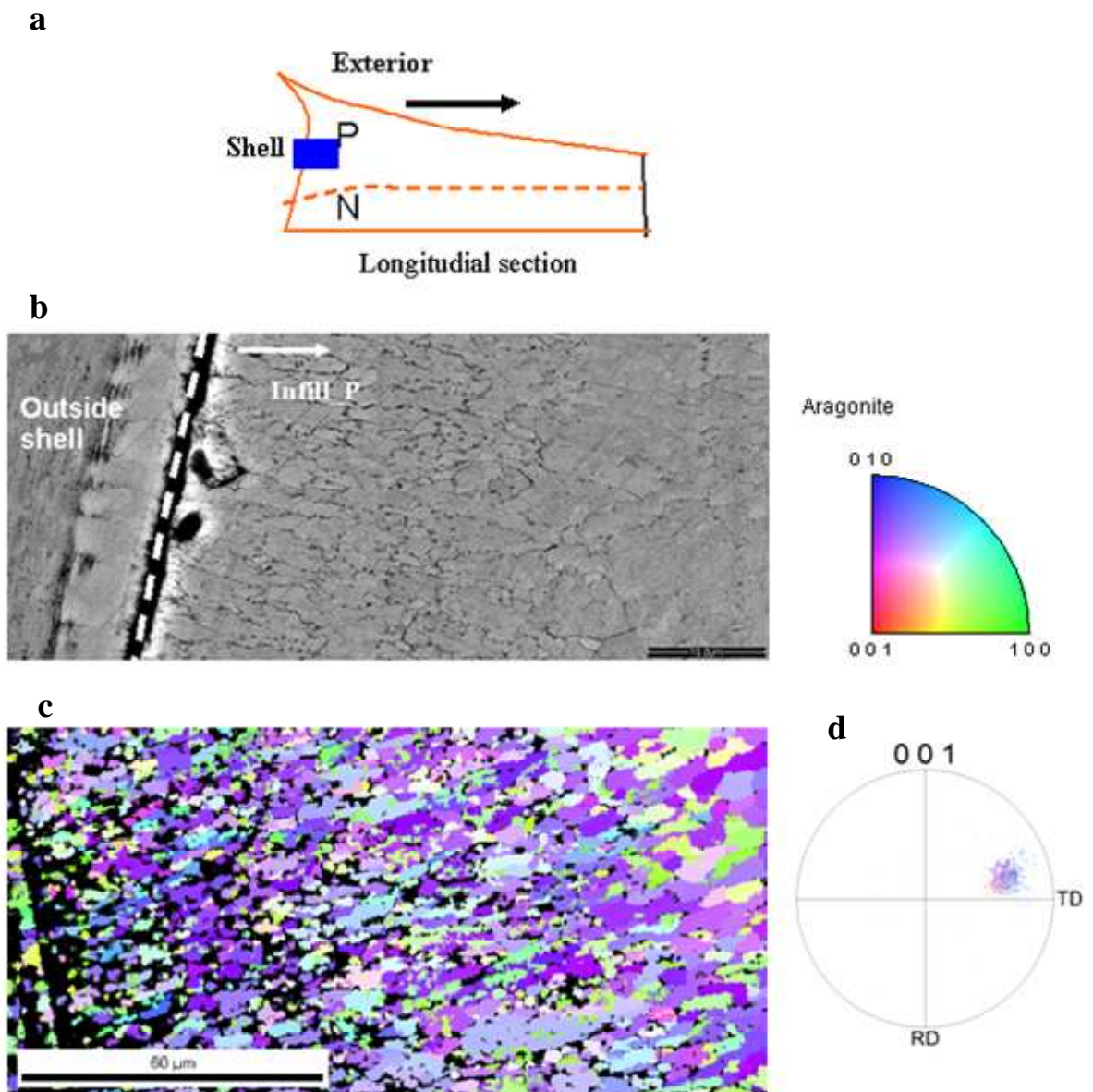
Figure 4.9   Crystallography of prismatic layer of aperture infill of *H. asinina* in longitudinal section

a. A sketch representation of longitudinal section sample with an analysed square in the prismatic layer (P). b. Backscatter electron image of area in (a) shows that the prisms grow granules firstly and then develop to polygonal shape with larger diameter. c. Crystal orientation map of area in (a) according to the aragonite colour key. d. Pole figure of the same area in (a) according to the crystal orientation map (c). Scale bars for b-c = 10, 60 μm respectively.

4.2.3.2 Nacreous layer of aperture infill

Using EBSD to analyse the nacreous layer of aperture infill in *H. asinina*, the c-axis of crystal orientation in the nacreous layer is perpendicular to the shell surface (Figure 4.10c, d), which is in accordance with crystal orientation of nacreous layer in shell (Figure 3.11b).
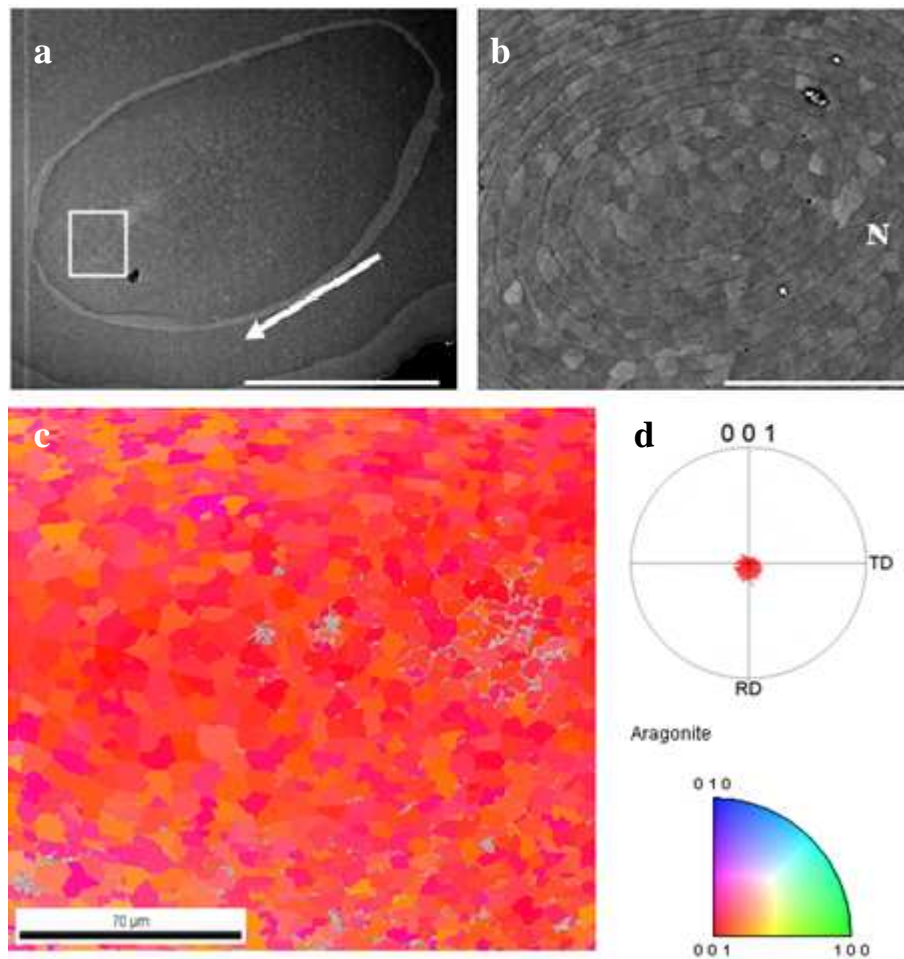
Figure 4.10 Crystallography of nacreous layer of aperture infill of *H. asinina* in plane section.

a. Backscatter electron image of a polished closed aperture showing the plan-view nacreous layer of aperture infill with an observed area (arrow shows the growth direction of infill and shell). b. Magnified backscatter electron image of the square area in (a) showing nacreous layer (N) in plan-view. c. Crystal orientation map of the area in (a) showing the c-axis of crystal orientation is perpendicular to the shell surface according to the aragonite colour key. d. Pole figure of the same area in (a) according to the crystal orientation map (c). Scale bars for a-c=500, 50, 70 μm respectively.

4.2.4 Cohesion between aperture infill and shell

Aperture infill occurs later than shell formation as the apertures are back filled forming a cohesive plug. The cohesion of this infill material with the shell material is interesting from a materials science perspective. Here the interface between shell and infill is investigated in terms of microstructure and crystallography.

4.2.4.1 Shell-infill interface microstructure

Both plan-view polished samples (Figure 4.11) and fracture of shell-infill interface (Figure 4.12) are preserved. In addition to one polished transverse-section infill sample with shell (Figure 4.13); it was polished twice along the growth direction of infill and shell.

There is a prism-like layer (L) between aperture infill (AI) and nacre of shell (S) (Figure 4.11b, c). The thickness of this intervening layer varies according to location (Figure 4.11c, f). It is presumed that the layer grows firstly on the shell nacreous layer and then aperture infill grows on it. The initiate aperture infill is observed porous (Figure 4.11d).
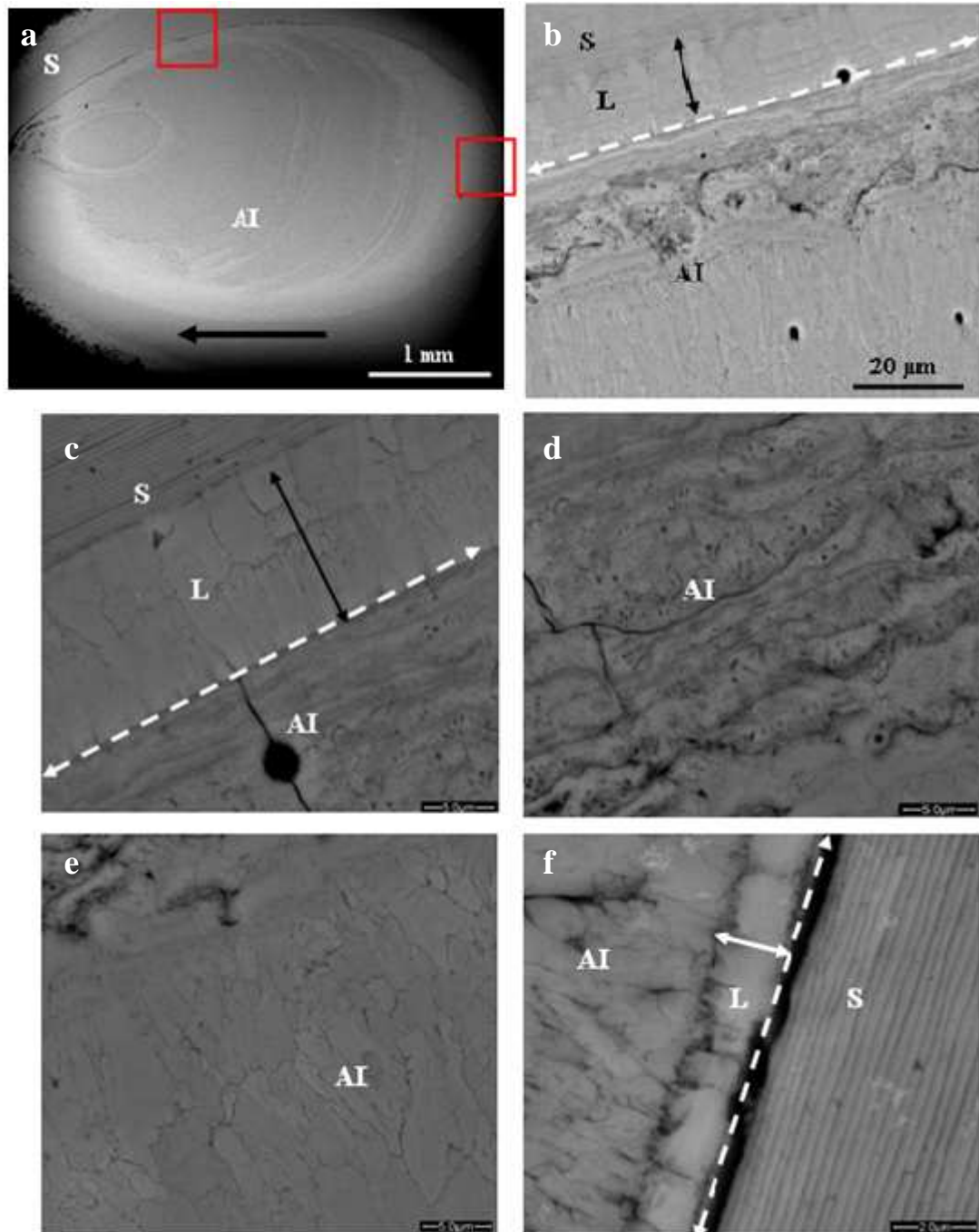
Figure 4.11 Backscatter electron images of aperture infill and surrounding shell of *H. asinina* in plan-view.

a. Aperture infill (AI) with 'b' and 'c' two detailed observed areas. b. Observed area 'b' in (a) including shell (S), prism-like layer (L) and AI. c. Magnified image of prism-like layer (L) of (b). d. Magnified image of porous area of (b). e. Magnified image of aperture infill of (b). f. Observed area 'c' in (a) including shell (S), prism-like layer (L) and AI. Scale bars for b-f=20, 5, 5, 5, 2 μm respectively.

Fracture section of aperture infill was observed in SEM in order to view features previously viewed in polished section, such as prism-like layer (Figure 4.12b), initial area (Figure 4.12c, d) and porous area of aperture infill (Figure 4.12e).
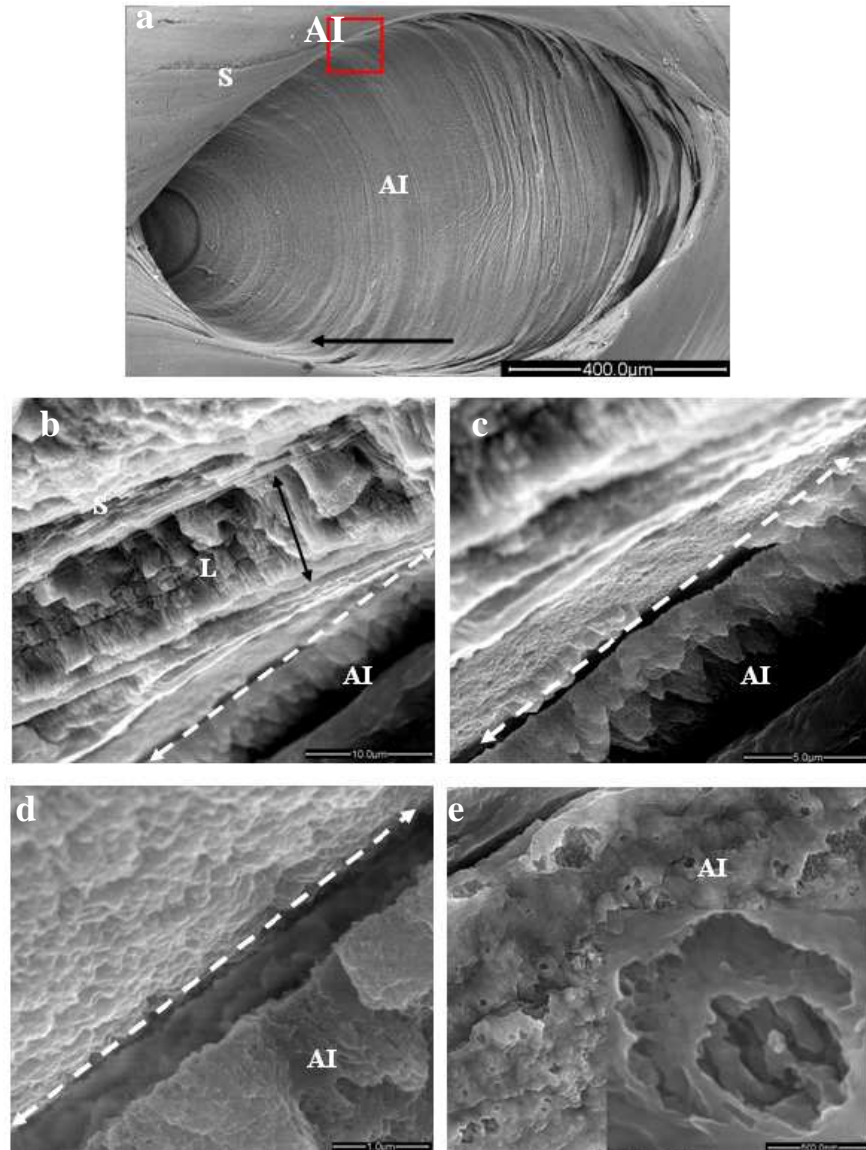
Figure 4.12 Secondary electron images of intact area of aperture infill and shell of fractured sample of *H. asinina* in plan-view

a. Aperture infill (AI) with one square area indicating area of fractured for images b-e (Arrow shows the growth direction of infill and shell). b. Square area in (a) including shell (S), prism-like layer (L) and AI. c. Magnified image of AI of (b) showing pyramid crystal morphology of initial AI growth. d. Magnified image of interface of (c) showing the gap area infilled by crystals. e. Porous area of initial AI (inset shows the detailed morphology). Scale bars for a-e= 400, 10, 5, 1, 0.5 µm respectively.

By viewing fractures section in middle of aperture infill and the polishing forwards anterior and final aperture infill, it is clear showing the aperture infill is always in contact with the shell nacre (Figure 4.13). In the aperture infill, the nacreous layer is of fairly constant thickness in all section analysed, *e.g.* Figure 4.13a, b.
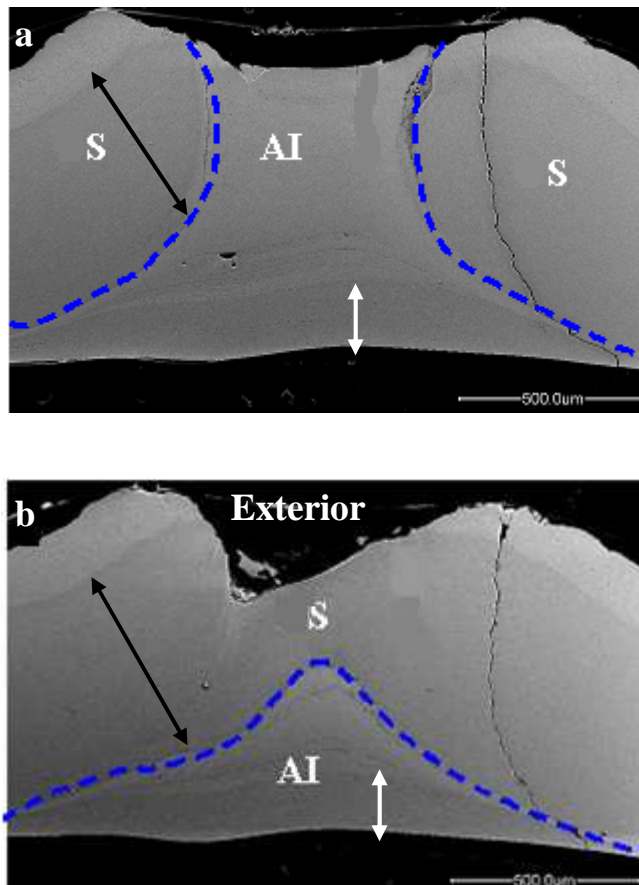
Figure 4.13 Backscatter electron images of polished sample including aperture infill and shell of *H. asinina* in transverse section

a. The first polished section through middle of infill including aperture infill (AI) and shell (S). b. Second time polished sample forwards anterior and final aperture infill including AI and S. (Black arrows show the thickness of shell nacreous layer; white arrows show the thickness of AI nacreous layer; dash lines show the range of AI).

4.2.4.2 Crystallographic viewpoint

Using EBSD to analyse the contact areas including shell, prism-like layer and aperture infill in plan-view, the crystal orientation relationship of the cohesive structure can be

determined. Although the three areas did not grow successively in a continuous time period, their c-axis of crystal orientation gradually changes to become parallel to the shell surface (Figure 4.14).
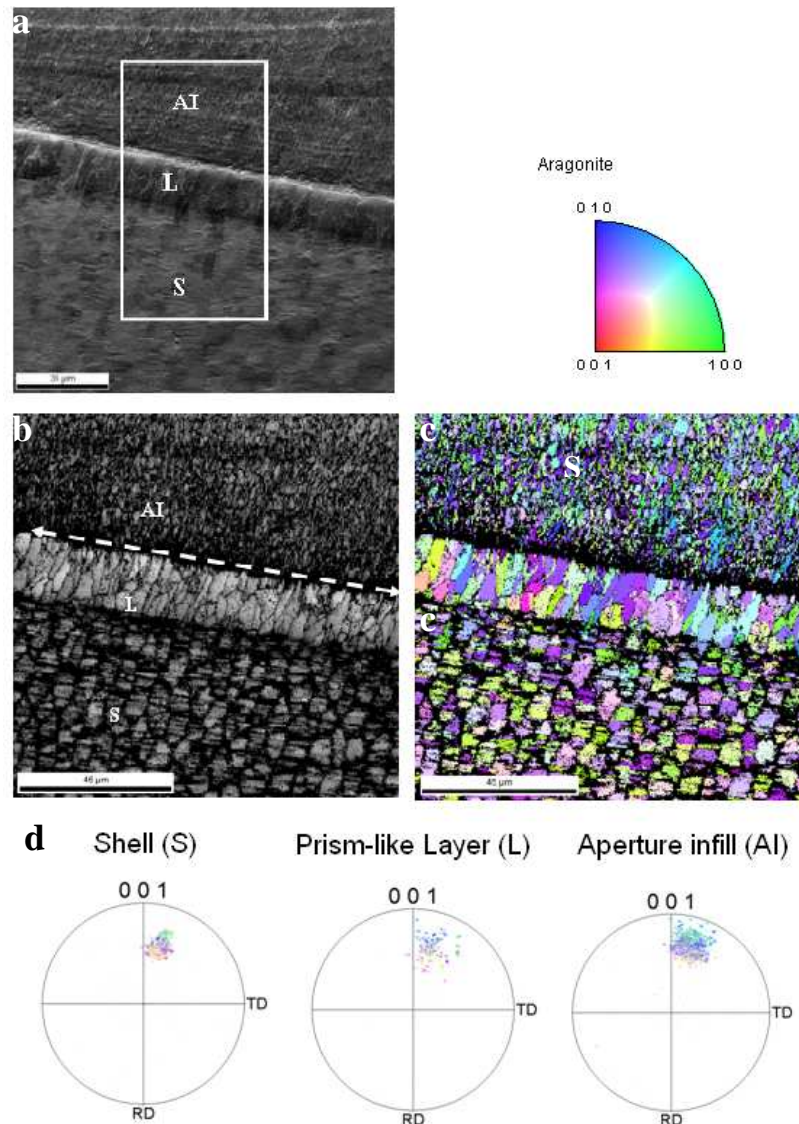
Figure 4.14 Crystallographic orientations of the contact areas including shell (S), prism-like layer (L) and aperture infill (AI) of *H. asinina* in plan-view

a. Secondary electron image showing the contact areas with rectangle indicating region of electron backscatter diffraction analysis. b. Diffraction intensity map of square area of (a). c. Crystal orientation map of the square area of (a) according to the aragonite colour key. d. Pole figures of S, L and AI separately according to (c). Scale bars for a-c=35, 45, 45 µm respectively.

4.3 Discussion

In abalone, the initial formation of shell take place in the contact zone between a layer of epithelial cells (the outer epithelium) and a layer of highly cross-linked proteins (the periostracum) (Figure 1.13). In molluscs, the epithelial cells secrete all of the components required to form the $CaCO_3$ shell: the crystal precursors Ca^{2+}, HCO_3^-, and possibly amorphous calcium carbonate (Addadi *et al.*, 2006), as well as several proteins and polysaccharides (Kröger, 2009). First, a layer of tightly stacked elongated prisms is formed and the prisms are oriented perpendicular to the longitudinal shell growth direction; then, the crystallization mode switches, and many layers of flat aragonite tablets are deposited (Figure 3.7). The aperture infill (Figure 4.4) has a similar structure to the shell. The prismatic layer consists of cylinder shape crystals perpendicularly grow on shell nacreous layer and parallel to the longitudinal shell growth direction (Figure 4.7b, c). Then, the aragonite tablets stacked along the c-axis the same as the shell nacre (Figure 4.7f). There are different volume ratios of prismatic layer *vs.* nacreous layer between shell structure (3:7) and aperture infill (7:3) (Figure 4.13). Whether aperture infill contains different mechanical properties from the shell is still unknown at the moment.

The environmental factors (such as temperature, salinity, ionic concentrations, *etc*.) have been reported to affect the crystal morphology (Wilbur, 1964). Another possible factor producing the observed difference between the normal shell and aperture infill is the periostracum, which is the outer covering of the shell and serves as the substratum of the outermost crystalline layer of shell (Beedham, 1958; Degens *et al*, 1967). It is a quinone-tanned protein (Degens *et al*, 1967) and present during normal shell growth, but lacking in shell regeneration after mechanical damage (Meenaksh *et al*., 1973). Whether abalone provides an equivalent of periostricum for the growing of aperture infill is to be investigated. According to calculate the growth rate of aperture infill, *H. asinina* (<6 month) shell grows about 60% faster than that of the aperture infill; while when individual was older than 6 months, the growth rate of shell and aperture infill occurs at nearly the same speed (Figure 4.3). However, it is also viewed that the changeable growth rate of aperture infill is in according with the growth rate of shell. Whether the infill has the same growth mechanism of shell or is also effected by environmental factors have not been known yet.

Both the aperture infill (Figure 4.9c; Figure 4.10c) and shell (Figure 3.10) of *H. asinina* are only found one polymorph aragonite in prismatic and nacreous layers. However, there is different crystallographic orientation of the prismatic layers in aperture infill and shell separately. The c-axis of crystal orientation of prismatic layer in aperture infill is parallel to shell exterior surface, and c-axis of crystal orientation of shell prismatic layer is perpendicular to the longitudinal shell growth direction. The elongated crystal shapes may reflect a faster growth rate such as in shell prismatic layer reported by Checa (*et al*., 2001), and so compared with aperture infill, which should have a different direction of faster growth rate.

The crystal orientation relationship of the cohesive structure of shell, prism-like layer and aperture infill is investigated. Although the three areas did not grow successively in a continuous time period; their c-axis of crystal orientation shows continuity (Figure 4.14). It may be one reason to explain why the aperture infill is so cohesive with the shell.

Based on the results of the microstructure and crystallography of aperture infill, there is still a lot of interesting work to do, such as to test the mechanical properties of the infill, analysis of crystallography of infill in other species and whether there is organic 'glue' effecting the cohesive property of infill.

5   Prismatic and Nacreous layers of *H. asinina*, *H. rufescens* and *H. gigantea*

5.1 Introduction

5.1.1 Specific research questions

In this chapter, the ultrastructure and crystallography of *H. asinina, H. rufescens* and *H. gigantea* three species (Figure 2.1) are investigated by EBSD analysis. Samples preparation is the same as described in Chapter 2 (refer to 2.2.4). This section focuses on the following questions.

- What is the mineralogy of the prismatic layers of the three species?

- Is the proportion of prismatic: nacreous layer thickness the same in all three species?

- What is the crystallographic orientation of the cross-section of shells of the three species?

5.1.2 Abalone shell structure

The abalone shell consists of two main layers, composed of calcium carbonate crystals with distinct microstructures (Nakahara *et al.*, 1982). It can be summarised by the outer prismatic layer and inner nacreous layer (refer to Chapter 3). Since nacre is always composed of aragonite, focus is placed on the prismatic layer. It has been reported that the prismatic layer of *H. rufescens* and *H. kamtschatkana* consist of calcite, while that of *H. asinina* consists of aragonite. *H. tuberculata, H. lamellosa* and *H. rotundata* have a mixture of various proportions of calcite and aragonite (Mutvei *et al.*, 1985; Dauphin *et al.*, 1989; Dauphin & Denis, 1995). These studies used energy dispersive X-ray spectroscopy (EDS), which provides indirect evidence for the calcium carbonate polymorph with higher concentrations of strontium, sodium and potassium indicating aragonite, and higher concentrations of manganese and magnesium indicating calcite. Here, EBSD is used to

provide direct evidence of the mineralogy of the prismatic layer of *H. asinina*, *H. rufescens* and *H. gigantea*.

5.1.3 Biological information

The composition of the prisms of three species from different locations is captured here. *H. asinina* is from Australia provided by Professor Jackson and Professor Degans (University of Queensland), *H. rufescens* is from American provided by Professor Taylor and Professor Claverie (University of California), and *H. gigantea* is from Japan provided by Professor Endo (University of Tokyo) (Figure 2.1, 2.2). Details of *H. asinina* are presented in Chapter 3 (Refer to 3.1.1), so the following section provides background information on *H. rufescens* and *H. gigantea*.

5.1.3.1 *H. asinina*

Haliotis asinina is common in the Pacific islands, southern Japan and northern Australia (Poutiers, 1998; Figure 2.2). Details biology information of *H. asinina* has been presented in Chapter 3 (refer to 3.1.1).

5.1.3.2 *H. rufescens*

H. rufescens is known under the common name of "red abalone". It is the largest species growing up to 313mm (Hutsell *et al.,* 1997) and mostly found in the northern part of California, U.S.A. (Figure 2.2). Red abalone lives in rocky areas with kelp; and they primarily feed on bull kelp and giant kelp (Cox, 1962; Mclean, 1966). The shell is heavy, somewhat oblong, arched and convex. The spiral is not elevated and hardly visible in dorsal view (Figure 5.1). Apertures are medium to large, oval, raised, and usually 3-5 open. Colours in variable width bands are red, pink, white, and green. Edges of bands are usually fuzzy (Geiger & Poppe, 2000).

5mm
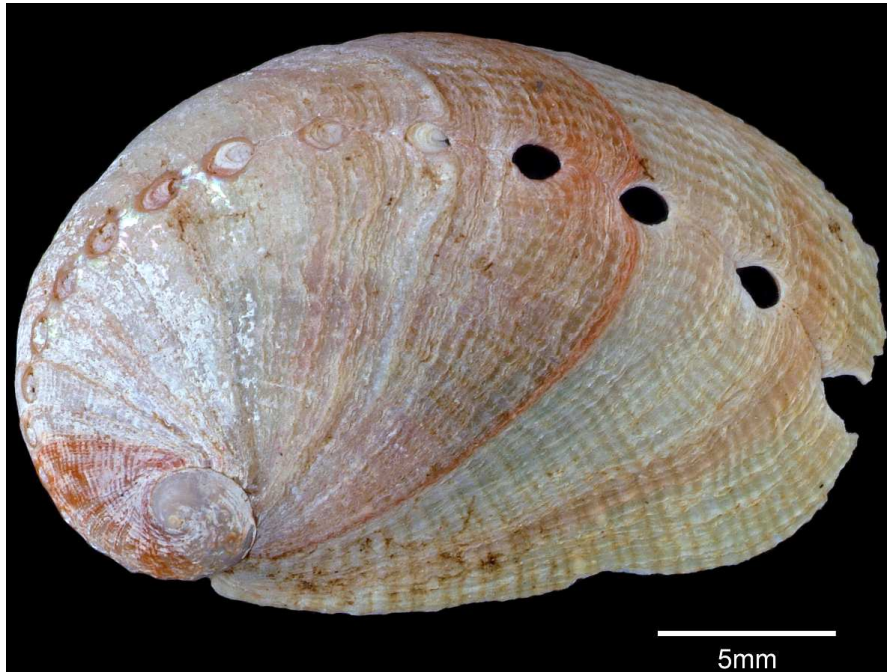
Figure 5.1 Dorsal view of *H. rufescens* shell

5.1.3.3 *H. gigantea*

H. gigantea are distributed along the southwest coast of Japan and are common and commercially important shellfish in the country (Figure 2.2). *H. gigantea* is large, growing up to 220mm (Hutsell *et al.,* 1997). The shell is elliptical, arched, and somewhat convex. Spire lines are depressed and barely visible in dorsal view (Figure 5.2). Apertures are medium size, round to oval, considerably raised, with usually 2-6 open. The dorsal surface is somewhat uneven with bumps and with low rounded spiral cords. Colour mostly is dull orange-red with radical bands in green, cream, and white (Geiger & Poppe, 2000).

Figure 5.2 Dorsal view of *H. gigantea* shell

5.2 Results

5.2.1 Mineralogy of prismatic layers of H. asinina, H. rufescens and H. gigantea

By EBSD analysis, the prismatic layer of *H. asinina* is composed entirely of aragonite, that of *H. rufescens* consists of calcite while *H. gigantea* has both aragonite and calcite in the prismatic layer (Figure 5.3).
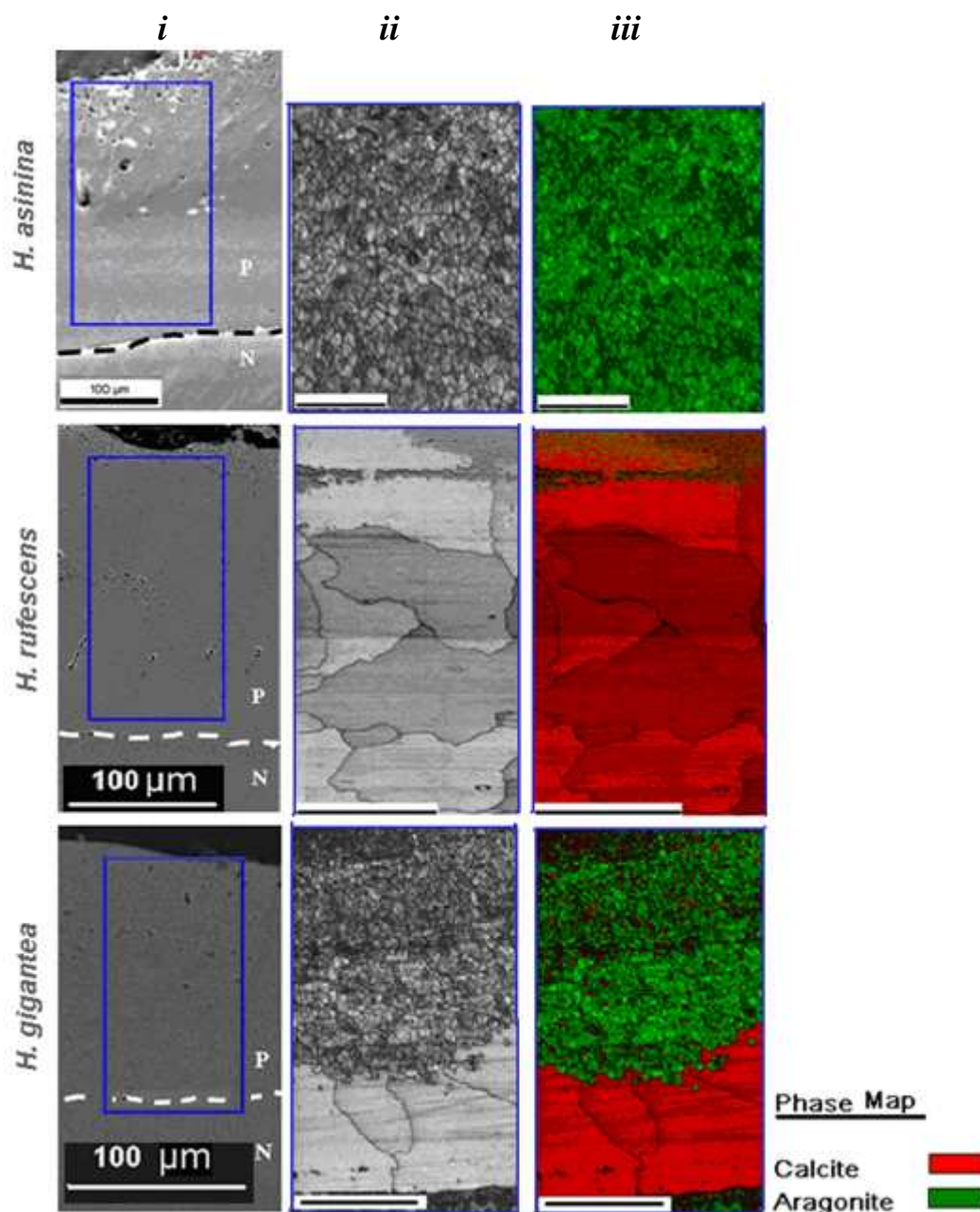
Figure 5.3 EBSD analysis of prismatic layer of *H. asinina, H. rufescens* and *H. gigantea* shells

(i) Secondary electron images of prismatic region, (ii) Diffraction intensity maps and (iii) Phase maps of three species separately. Diffraction intensity maps (ii) and phase maps (iii) are shown corresponding to the blue box of secondary electron images (i). According to the colour key, the prismatic layer of H. asinina is composed entirely of aragonite, that of H. rufescens consists of only calcite while H. gigantea has both aragonite and calcite in the prismatic layer Scale bar for ii and iii = 40 µm.

5.2.2 Relationship between thickness of prismatic layer and that of the whole shell of H. asinina, H. rufescens and H. gigantea

The prismatic regions of the three species have different mineralogy (Figure 5.3). Here, the thickness percent of the prismatic layer compared to whole shell has been investigated in the three species in order to determine whether the thickness of the primatic layer simply relates to overall shell thickness. Figure 5.4 shows the thickness relationship of prismatic layer and the corresponding shell thickness. *H. gigantea* shell is the thickest at just under 1 mm, *H. rufescens* is the thinnest at around 600~700 µm and *H. asinina* is about 800 µm thick (Figure 5.4a). The calcite prismatic layer (*H. rufescens*) takes up about 50% of the shell thickness compared with aragonite prismatic layer (*H. asinina*) of about 20~30%, and the prismatic layer consisting of calcite and aragonite (*H. gigantea*) is between the two at over 30% of total shell thickness (Figure 5.4b).

a

b
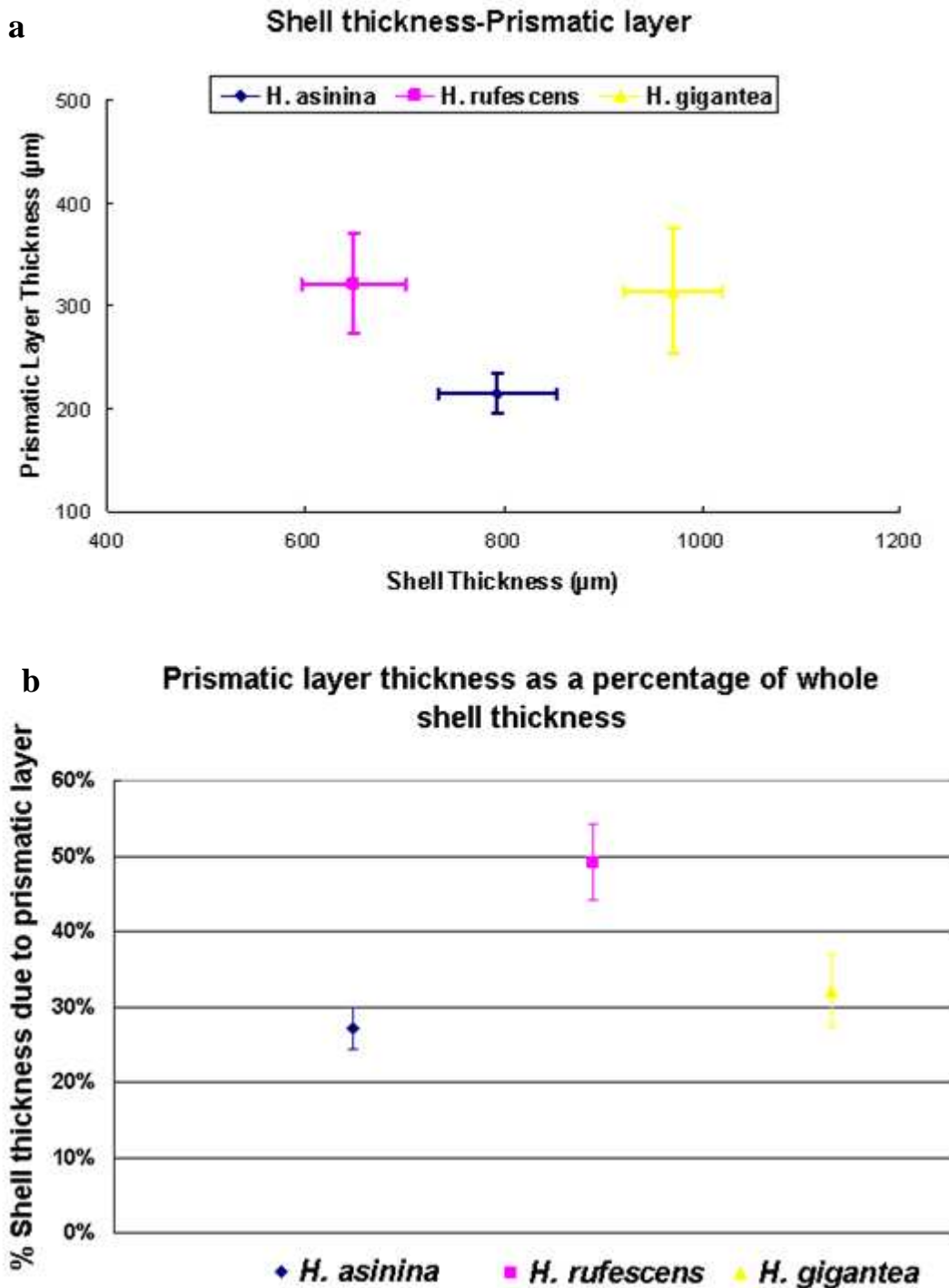
Figure 5.4   Thickness relationships of prismatic layer and the corresponding cross-section shell in three abalone species, *H. asinine*, *H. rufescens* and *H. gigantea*

a. The average (n of 24) thickness and standard deviation (S.D.) of cross-section shell and prismatic layer. b. The average (n of 24) thickness of prismatic layer as a percentage of whole shell thickness and S.D.

5.2.3 Crystallographic orientation of prismatic and nacreous layers of H. asinina, H. rufescens and H. gigantea

The crystal orientation of *H. asinina* shell has been investigated in Chapter 3. The shell of *H. asinina* is comprised of aragonite in both prismatic and nacreous layers, with c-axis of crystal orientation throughout the prismatic and nacreous layers of the shell. Towards the prismatic-nacreous interface, crystallographic alignment becomes much more tightly constrained. The c-axis is more tightly constrained in the nacreous layer than in the prismatic layer (Figure 5.5). Using the same approach of EBSD to analyse *H. rufescens* and *H. gigantea* shells, it reveals that both species contain aragonite nacreous layer and there is also the same higher crystallographic constraint in nacreous layer than in the prisms (Figure 5.5). The prismatic layer of *H. rufescens* shell is composed of calcite, with preliminary analyses indicating that the c-axis of crystal orientation is perpendicular to the shell surface. The prismatic layer of *H. gigantea* shell consists of calcite and aragonite. A small number of preliminary analyses suggest that the c-axis of aragonite is perpendicular to the shell surface and that of the calcite of the prisms is parallel to the shell surface (Figure 5.5).
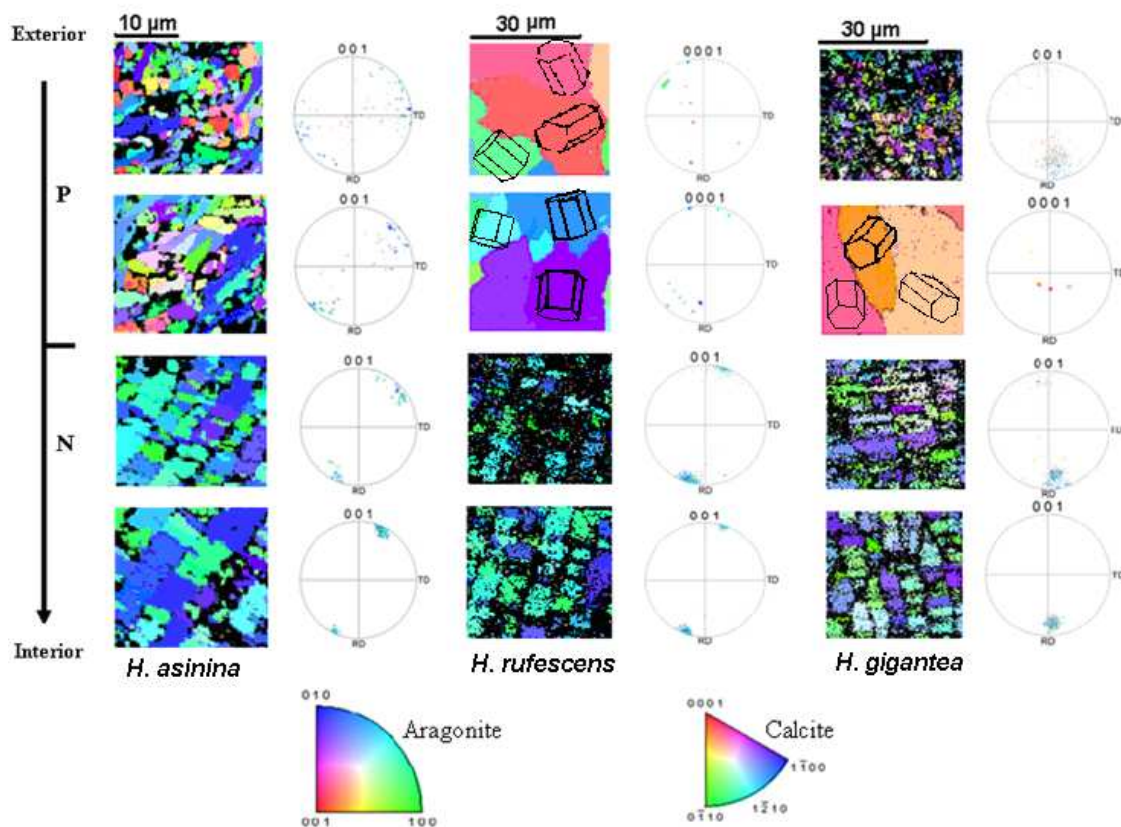
Figure 5.5   Crystallographic orientations of prismatic and nacreous layers in *H. asinina, H. rufescens* and *H. gigantea* shells

Crystallographic orientation maps and pole figures of statements and innermost regions of prismatic and nacreous layer according to the colour key for aragonite and calcite. There are wire frames in the calcite prismatic layer of H. rufescens and H. gigantea. Arrow shows the direction from exterior to interior of cross-section shell samples, which are divided to prismatic (P) and nacreous (N) layers.

5.3 Discussion

The prismatic layer in *H. asinina* is composed of aragonite, in *H. rufescens* the prismatic layer consists of calcite, while in *H. gigantea* the prismatic layer contains both calcite and aragonite (Figure 5.3). The fact that the prismatic layer in *H. asinina* is aragonite and in *H. rufescens* is calcite has proved before report by Mutvei *et al*. (1985) & Dauphin *et al*. (1989) using energy dispersive X-ray spectroscopy (EDS) analysis method. The calcite prismatic layer (*H. rufescens*) is about 300µm thick accounting for ~ 50% of total shell thickness, compared with that of aragonite prismatic layer (*H. asinina*) is about 200µm

thick which is about 20~30% of shell thickness, and that of the prismatic layer composed of two polymorphs, calcite and aragonite (*H. gigantea*) is over 300µm thick, accounting for 30% of shell thickness (Figure 5.4b). It reveals that the calcite prismatic layer (*H. rufescens*) takes more shell volume percent than that of aragonite prismatic layer (*H. asinina*). However, whether it is applicable in other species requires more investigations. Whether the prismatic layer of different mineralogy possesses different mechanical properties need further investigation.

Why do the prisms of abalone shells have different mineralogy? The distribution of shell mineralogy among biomineralising taxa has long posed a puzzle to paleontologists and biologists alike (*e.g*. Boggild, 1930; Lowenstam & Weiner, 1989; Weiner & Addadi, 1997). This may be determined by biology, environment or a combination of the two. The evolution success of mollusca can be attributed to an ability to assemble a wide diversity of mineralised structures (Weiner & Dove, 2003; Lowenstam & Weiner, 1989). The capacity, in combination with environmental changes at the end of the Proterozoic (Brennan *et al*., 2004; Feng & Weiner, 2003), has been proposed as one of the biological characters that aided the Cambrian radiation (Knoll, 2003). However, it is still unknown if the genetic programming directing the biofabrication of calcified and other mineralised structures in disparate animals is homologous (Knoll, 2003). Porter (2010) indicates that calcite and aragonite seas may initially play a primary role in determining carbonate skeletal mineralogy, but after carbonate skeletons have evolved, their influence on skeletal mineralogy is limited. This reflects that the diverse suite of proteins involved in shell mineralisation, many of which are polymorph-specific (*e.g.* Belcher *et al.*, 1996; Falini *et al.*, 1996; Zaremba *et al.*, 1996; Zhang & Zhang, 2006). Although a number of proteins implicated in the calcification process have been identified from the abalone shells (Fu *et al*., 2005; Shen *et al*., 1997; Weiss *et al.,* 2001; Mann *et al*., 2000); only a handful of genes are currently known to play a role in the biomineralisation (Himan *et al*., 2003; Jackson *et al*., 2007).

The shell of *H. asinina* is comprised of aragonite in both prismatic and nacreous layers, with c-axis orientation throughout the shell. Towards the prismatic-nacreous interface, crystallographic alignment becomes much more tightly constrained. The c-axis is tightly constrained in the nacreous layer than in the prismatic layer. In many cases,

crystallographic continuity persists across several laminae (Figure 5.5). The prismatic layer of *H. rufescens* shell is composed of calcite, the c-axis of crystal orientation is normal to the shell surface. The prismatic layer of *H. gigantea* shell consists of calcite and aragonite, the c-axis of aragonite is normal to the shell surface and that of calcite analysed area is parallel to the shell surface (Figure 5.5). Whether the c-axis of the calcite layer in *H.gigantea* always parallel to the shell surface or not need to do further analysis. In these three species, there is higher crystallographic constraint in the nacreous layer than in the prisms. Furthermore, in the nacreous layer of *H. asinina*, it has been revealed that there are tablets of co-oriented column varying between 2 and 50 (Figure 3.11c). In *H. rufescens* and *H. gigantea*, they are observed to compose of 2 and 40 varying co-oriented tablets (Figure 5.5). The same result of *H. rufescens* has been presented by Metzler *et al*. (2007). These observations support the possible formation mechanisms of "mineral bridges" for nacre growth (Schaffer *et al*., 1997) that best resembles bulk columnar nacre morphology as presented by Gilbert *et al*. (2008).

Unfortunately, the external shells of the samples *H. rufescens* and *H. gigantea* were not clean and encrusted with their calcium carbonate biominerals which can not be removed without damaging the shell and thus removing the information being sought. There were no special and clear findings on the protoconch areas of the two species like that of *H. asinina* and so there is no compare among them. However, further work need to do on the protoconch patterns of different abalone species.

6 Discussion and Future Work

6.1 Nacreous Layer of Abalone Shells

In *H. asinina*, the non-uniformity of nacreous tablet thickness was investigated in three polished samples from mature *H. asinina* shell from posterior to anterior (Figure 3.8a). Each sample is chosen three regions in nacreous layer: outer (near the prismatic layer), mid and inner (near the interior surface of shell) (Figure 3.8b) and measuring the thickness of 30~40 continuous tablets separately. It is found there is a pattern of more recently formed tablets being thicker; and the tablet thickness increasing gradually between 0.45~0.70 µm from the exterior to the shell interior (Figure 3.9). There are still many further questions such as whether the changeable thickness of nacre tablets in *H. asinina* could interpret the environmental factors affecting shell growth, or whether there is a characteristic thickness of nacre tablets in different species.

In *H. asinina* shell, the interior shell of nacre is associated with tiled aragonite growth (Shen *et al*., 1997; Zaremba *et al*., 1996; Fritz *et al*., 1994; Fritz & Morse, 1998; Figure 3.4b). In the microstructure of *H. asinina* nacre the nanoscale asperities are easily observed on the aragonite platelet surface (Figure 3.5b, 3.7c) and they were confirmed being remnants of mineral bridges by transmission electron microscopy (TEM) (Lin *et al*., 2008). Between the tablet there is organic 'glue' (Lin & Meyers, 2009), which is evident in Figure 3.5b. In the nacreous layer of *H. asinina*, it has been revealed that there are tablets of co-oriented column varying between 2 and 50 (Figure 3.11c). In *H. rufescens* and *H. gigantea*, they are observed to compose of 2 and 40 co-oriented tablets. The same result of *H. rufescens* has been provided by Metzler *et al*. (2007).

6.2 Prismatic Layer of Abalone Shells

The distribution of shell mineralogy among biomineralising taxa has long posed a puzzle to palaeontologists and biologists alike (*e.g.* Boggild, 1930; Lowenstam & Weiner, 1989; Weiner & Addadi, 1997). This mineralogy and proportions of calcium carbonate polymorphs produced in bimineralic systems have been studied and it showed that

environmental variation in salinity and temperature could produce distinct variation in proportions of calcite and aragonite between specimens and ontogenic stages (Lowenstam, 1954; Dodd, 1964; Eisma, 1966; Checa *et al.*, 2007). Since the initial recognition of calcite and aragonite seas, there has been abundant speculation about their effects on skeletal mineralogy (Porter, 2010). The primary driver of these oscillations is generally thought to be changes in the ratio of magnesium to calcium in seawater (*e.g.* Hardie, 1996; Morse *et al.*, 1997; Stanley & Hardie, 1998; Lowenstein *et al.*, 2001). Morse *et al.* (1997) has indicated that both the Mg/Ca ratio and temperature control the calcium carbonate mineral that forms from seawater. Such as calcite forms over a wide temperature range (0-35℃) in Mg-free seawater, but only below about 8℃ in seawtawer of normal Mg/Ca ration (~5/1). However, Porter (2010) still indicate that calcite and aragonite seas may initially play a primary role in determining carbonate skeletal mineralogy, but after carbonate skeletons have evolved, their influence on skeletal mineralogy is limited. This reflects that the diverse suite of proteins involved in shell mineralisation, many of which are polymorph-specific (*e.g.* Belcher *et al.*, 1996; Falini *et al.*, 1996; Zaremba *et al.*, 1996; Zhang & Zhang, 2006).

Prismatic layer of *H. asinina* is composed of aragonite, that of *H. rufescens* is calcite, and in *H. gigantea* the prismatic layer contains both calcite and aragonite (Figure 5.3). The fact of the aragonite prismatic layer in *H. asinina* and calcite prismatic layer in *H. rufescens* had been confirmed by EDS analysis method (Nakahara & Bevelander, 1982; Dauphin *et al.,* 1989; Mutvei *et al.*, 1985). Prisms of some other abalone species had also been identified with EDS analysis method, such as *H. kamtschatkana* is calcite (Dauphin *et al.,* 1989), *H. tuberculata, H. lamellosa* and *H. rotundata* have a prismatic layer of various proportions of calcite and aragonite (Mutvei *et al.*, 1985; Dauphin & Denis, 1995). The EDS analysis method indirectly recognized each by aragonite containing relative abundant Sr, Na and K; and calcite containing relative abundant Mg and Mn separately. This method is different from the direct EBSD analysis method using in my study.

The calcite prismatic layer (*H. rufescens*) is accounting for ~ 50% of total shell thickness, compared with that of aragonite prismatic layer (*H. asinina*) is about 20~30% of shell thickness, and the prismatic layer composed of calcite and aragonite two polymorphs (*H. gigantea*) is accounting for ~ 30% of shell thickness (Figure 5.4b). However, whether it is

applicable in other species, such as the calcite prismatic layer takes more shell volume percent than that of aragonite prismatic layer, needing further investigation. On the other side, whether the prismatic layers of different mineralogy contain different mechanical properties also need further investigation.

6.3 Crystallography of Prismatic and Nacreous Layers of Abalone Shells

The shell of *H. asinina* is comprised of aragonite in both prismatic and nacreous layers, with c-axis orientation throughout the shell. Towards the prismatic-nacreous interface, crystallographic alignment becomes much more tightly constrained. The c-axis is tightly constrained in the nacreous layer than in the prismatic layer. In many cases, crystallographic continuity persists across several laminae (Figure 5.5). Using the same approach of EBSD to analyse *H. rufescens* and *H. gigantea* shells, it reveals that both species contain aragonite nacreous layer and there is also the same higher crystallographic constraint in nacreous layer than in the prisms (Figure 5.5). The prismatic layer of *H. rufescens* shell is composed of calcite, with preliminary analyses indicating that the c-axis of crystal orientation is normal to the shell surface. The prismatic layer of *H. gigantea* shell consists of calcite and aragonite. A small number of preliminary analyses suggest that the c-axis of aragonite is normal to the shell surface while c-axis of calcite area is parallel to the shell surface (Figure 5.5), whether it is uniform in the whole calcite layer needs more analysis. In all, there is higher crystallographic constraint in the nacreous layer than in the prisms in the three species.

Mann (1988) indicated that to produce a certain polymorph, a matrix surface must be present to provide the optimum orientation geometry for nucleation of a crystal face. Thompson *et al.* (2000) and Belcher *et al.* (1996) demonstrated that aragonite can be produced without the need for the initial protein template; the soluble proteins would facilitate the direct growth of polymorph calcium carbonate. Other researchers (Levi *et al.*, 1998; Falini *et al.*, 1996; Addadi *et al.*, 2006; Cartwright & Checa, 2006) show the insoluble fractions to be of significant importance at least for controlling the nucleation of crystallisation. Although a number of proteins implicated in the calcification process have been identified from the abalone shells (Fu *et al.*, 2005; Shen *et al.*, 1997; Weiss *et al.*,

2001; Mann *et al*., 2000); only a handful of genes are currently known to play a role in the biomineralisation (Himan *et al*., 2003; Jackson *et al*., 2007). There is still a lot work to do on the transition process from prismatic layer to nacreous layer.

6.4 Comparison of Aperture Infill and Abalone Shell

The aperture infill (Figure 4.4) has a similar structure to the shell. The prismatic layer consists of cylinder shape crystals growing perpendicular to the shell nacreous layer and parallel to the longitudinal shell growth direction (Figure 4.7b, c). The aragonite tablets stacked along the c-axis as in the shell nacre (Figure 4.7f). It is also found the different volume ratios of prismatic layer *vs.* nacreous layer between shell structure (3:7) and aperture infill (7:3) (Figure 4.13). Whether aperture infill contains different mechanical properties is still unknown at the moment. One possible factor producing the observed difference between the normal shell and aperture infill is the periostracum, which is present during initial shell growth, but is lacking in shell regeneration after mechanical damage (Meenaksh *et al*., 1973) and presumably in aperture infill. The periostracum is a quinone-tanned protein, outer covering and serving as the substratum of the outermost crystalline layer of shell (Beedham, 1958; Degens *et al*, 1967). Whether abalone provides an equivalent of periostracum for the growing of aperture infill is to be investigated. One possible approach would be to dissolve away infill to reveal organic components such as analysis the matrix surfaces of mollusc shells *Atrina* and *Nautilus* by Nudelman *et al.* (2006).

In *H. asinina*, both the aperture infill (Figure 4.9c; Figure 4.10c) and shell (Figure 3.10) contain only aragonite. It is interesting to find the different crystallographic orientation of the prismatic layer between aperture infill and shell. The c-axis of the prismatic layer of aperture infill is parallel to shell exterior and that of shell is perpendicular to the shell exterior. Analysis of infill in other abalone species is required to determine how the infill mineralogy and crystallographic orientation compare. In addition to this suggestions for further work are presented below.

6.5 Ideas for Further Work

Jackson *et al*. (2007) have investigated the development of nine mantle genes during the life of the abalone *Haliotis asinina*. It is still unknown if ontogenetic changes in skeletal construction are the result of the expression of different batteries of biomineralisation genes. Ultrastructure analysis of ontogenetic stages throughout shell developments *of H. asinina* may shed light on the shell construction throughout ontogeny. Identifying changes in shell chemistry and crystallography and any relationship between them will contribute to our understanding of biomineralisation as well as the interpretation of climate proxies. Furthermore, investigation into the mineralising extrapallial fluid through ontogeny would provide a better insight to understand the biomineralising process. This would entail a detailed study of the chemistry of the fluid at different stages of ontogeny and protein composition.

Mutvei *et al*. (1985) and Dauphin *et al*. (1989) studied a range of abalone species and demonstrated that the prismatic layers consisted of aragonite or calcite, or both minerals in different proportions. Why do the prisms of abalone shells have different mineralogy? Whether the proportion of aragonite and calcite is related with the environments, such as trace elements, salinity, and temperature require further investigation. The Mg/Ca ratio and temperature influence the calcium carbonate mineral that forms from seawater (Morse et al., 2007). Calcite and aragonite seas may initially play a primary role in determining carbonate skeletal mineralogy and little effecting after carbonate skeletons have evolved (Porter, 2010). Thus, the selection of crystal polymorph or the 'calcite-aragonite' problem (Mann, 2001) is still unresolved at present. Analysis of the shell chemistry of the three species (*H. asinina. H. rufescens* and *H. gigantea*) may reveal a relationship between trace elements and the polymorph switch. Whether or not the proportion of aragonite and calcite is related to the mechanical properties of the prismatic layer should be investigated.

Aperture infill brings research into molluscs into the domain of material science. The infill has different proportions of prismatic and nacreous layers compared to the shell, and contains different crystallographic orientation in prismatic layer. It would be interesting to measure the mechanical property of aperture infill, compared with shell nacre which has

excellent properties of stiffness, strength and toughness (Curry, 1977; Jackson *et al.*, 1988; Wang *et al.*, 1995).

References

Adams, B.L., Wright, S.I. & Kunze, K. 1993 Orientation imaging- the emergence of a new microscopy. *Metallurgical Transactions A-Physical Metallurgy and Materials Science* **24**, 819-813.

Addadi, L., Joester, D., Nudelman, F. and Weiner, S. 2006 Mollusk shell formation: a source of new concepts for understanding biomineralisation process. *Chemistry A Eruopean Journal* **12**, 980-987.

Addadi, L., Raz, S. & Weiner, S. 2003 Taking advantage of disorder: Amorphous calcium carbonate and its roles in biomineralization. *Advanced Materials* **15**, 959-970.

Addadi, L. & Weiner, S. 1997 Biomineralization - A pavement of pearl. *Nature* **389**, 912-915.

Addadi, L. & Weiner, S. 1992 control and design principles in biological mineralization. *Angewandte Chemie* **31**, 153-169.

Addadi, L & Weiner, S. 1985 Interactions between acidic proteins and crystals-stereochemical requirements in biomineralization. *Proceedings of the National Academy of Sciences of the United States of America* **82**, 4110-4114.

Atlan, G., Delattre, O., Berland, S., LeFaou, A., Nabias, G., Cot, D. & Lopez, E. 1999 Interface between bone and nacre implants in sheep. *Biomaterials* **20**, 1017-1022.

Barthelat, F., Li, C.M., Comi, C. & Espinosa, H.D. 2006 Mechanical properties of nacre constituents and their impact on mechanical performance. *Journal of Material Research* **21**, 1977-1986.

Beedham, G.E. 1958 Observations on the non-calcareous components of the shell of the *Lamellibranchia. The Quarterly Journal of Microscopical Science* **99**, 341–357.

Beesley, P.L., Ross, G.J.B. & Wells, A. 1998. *Mollusca: The Southern sysnthesis. Fauna of Australia.* Melbourne: CSIRO Publishing. pp.667-669.

Belcher, A.M.B, Wu, X.H., Christensen, R.J., Hansma, P.K., Stucky, G.D. & Morse, D.E. 1996 Control of crystal phase switching and orientation by soluble mollusk-shell proteins. *Nature* **381**, 56-58.

Belcher A.M. 1996 Spatial and temporal resolution of interfaces, phase transitions and isolation of three families of proteins in calcium carbonate-based biocomposite materials. *Ph.D. thesis*. University of California, Santa Barbara, CA.

Beniash, E., Aizenberg, J., Addadi, L. & Weiner, S. 2007 Amorphous calcium carbonate transforms into calcite during sea urchin larval spicule growth. *Proceedings of the Royal Society of London Series B-Biological Sciences* **264**, 461-465.

Bevelander, G. & Nakahara, H. 1969 An electron microscope study of the formation of the nacreous layer in the shell of certain bivalve mollusks. *Calcified Tissue Res*earch **3**, 84-92.

Bezares, J., Asaro, R.J. & Hawley, M. 2008 Macromolecular structure of organic framework of nacre in Haliotis rufescens: implications for growth and mechanical behavior. *Journal of Structural Biology* **163**, 61-75.

Boggild, O.B. 1930 The shel structure of the mollusks. *Det Kontelige Danske Videnskabernes Selskabs Skrifter, Naturvidenskabelig og Mathematisk Afdeling* **2**, 231-326.

Brennan, S.T., Lowenstein, T.K. & Horita, J. 2004 Seawater chemistry and the advent of biocalcification. *Geology* **32**, 473-476.

Capinpin, E.C.J., Encena, V.C. III & Bayona, N.C. 1998 Studies on the reproductive biology of the Donkey's ear abalone, *Haliotis asinina Linne*. *Aquaculture* **166**, 141–150.

Cartwright, J.H.E. & Checa, A.G. 2006 The dynamics of nacre self-assembly. *Journal of the Royal Society Interface* **4**, 491-504.

Carter, J.G. & Hall, R.M. 1990 Polyplacophora, Scaphopoda Archaeogastropoda and Paragastropoda (Mollusca). In Cater, J.G. (ed.) *Skeletal Biomineralization: Patterns, Processes and Evolutionary Trends* **2**, 29-51.

Carter, J. G. and Clark II, G. R. 1985 Classification and phylogenitc significance of molluscan shell microstructure. *In: Bottjer D J Hickman, C.S, Ward, P D Broadhead T W (Eds), Molluscs, Note for a short Course. University of Tenessee, Department of Geological Sciences Studies in Geology,* 50-71.

Chateigner, D., Hedegaard, C. & Wenk, H.-R. 2000 Mollusc shell microstructures and crystallographic textures. *Journal of Structural Geology* **22**, 1723-1735.

Checa, A.G. & Rodriguez-Navarro, A.B. 2005 Self-organisation of nacre in the shells of *Pterioida* (Bivalvia : Mollusca). *Biomaterials* **26**, 1071-1079.

Checa, A.G. & Rodriguez-Navarro, A. 2001 Geometrical and crystallographic onstraints determine the self-organization of shell microstructures in Unionidae (Bivalvia: Mollusca). *Proceedings of the Royal Society B: Biological Sciences* **268**, 771-778.

Clark, G.R. 1974. Growth lines in invertebrate skeletons. *Annual Review of Earth and Planetary Sciences* **2**, 77-99.

Cölfen, H. & Antonietti, M. 2005 Mesocrystals: Inorganic superstructures made by highly paralle crystallization and controlled alignment. *Angewandte Chemie* **44**, 5576-5591.

Cölfen, H. & Mann, S. 2003 Higher-order organization by mesoscale self-assembly and transformation of hybrid nanostructures. *Angewandte Chemie* **42**, 2350-65.

Coppersmith, S.N., Gilbert, P.U.P.A. & Metzler, R.A. 2009 Theoretical characterization of a model of aragonite crystal orientation in red abalone nacre. *Journal of Physics A-Mathematical and Theoretical* **42**, 125101 (1-17).

Cox, K.W. 1962 California Abalone, Family Haliotidae. *California Department of Fish and Game Fish Bulletin* **118**, 133.

Crenshaw, M.A.& Ristedt, H. 1976 The histochemical localization of reactive groups in septal nacre from *Nautilus pompilius* L. *Belle W. Baruch Library in Marine Science* **5**, 355-367.

Cuif, J-P. & Dauphin, Y. 1996 Occurrence of mineralization disturbance in nacreous layers of cultivated pearls produced by *Pinctada margaritifera* var. *cumingi* from French Polynesia. Comparison with reported shell alterations. *Aquatic Living Resources* **9**, 187-193.

Currey, J.D. 1977 Mechanical properties of mother of pearl in tension. *Proceeding of the Royal Society London B* **196**, 443-463.

Cusack, M & Freer, A. 2008 Biomeralization: elemental and organic influence in carbonate systems. *Chemical Reviews* **108**, 4433-4454.

Cusack, M., England, J., Parkinson, D., Dalbeck, P., Lee, M., Curry, G.B. & Fallick, A.E. 2008b. Oxygen isotope composition, magnesium, distribution and crystallography of Terebratulina retusa. *Fossils & Strata* **54**, 259-267.

Dalbeck, P.C. 2008 Crystallography, stable isotope and trace element analysis of Mytilus edulis shells in the context of ontogeny. Ph.D. thesis. University of Glasgow. pp249.

Day, R. W. & Fleming, A. E. 1992 The determinants and measurement of abalone growth. Abalone of the World, Biology, Fisheries and Culture. Proceedings of the 1st International Symposium on Abalone, 1989, La Paz, Mexico.

Dauphin, Y. & Denis, A. 1995 Impications of statistical-analyses based on localized chemical contents on some species Haliotis shells (Mollusca, Archaeogastropoda). *Annales des Sciences Natutrelles-Zoologie et Biologie Animale* **16**, 7-19.

Dauphin, Y., Cuif, J.P., Mutvei, H. & Denis, A. 1989 Mineralogy, chemistry and ultrastructure of the external shell-layer in ten species of *Haliotis* with reference to *Haliotis tuberculata* (Mollusca: Archaeogastropoda). *Bulletin of the Geological Institutions of the University of Uppsala*, 7-37.

Degens, E.T., Spencer, D.W. & Parker, R.H. 1967 Paleobiochemistry of molluscan shell proteins. *Comparative Biochemistry and Physiology* **20**, 553–579.

Dey, A., With, G. & Sommerdijk, N.A.J.M. 2010 *In situ* techniques in biomimetic mineralization studies of calcium carbonate. *Chemical Society Reviews Articles* **39**, 397-409.

Dodd, J.R. 1965 Environmental control of strontium and magnesium in *Mytilus*. *Geochimica et Cosmochimica Acta* **29**, 385-398.

Dodd, J.R. 1964 Environmentally controlled variation in the shell structure of a Pelecypod species. *Journal of Paleontology* **38**, 1065-1071.

Eisma, D. 1966 Influence of salinity on mollusc shell mineralogy-a discussion. *Journal of Geology* **74**, 89-94.

Falini, G., Albeck, S., Weiner, S. & Addadi, L. 1996 Control of aragonite or calcite polymorphism by mollusk shell macromolecules. *Science* **271**, 67-69.

Feng, W. & Weiner, S. 2003 Phosphate replicated and replaced microstructure of olluscan shells from the earliest Cambrian of China. *Acta Paleontologica Polonica* **48**, 21-30.

Frankel, R.B., Bazylinski, D.A. 2003 Biologically induced mineralization by bacteria. *Review in Mineralogy and Geochemistry* **54**, 95-114.

Fritz, M. & Morse, D.E. 1998 The formation of highly organized biogenic polymer/ceramic composite materials: the high-performance microaluminate of molluscan nacre. *Current Opinion in Colloid & Interface Science* **3**, 55-62.

Fritz, M., Belcher, A.M., Radmacher, M., Walters D.A., Hansma, P.K., Stucky, G.D., Morse, D.E. & Mann, S. 1994 Flat pearls from biofabrication of organized composites on inorganic substrates. *Nature* **371**, 49-51.

Fu, G., Valiyaveettil, S., Wopenka, B. & Morse, D.E. 2005 CaCO$_3$ biomineralization: acidic 8-kDa proteins isolated from aragonitic abalone shell nacre can specifically modify calcite crystal morphology. *Biomacromolecules* **6**, 1289-1298.

Fuge, R., Palmer, T.J., Pearce, N.J.G. & Perkins, W.T. 1993 Minor and trace element chemistry of modern shells: A laser ablation inductively coupled plasma mass spectrometry study. *Applied Geochemistry, Suppl.* **2**, 111-116.

Gao, H., Ji, B., Jer, I.L., Arzt, E., Fratzl, P. 2003 Materials become insensitive to flaws at nanoscale: lessons from nature. *Proceedings of the National Academy of Sciences* **100**, 5597-5600.

Geiger, D.L. & Poppe, G.T. 2000 *The Family Haliotidae*. 1st Edn. Germany: ConchBooks (formerly Christa Hemmen). ISBN: 3925919279. pp135.

Geiger, D.L. 1998a Recent genera and species of the family *Haliotidae rafinesque,* 1815 (Gastropoda: Vetigastropoda). *The Nautilus* **111**: 85-116.

Gilbert, P.U.P.A., Metzler, R.A., Zhou, D., Scholl, A., Doran, A., Young, A., Kunz, M., Tamura, N. & Coppersmith, S.N. 2008 Gradual ordering in red abalone nacre. *Journals of the American Physical Society* **130**, 17519–17527

Goldstein, J.I., Newbury, D.E., Echlin, P., Joy, D.C., Fiori, C. & Lifshin, E. 1981 Scanning electron microscopy and X-ray microanalysis. Plenum Press, New York. ISBN: 030640768x. pp689.

Greenaway, P. 1985 Calcium balance and moulting in the crustacea. *Biological Reviews of the Cambridge Philosophical Society* **60**, 425-454.

Gregoire, C. 1972 *Structure of the molluscan shell. In: M.Florkin and B.T.Scheer, Editors, Chemiceal Zoology* Vol. VII, Academic Press, New York, pp45-102.

Gregoire, C. 1957 Topography of the organic components in mother-of-pearl. *Journal of Biophysical and Biochemical Cytology* **3**, 797-808.

Hardic, L.A. 1996 Secular variation in seawater chemistry: an explanation for the coupled secular variation in the mineralogies of marine limestones and potash evaporates over the past 600 m.y. *Geology* **24**, 279-283.

Hart, S.R. & Blusztajn, J. 1998 Clams as recorders of ocean ridge volcanism and hydrothermal vent field activity. *Science* **280**, 883-886.

Haszprunar, G. 2001 Mollusca. In: *Encyclopedia of Life Sciences*. Macmillian Referece Ltd. Hampshire. 6pp.

Hedegaard, C. & Wenk, H.-R., 1998 Microstructure and texture patterns of mollusc shells. *Journal of Molluscan Studies* **64**, 133-136.

Heuer, A.H., Fink, D.J., Laraia, V.J., Arias, J.L., Calvert, P.D., Kendall, K., Messing, G.L., Blackwell, J., Rieke, P.C. and Thompson, D.H. 1992 Innovative materials processing strategies: a biomimetic approach. *Science* **255**, 1098-1105.

Hinman, V.F., O'Brein, E.K., Richards, G.S. & Degnan, B.M. 2003 Expression of anterior Hox genes during larval development of the gastropod Haliotis asinina. *Evolution & Development* **5**, 508-521.

Hubbard, F., McManus, J. & Al-Dabbas, M. 1981 Evironmental influences on the shell mineralogy of *Mytilus edulis*. *Geo-Marine Letters* **1**, 267-269.

Hutsell, K.C., Hutsell, L.L. & Pisor, D.L. 1997 *Registry of World Record Size Shells*. Snail's Pace Productions, San Diego. pp101.

Ino, T. 1952. Biological studies on the propagation of Japanese abalone (Genus *Haliotis*). *Bulletin of theTokai Regional Fisheries Research Laboratory* **5**, 1-102, pls.1-34.

Jackson, A.P., Vincent, J.F., Turner, R.M. 1990 Comparison of nacre with other ceramic composites. *Journal of Materials Science* **25**, 3173-3178.

Jackson, A.P., Vincent, J.F., Turner, R.M. 1988 The mechanical design of nacre. *Proceedings of the Royal Society London* **B 234**, 415-440.

Jackson, D.J., Wörheide, G & Degnan M.B. 2007 Dynamic expression of ancient and novel molluscan shell genes during ecological transitions. *BMC Evolutionary Biology* **7**, 160-176.

Jackson, D.J., Ellemor, N., Degnan B.M. 2005 Correlating gene expression with larval competence, and the effect of age and parentage on metamorphosis in the tropical abalone *Haliotis asinina*. *Marine Biology* **147**, 681-697.

Jackson, D.J., Leys, S.P., Hinman, V.F., Woods, R., Lavin, M.F. & Degnan, B.M. 2002 Ecological regulation of development: induction of marine invertebrate metamorphosis. *International Journal of Developmental Biology* **46**, 679-686.

Ji, B.H., Ga, H.J. & Hsia, K.J. 2004 How to slender mineral crystals resist buckling in biolocial materials? *Philosophical Magazine Letters* **84**, 631-641.

Ji, B.H. & Ga, H.J. 2004 Mechanical properties of nanostructure of biological materials. *Journal of the Mechanics and Physics of Solids* **52**, 1963-1990.

Kamat, S., Su, X., Ballarini, R., Heuer, A.H. 2000 Structural basis for the fracture toughness of the shell of the conch *strombus gigas*. *Nature* **405**, 1036-1040.

Keeton, W. T. & Gould, J. L. 1986 *Biological Science. 4th ed.* W.W.Norton and Company, New York.1175pp.

Kniprath, E. 1981 Ontogeny of the molluscan shell field-a review. *Zool Scripta* **10**, 61-79.

Knoll, A.H. 2003 Biomineralisation and evolutionary history. *Review Mineral Geochemistry* **54**, 329-356.

Kobayashi, I. & Samata, T. 2005. Bivalve shell structure and organic matrix. *Materials Science and Engineering C* **26**, 692-698.

Kröger, N. 2009 The molecular basis of nacre formation. *Science* **325**, 1351-1352.

Leighton, D. L. 2000 *The Biology and Culture of the California Abalones*. Pittsburgh, PA,Dorrance Publishing Co., Inc. 216.

Levi-Kalisman, Y., Falini, G., Addadi, L., et al. 2001 Structure of nacreous organic matrix of a bivalve mollusc shell examined in the hydrated state using Cryo-TEM. *Journal of Structural Biology* **135**, 8-17.

Levi, Y., Albeck, S., Brack, A., Weiner, S. & Addadi, L. 1998 Control over aragonite crystal nucleation and growth: An in vitro study of biomineralization. *Chemistry-A European Journal* **4,** 389-396.

Lin, A.Y.M. & Meyers, M.A. 2009 Interfacial shear strength in abalone nacre. *Journal of the Mechanical Behavior of Biomedical Materials* **2**, 607-612.

Lin, A.Y.M., Chen, P.Y. & Meyers, M.A. 2008 The growth of nacre in the abalone shell. *Acta Biomaterialia* **4**, 131-138.

Lin, A.Y.M. & Meyers, M.A. 2005 Growth and structure in abalone shell. *Materials Science and Engineering A-Structural materials properties microstructure and processing* **390**, 27-41.

Lipmann, F. 1973 Nornribosomal polypeptide synthesis on polyenzyme templates. *Accounts of Chemical Research* **6**, 361-367.

Livingston, B.T., Killian, C.E., Wilt, H., Camerron, A., Landrum, M.J., Ermolaeva, O., Sapojnikov, V., Maglott, D.R., Buchanan, A.M., Ettensohn, C.A. 2006 Agenome-wide analysis of biomineralization-related proteins in the sea urchin *Strongylocentrotus purpuratus*. *Developmental Biology* **300**, 335-348.

Lopez, E., Vidal, B., Berland, S., Camprasse, C., Camprasse, G. & Silve, S. 1992. Demonstration of the capacity of nacre to induce bone formation by human osteoblasts maintained in vito. *Tissue Cell* **24**, 667-679.

Lorens, R.B. & Bender, M.L. 1980 The impact of solution chemistry on *Mytilus edulis* calcite and aragonite. *Geochimica et Cosmochimica Acta* **44,** 1265-1278.

Lowenstam, T.K., Timofeef, M.N., Brennan, S.T., Hardie, L.A. & Demicco, R.V. (2001) Oscillations in Phanerozoic seawater chemistry: evidence from fluid inclusions. *Science* **294**, 1086-1088.

Lowenstam, H.A. & Weiner, S. 1989 *On Biomineralization*. New York, Oxford University Press. pp324.

Lowenstam, H.A. 1981 Minerals formed by organisms. *Science* **211**, 1126-1131.

Lowenstam, H.A. & Margulis, L. 1980 Evolutionary prerequisites for early phanerozonic calcareous skeletons. *Biosystems* **12**, 27-41.

Lowenstam, H.A. 1954 Factors affecting the aragonite: calcite ratios in carbonate secreting marine organisms. *Journal of Geology* **62**, 284-322.

Luz, G.M. & Mano, J.F. 2009 Biomimetic design of materials and biomaterials inspired by the structure of nacre. *Philosophical Transactions of the Royal Society A.* **367**, 1587-1605.

Mahway, E. 2005 OIM User's Manual: New Jersey, EDAX-TSL.

Mann, K., Weiss, I.M., Andre, S., Gabius, H.J. & Fritz, M. 2000 The amino-acid sequence of the abalone (*Haliotis laevigata*) nacre protein perlucin. Detection of a functional C-type lectin domain with galactose/mannose specificity. *European Journal of Biochemistry* **267**, 5257–5264.

Mann, S. 2001 *Biomineralization: Principles and Concepts in Bioinorganic Materials Chemistry*. Oxford, Oxford University Press. ISBN: 0198508824 (pbk). pp193.

Mann, S. 1994 Atomic force microscopy of the nacreous layer in mollusc shells. *Proceeding of the Royal Society B* **256**, 17-23.

Marin, F. & Luquet, G. 2004 Molluscan shell proteins. *Comptes Rendus Palevol* **3**, 469-492.

Mayer, G. 2005 Rigid biological systems as models for synthetic composites. *Science* **310**, 1144-1147.

Mclean, J. 1962 Sublittoral ecology of kelp beds of the open coast areas near Carmel, California. *The Biological Bulletin (Woods Hole, Mass.)* **122**, 95-114.

Meenakshi, V.R., Blackwelder, P.L. & Wilbur, K.M. 1973 An ultrastructural study of shell regeneration in *Mytilus edulis* (Mollusca: Bivalvia). *Journal of Zoology, London* **171**, 475-484.

Meenakshi, V.R., Hare, P.E. & Wilbur, K.M. 1971. Amino acids of the organic matrix of neogastropod shells. *Comparative Biochemistry and Physiology Part B: Comparative Biochemistry* **40**, 1037-1043.

Mening, R., Meyers, M.H., Meyers, M.A. & Vecchio, K.S. 2000 Quasi-static and dynamic mechanical response of *Haliotis rufescens* (abalone) shell. *Acta Materialia* **45**, 2383-2398.

Metzler, R.A., Abrecht, M., Olabisi, R.M., Ariosa, D., Johnson, C.J., Frazer, B.H., Coppersmith, S.N. & Gilbert, P.U.P.A. 2007 Architecture of columnar nacre, and implications for its formation mechanism. *Physics Review Letters* **98**, (268102-)1-4.

Meyers, M.A., Chen, P.-Y., Lin, A.Y.-M. & Seki, Y. 2008 Biological materials: structure and mechnial properties. *Progress in Materials Science* **53**, 1-206.

Meyers, M.A., Lin, A.Y.-M., Chen, P.Y. & Muyco, J. 2008 Mechanical strength of abalone nacre: role of the soft organic layer. *Journal of The Mechanical Behaviour of Biomedical Materials* **1**, 76-85.

McNamara, D.C. & Johnson, C.R. 1995 Growth of the ass's ear abalone (*Haliotis asinina Linne*) in Heron Reef, Tropical Eastern Australia. *Marine and Freshwater Research* **46**, 571–574.

Morse, J.W., Arvidson, R.S. & Luttge, A. 2007 Calcium carbonate formation and dissolution. *Chemical Reviews* **107**, 342-381.

Morse, J.W., Wang, Q. & Tsio, M.Y. 1997 Influences of temperature and Mg:Ca ratio on the mineralogy of CaCO3 precipitated from seawater. *Geology* **25**, 85-87.

Morse, D.E., Hooker, N., Duncan H. & Jensen, L. 1979 g-aminobutyric acid, a neurotransimitter, induces planktonic abalone larvae to settle and begin metamorphosis. *Science* **204**, 407-410.

Mutvei, H., Dauphin, Y. & Cuif, J-P. 1985 Observations on structure of the external layer of shell of *Haliotis* Gastropoda an exceptional case mineralogical and microstructural variability. *Bulletin du Museum National d'Histoire Naturelle Section A Zoologie Biologie et Ecologie Animales* **7**, 73-92.

Mutvei, H. 1977 Nacreous layer in *Mytilus, Nucula*, and *Unio* (Bivalvia)-crystalline composition and nucleation of nacreous tablets. *Calcified Tissue Research* **24**, 11-18.

Nakahara, H. 1991. Nacre formation in bivalve and gastropod molluscs. In: Suga S, Nakahara H, editors. *Mechanisms and phylogeny of mineralizaion in biological systems*. New York: Springer-Verlag. pp343.

Nakahara, H., Bevlander, G. & Kakei, M. 1982 Electron microscopic and amino-acid studies on the outer and inner shell layers of *Haliotis rufescens*. *Venus the Japanese Journal of Malacology* **41**, 33-46.

Nakahara, H., Kakei, M. & Bevelander, G. 1980 Fine structure and amino acid composition of the organic "envelope" in the prismatic layer of some bivalve shells. *Venus* **39**, 167-177.

Nassif, N. Pinna, N., Gehrke,N., Antonietti, M., Jager, C. & Colfen, H. 2005 Amorphos layer around aragonite platelets in nacre. *Proceedings of the National Academic of Sciences* **102**, 12653-12655.

Nowell, M.M., Witt, R.A. & True, B. 2005 EBSD sample preparation: Techniques tips and tricks. *Microscopy and Microanalysis* **11**, 504-505.

Nudelman, F., Gotliv, B.A., Addadi, L. & Weiner, S. 2006 Mollusk shell formation: Mapping the distribution of organic matrix components underlying a single aragonitic tablet in nacre. *Journal of Structural Biology* **153**, 176-187.

Penn, R.L. 2004. Kinetics of oriented aggregation. *The Journal of Physical Chemistry B* **108**, 12707-12712.

Penn, R.L. & Banfield, J.F. 1998 Imperfect oriented attachment: Dislocation generation in defect-free nanocrystals. *Science* **281**, 969-971.

Pérez-Huerta, A. & Cusack, M. 2009 Optimizing electron backscatter diffreation of carbonate biominerals-resion type and carbon coating. *Microscopy and Microanalysis* **15**, 197-203.

Politi, Y., Arad, T., Klein, E., Weiner, S & Addadi, L. 2004 Sea urchin spine calcite forms via a transient amorphous calcium carbonate phase. *Science* **306**, 1161-1164.

Pollard, G. 2001. Abalone fishing in South Australia. *South Pacific Underwater Medicine Society Journal* **31**, 150-152.

Porter, S.M. 2010 Calcite and aragonite seas ad the de novo acquisition of carbonate skeletons. *Geobiology* **8**, 256-277.

Poutiers, J.M. 1998. In: Carpenter, K.E. & Niem, V.H. (eds). *FAO species identification guide for fishery purposes: the living marine resources of the Western Central Pacific Volume 1: Seaweeds, corals, bivalves and gastropods.* 385p. ISBN: 9251040516.

Prior, D.J., Boyle, A.P., Brenker, F., Cheadle, M.C., Day, A., Lopez, G., Peruzzo, L., Potts, G.J., Reddy, S., Spiess, R., Timms, N.E., Trimby, P., Wheeler, J. & Zetterstrom, L. 1999 The application of electron backscatter diffraction and orientation contrast imaging in the SEM to textural problems in rocks. *American Mineralogist* **84**, 1741-1759.

Raz, S., Weiner, S. & Addadi, L. 2000 The formation of high magnesium calcite via a transient amorphous colloid phase. *Advanced Materials* **12**, 38-42.

Reimer, L. 1985 Image recording and processing. *Scanning Electron Microscopy*. Physics of Image Formation and Microanalysis. pp214-215. Springer, Berlin..

Rhoads, D.C. & Lutz, R.A. 1980. *Skeletal Growth of Aquatic Organisms. Biological Records of Enviromental Change.* New York, London. ISBN 0306402599. pp750.

Rousseu, M., Lopez, E., Stempfle, P., Brendle, M., Franke, L., Guette, A., Naslain, R. and Bourrat, X. 2005 Multiscale structure of sheet nacre. *Biomaterials* **26**, 6254-6262.

Rubner M. 2003 Materials science: Synthetic sea shell. *Nature* **423**, 925-926.

Ruppert, E.E., Fox, R.S., & Barnes, R.D. 2004 *Invertebrate Zoology, A Functional Evolutionary Approach* (7 ed.). Brooks Cole Thomson, Belmont, C.A. pp963.

Schaffer, T.E., Inoescu-Zanetti, C., Proksch, R., Fritz, M., Walters, D.A., Almqvist, N., Zaremba, C.M., Belcher, A.M., Smith, B.L., Stucky, G.D., Morse, D.E. & Hansma, P.K. 1997 Does abalone nacre form by heteroepitaxial nucleation or by growth through mineral bridges? *Chemistry of Materials* **9**, 1731-1740.

Schwahn, D., Ma, Y. & Cölfen, H. 2007 Mesocrystal to single crystal transformation of D, L-Alanine evidenced by small angle neutron scattering. *The Journal of Physical Chemistry* **8**, 3324-3227.

Schwartz, A.J., Kumar, M. & Adams, B.L. 2000. Editors. *Electron Backscatter Diffraction in Material Science.* New York: Kluwer Academic/Plenum Press. ISBN: 9780387881355. pp403.

Schwarzer, R.A. 1997a Advances in crystal orientation mapping with the SEM and TEM. *Ultramicroscopy* **67**, 19-24.

Schwarzer, R.A. 1997b Automated crystal lattice orientation mapping using a computer controlled SEM. *Micron* **28**, 249-265.

Shen, X.Y., Belcher, A.M., Hansma, P.K., Stucky, G.D. & Morse, D.E. 1997 Molecular cloning and characterization of lustrin A, a matrix protein from shell and pearl nacre of Haliotis rufescens. *Journal of Biological Chemistry* **272**, 32472-32481.

Silve, C., Lopez, E., Vidal, B. & Smith, D.C. 1992 Nacre initiates biomineralization by human osteoblasts maintained in vitro. *Calcified Tissue International* **51**, 363-369.

Simkiss, K. & Wilbur, K.M. 1989 *Biomineralization: Cell Biology and Mineral Deposition*. San Diego, New York, Berkeley, Boston, London, Sydney, Tokyo, Toronto: Academic Press. ISBN: 0126438307. pp337.

Sinclair, M. 1963 Studies on the Paua, *Haliotis iris* Martyn, in the Wellington district 1945-46. *Zoological Publications, Victoria University, Wellington* **35**, 1-16.

Song, F. & Bai, Y.L. 2003 Effects of nanostructures on the fracture strength of the interfaces in nacre. *Journal of Materials Research* **18**, 1741-1744,

Song, F., Zhang, X.H. & Bai, Y.L. 2002 Microstructure and characteristics in the organic matrix layers of nacre. *Journal of Materials Research* **17**, 1567-1570.

Stanley, S.M. & Hardie, L.A. 1998 Secular oscillations in the carbonate mineralogy of reef-building and sediment-producing organisms driven by tectonically forced shifts in seawater chemisty. *Palaeogeography, Palaeoclimatology, Palaeoecology* **144**, 3-19.

Stecher III, H.A., Krantz, D.E., Lord III, C.J., Luther III, G.W. & Bock, K.W. 1996 Profiles of strontium and barium in *Mercenaria mercenaria* and *Spisula solidissima* shells. *Geochimica et Cosmochimica Acta* **60**, 3445-3456.

Tang, Z., Kotov, N.A., Magonov, S., Ozturk, B. 2003 Nanostructured artificial nacre. *Nature Materials* **2**, 413-418.

Taylor, J., Kennedy W.J. & Hall, A. 1969 Shell structure and mineralogy of the Bivalvia (Nuculacea-Trigonacea): Bulletin of the British Museum (Natural History). *Zoology* **3**, 1-125.

Thomapson, J.B., Paloczi, g.t., Kindt, J.H., Michenfelder, M., Smith, B.L., Stucky, G., Morse, D.E. & Hansma, P.K. 2000 Direct observation of the transition from calcite to aragonite growth as induced by abalone shell proteins. *Biophysical Journal* **79**, 3307-3312.

Thompson, D.W. 1968 *On growth and form.* 2nd ed., reprinted. Cambridge: Cambridge University Press. pp1116.

Tissot, B.N. 1992 Water movement and the ecology and evolution of the Haliotidae. In: Shepherd, S.A., M.J.Tegner & S.A.Guzman del Proo(eds.). *Abalone of the world: Biology Fisheries and Cultrue*. Fishing News Books, Oxford, pp34-45.

Voltzow, J. & Collin, R. 1995 Flow through mantle cavities revisited: Was sanitation the key to fissurellid evolution? *Invertebrate Biology* **114**, 145-150.

Wada, K. 1972 Nucleation and growth of aragonite crystal in the nacre of some bivalve molluscs. *Biomineralization* **6**, 141-151.

Wada, K. 1968 Electron microscope observations of the formation of the periostracum of *Pinctada fucata. Material of the National Pearl Research Laboratory* **13**, 1540-1560.

Walters, D.A., Smith, B.L., Belcher, A.M., Paloczi, G.T., Stucky, G.D., Morse, D.E. & Hansma, P.K. 1997 Modification of calcite crystal growth by abalone shell proteins: an atomic force microscope study. *Journal of Biophysics* **72**, 1425-1433.

Wang, R.Z., Suo, Z., Evans, A.G., Yao, N. & Aksay, I.A. 2001 Deformation mechanisms in nacre. *Journal of Materials Research Soc*iety **16**, 2485-2493.

Wang, R.Z., Wen, H.B., Cui, F.Z., Zhang, H.B. & Li, H.D. 1995 Observations of damage morphologies in nacre during deformation and fracture. *Journal of Materials Science* **30**, 2299-2304.

Watabe, N. 1965 Studies on shell formation.11. Crystal-matrix relationship in inner layers of mollusc shells. *Journal of Ultrastructure Research* **12**, 351-370.

Weiner, S. & Dove, P.M. 2003 An overview of biomineralisation processes and the problem of the vital effect. *Biomineralisation Volume* **54**. Edited by: Dove, P.M., DeYoreo, J.J., Weiner, S. Washington, D.C., Mineralogical Society of America: 1-29p.

Weiner, S. & Addadi, L. 2002 Calcium carbonate formation in biology: the involvement of an amorphous calcium carbonate precursor phase. *Geochimica et Cosmochimica Acta* **66**, A827.

Weiner, S. & Addadi, L. 1997 Design strategies in mineralized biological materials. *Journal of Materials Chemistry* **7**, 689-702.

Weiner, S. & Traub, W. 1984 Macromolecules in mollusc shells and their functions in biomineralization. *Philosophical Transactions of the Royal Society of London B* **304**, 425-434.

Weiner, S., Talmon, Y. & Traub, W. 1983. Electron diffraction of mollusk shell organic matrixes and their relationship to the mineral phase. *International Journal of Biological Macromolecules* **5**, 325-328.

Weiner, S. & Traub, W. 1980 X-Ray-diffraction study of the insoluble organic matrix of mollusk Shells. *FEBS Letters* **111**, 311-316.

Weiner, S. 1979 Aspartic acid-rich proteins-major components of the soluble organic matrix of mollusc shells. *Calcified Tissue International* **29**, 163-167.

Weiss, I.M., Gohring, W., Fritz, M. & Mann, K. 2001 Perlustrin, a Halitois laevigata (Abalone) nacre protein, is homologous to the insulinlike growth factor binding protein N-terminal module of vertebrates. *Biochemical Biophysical Research Communications* **285**, 244-249.

Wilbur, K.M. 1964 Shell formation and regeneration. In: *Physiology of Mollusca I* (Wilbur, K.M., Yonge, C.M., eds.). New York: Academic Press, 243-282.

Wise, S. 1970 Microarchitecture and mode of formation of nacre (mother-of-pearl) in pelecypods, gastropods, and cephalopods. *Eclogae Geologicae Helvetiae* **63**, 775-797.

Wright, S.I., Gray, G.T. & Rollett, A.D. 1994 Textural and microstructural gradient effects on the mechanical-behaviour of a tantalum plate. *Metallurgical Transactions a-Physical Metallurgy and Materials Science* **25**, 1025-1031.

Wright, S.I. & Adams, B.L. 1992 Automatic-analysis of electron backscatter diffraction patterns. *Metallurgical Transactions A-Physical Metallurgy and Materials Science* **23**, 759-767.

Wright, S.I. & Adams, B.L. 1991 Automated lattice orientation determination from electron backscatter kikuchi diffraction patterns. *Textures and Microstructures* **14**, 273-278.

Wu, G. & Jensen, D.J. 2008 Automatic determination of recrystallization parameters based on EBSD mapping. *Materials Characterization* **59**, 794-800.

Yuwono, V.M., Burrows, N.D., Soltis, J.A. & Penn R.L. 2010 Oriented aggregation: Formation and transformation of mesocrystal intermediates revealed. *Journal of the American Chemical Society* **132**, 2163-2165.

Zaremba, C.M., Belcher, A.M., Fritz, M., et al. 1996 Critical transitions in the biofabrication of abalone shells and flat pearls. *Chemistry of Materials* **8**, 679-690.

Zeng, H.C. 2007 Oriented attachment: a versatile approach for construction of nanomaterials. *International Journal of Nanotechnol*ogy **4**, 329-346.

Zhang, Q., Liu, S.J. & Yu, S.H. 2009 Recent advances in oriented attachment growth and synthesis of functional materials: concept, evidence, mechanism, and future. *Journal of Materials Chemisty* **19**, 191-207.